UNIVERSITÀ
DEGLI STUDI
DI PADOVA

UNIVERSITA' DEGLI STUDI DI PADOVA

Department of Industrial Engineering DII

Master's degree course in Ingegneria Energetica

Aquifer Thermal Energy Storage:

Development of a simplified model for building and district simulation tools

Supervisor: Prof. Zarrella Angelo (UniPD)

Co-supervisor: Asst. Prof. Maccarini Alessandro (AAU)

Candidate: Varesano Davide 2027554

Academic Year 2022/2023

Abstract:

The main goal of this master thesis is the development of a model of an Aquifer Thermal Energy Storage (ATES) for building and district simulations tools. An ATES system consists of two or more groundwater wells where the storage and recovery of thermal energy is achieved by extraction and injection of water. Usually, the performance study of an ATES requires complex fluid dynamics simulations which have limited capability of integrating energy tools. In the proposed simplified model, which was developed using a *MATLAB* code, the radial temperature variation of the groundwater is calculated using a finite difference method with a lumped parameters system to solve the transient heat and mass transfer equations in the porous media. The model was validated with measured data retrieved from an ATES system located in Delft (Netherlands). To demonstrate the use of the above mentioned model, a simulation-based case study was carried out by connecting the ATES model with an office building energy model. Thermal loads from the office building simulation have been integrated in the ATES model assuming that the system works with a groundwater heat pump for heating and a heat exchanger for cooling. Simulations were performed under three different climate conditions (Verona, Frankfurt, and Helsinki).

Riassunto esteso in italiano:

L'*Aquifer Thermal Energy Storage* (ATES) è una tecnologia di accumulo di energia termica che utilizza l'acqua di falda racchiusa in strati geologici impermeabili come sorgente termica.

È una tecnologia di accumulo stagionale poiché, durante l'inverno, l'acqua di falda viene estratta da un pozzo detto caldo e, successivamente, viene iniettata nel pozzo cosiddetto freddo. Viceversa, durante l'estate, l'acqua viene estratta dal pozzo freddo e immessa in quello caldo.

Il principale vantaggio per l'accumulo stagionale è la possibilità dell'incontro tra l'energia fornita dall'ATES e quella richiesta dall'utenza quando queste non coincidono nel tempo. Questi sistemi di accumulo possono anche essere accoppiati con pompe di calore geotermiche o direttamente con scambiatori di calore. Gli stessi sistemi sono particolarmente indicati per carichi su larga scala, come grandi edifici o reti di teleriscaldamento e teleraffrescamento.

I modelli di ATES vengono generalmente studiati e sviluppati utilizzando complessi *software* di analisi fluidodinamica che hanno un'elevata precisione in quanto trattano anche il comportamento e l'influenza della pressione nella falda. Contestualmente, richiedono lunghi tempi di simulazione e offrono una bassa interoperabilità in termini di integrazione con strumenti di simulazione energetica.

Lo scopo di questa tesi è quello di creare un modello semplice e flessibile di un ATES per *software* di analisi energetica.

Nel merito, dopo aver introdotto a carattere generale, i sistemi geotermici ed in particolare i sistemi ad accumulo termico in falda acquifera a bassa temperatura, il presente lavoro si concentra sulla creazione di un modello che simuli un ATES. L'elaborato parte da un precedente lavoro di ricerca, *"An aquifer thermal energy*

storage model for efficient simulations of district systems", di Elisa Scalco, Angelo Zarrella, Alessandro Maccarini e Alireza Afshari relativo allo sviluppo di un modello, un codice *MATLAB*, che utilizza un approccio alle differenze finite per risolvere le equazioni di conduzione del calore e le equazioni di trasferimento di massa nel mezzo poroso della falda in due dimensioni. I pozzi vengono raffigurati da cilindri indipendenti immersi nella falda acquifera circostante la quale, secondo l'ipotesi del seguente studio, è rappresenta con dischi radialmente simmetrici. In questo modo, il modello risulta semplice in quanto il comportamento del sistema pozzo/falda viene studiato tramite parametri concentrati. Inoltre, nel modello proposto, viene trascurato il calcolo della pressione che richiederebbe l'analisi fluidodinamica ritenuta non essenziale per la semplicità del progetto. Il modello, in sintesi, calcola solamente le temperature della falda nello spazio e nel tempo.

La validazione del modello è stata effettuata sia con dati provenienti da un articolo di Julian E. Mindel et al. *"Benchmark study of simulators for thermo-hydraulic modelling of low enthalpy geothermal processes"* riguardante dei test eseguiti con diversi *software* di simulazione fluidodinamica e sia con dati reali provenienti da un impianto ATES situato nella città di Delft nei Paesi Bassi.

Nell'ultima parte di questo lavoro, invece, è descritta l'integrazione dei dati provenienti dalla simulazione energetica eseguita con *EnergyPlus*. Nel modello, quindi, sono inseriti i carichi termici richiesti dall'edificio, o da reti di teleriscaldamento/raffrescamento, i quali determinano la quantità d'acqua estratta e successivamente iniettata necessaria per soddisfare il fabbisogno energetico.

Si è scelto, infine, di analizzare differenti casi relativi ad un medesimo grande edificio adibito per uffici alimentato da un ATES, localizzato però in diverse località e quindi con carichi differenti in modo da avere: raffreddamento dominante (Verona), carico bilanciato (Francoforte) e riscaldamento dominante

(Helsinki). All'ATES sono stati aggiunti una pompa di calore funzionante durante la fase di riscaldamento ed alimentata dall'acqua del pozzo caldo e uno scambiatore di calore per il raffreddamento che utilizza direttamente l'acqua proveniente dal pozzo freddo.

Acknowledgements:

During these years of my master's degree in energy engineering, I got interested in HVAC and building energy sectors, which require, as soon as possible, to be decarbonize. In addition to the most common known renewable energy technologies, I was fascinated by geothermal energy, mainly in the geothermal system used for heating and cooling purposes.

The development of this work has been possible thanks to my supervisor, Prof. Angelo Zarrella, who proposed a thesis to me about his former research work on aquifer thermal energy storage systems conducted with my co-supervisor Assistant Prof. Alessandro Maccarini of the department of Build Environment of Aalborg University.

I sincerely thank you both for all the time dedicated to me, for all the advices, documents, and materials provided, but above all for the possibility of continuing your interesting work.

Further thanks too Prof. Martin Bloemendal of the Delft University of Technology who helped us in the validation work providing papers and data of a real plant.

Finally, I would like to thank all the Padua University, all the Professors and collaborators of the energy engineering course that I've had in these years who have proved to be prepared and of a high level.

Acronyms:

ATES: Aquifer Thermal Energy Storage

GSHP: Ground Source Heat Pump

GCHP: Ground Coupled Heat Pump

GWHP: Ground Water Heat Pump

SWHP: Surface Water Heat Pump

UTES: Underground Thermal Energy Storage

PTES: Pit Thermal Energy Storage

TTES: Tank Thermal Energy Storage

BTES: Borehole Thermal Energy Storage

FDM: Finite Difference Method

HVAC: Heating Ventilation Air Conditioning

COP: Coefficient Of Performance

RMSE: Root Mean Square Error

Nomenclature:

Φ: porosity [-]

ϱ: density [kg/m^3]

c_p: specific heat [J/kgK]

λ: thermal conductivity [W/mK]

α: thermal diffusivity [m^2/s]

Δτ: time step [s]

T: temperature [°C]

R: thermal resistance [K/W]

V: Volumetric flow rate [m^3/s]

Cs: Volumetric heat capacity [J/m^{3}K]

Vol: Volume [m^3]

C_{exp}: expansion coefficient [-]

r_M: barycentric medium radius

h: height

s: annulus thickness [m]

r_i: internal radius [m]

l: leakage coefficient [m^3_{water}/m^3_{aq}]

Q: Thermal load [W]

T_{WLC}: water temperature leaving the condenser [K]

T_{WLE}: water temperature leaving the evaporator [K]

ΔT: temperature difference [°C]

η_{carnot}: carnot efficiency [-]

R_{th}: thermal radius

Subscripts and Superscripts

p: time instant

i: generic active node

wb: well bore

ax: axial

g: ground

aq: aquifer

r: rock matrix

w: water

ext: extracted

inj: injected

H: heating

C: cooling

pp: pinch point

ev: evaporator

cond: condenser

Index:

Introduction:

According to the most recent report of the International Energy Agency [1], the operation of the building sector accounted for 30% of global final energy consumption and 27% of total energy sector emissions, including 8% being direct emissions in buildings and 19% indirect emissions from the production of electricity and heat used in buildings. Minimum performance standards for building energy are increasing in both scope and stringency, and the use of more efficient and renewable energy technology in buildings is contributing to lower these consumptions.

The operation of HVAC plant in buildings is one of the most important factors, as it is responsible for emissions and energy demand.

Concerning the heating sector, both for space heating and domestic hot water production, about 60% of the energy demand is covered by fossils fuels especially natural gas (45% of the total) in Europe [1].

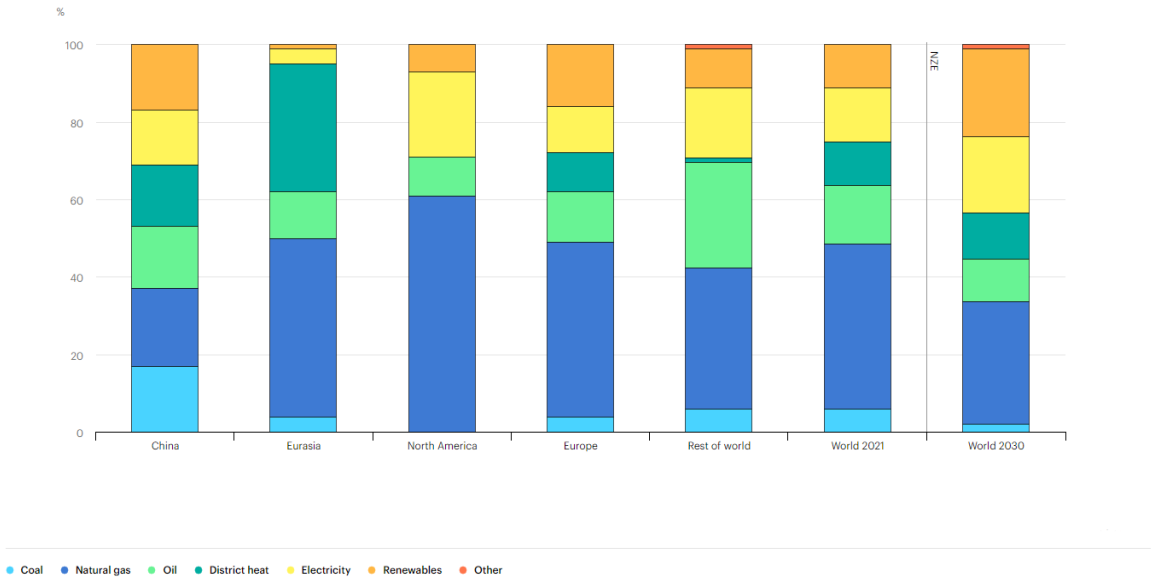

Figure 1: Different fuels for space heating

The sector is responsible for 2450 Mt of direct CO_2 emissions in 2021 [1].

According to the Net Zero Emissions (NZE) scenario, in 2030, the direct emissions must be reduced by 10% each year; this is possible by investing on technologies which are already available and mature in the market: new condensation gas boilers, heat pumps or renewables like solar thermal collectors, geothermal energy or bio-energies.

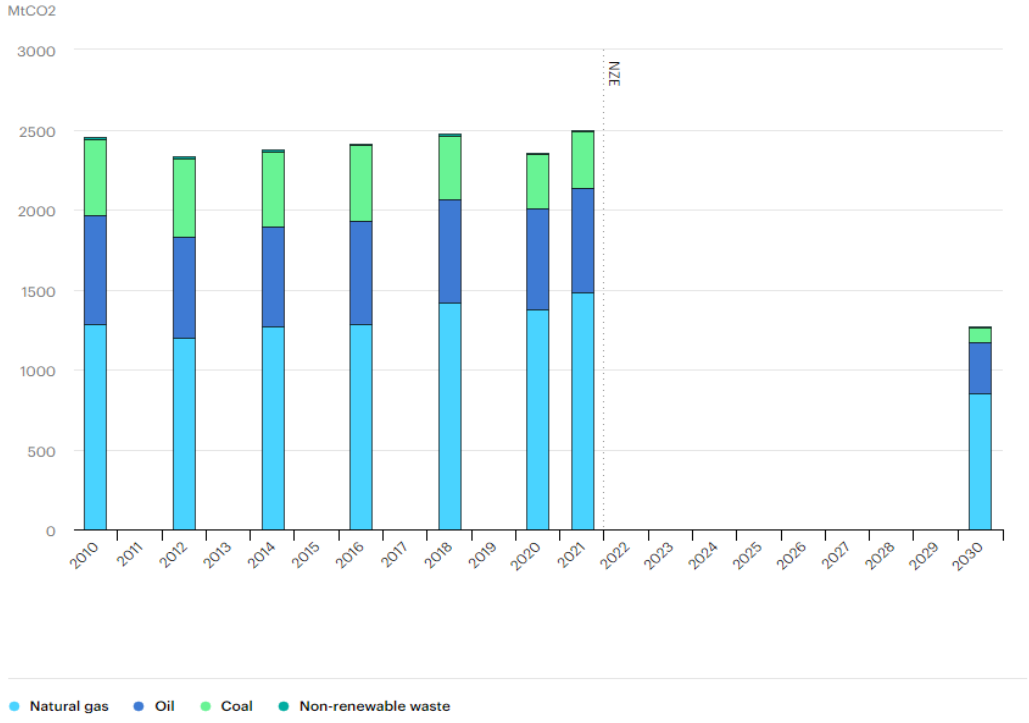

Figure 2: Emission of CO2 from different fuel

Important factors to be considered are population growth and the evolution of living standards, these increase heating consumption, for this reason the building sector should invest also on energy efficiency.

On the other hand, the space cooling sector has more than tripled its energy consumption since 1990 [1]. This is, due to rapid urbanization, particularly in developing countries, and hotter weather and it will surely increase in the next few years, resulting in it being as a primary topic to be analysed in terms of energy consumption.

In 2021, 16% (about 2000 TWh) of the final electricity consumption for building came from the cooling demand and the carbon dioxide emissions for the cooling sector was almost 1000 Mt [1].

Space cooling equipment performance is improving continuously, and electricity production is becoming less carbon-intensive; by 2030 a single air conditioning unit have to emit less than 150 $kgCO_2$ (figure 3). However, these figures do not consider the emissions of greenhouse gases due to refrigerant leakages. According to the "*Kigali amendment*" signed in 2016, the use of hydrofluorocarbons fluids has been regulated in order to cut their consumption and invest more in new refrigerants like the new hydrofluoroolefins.

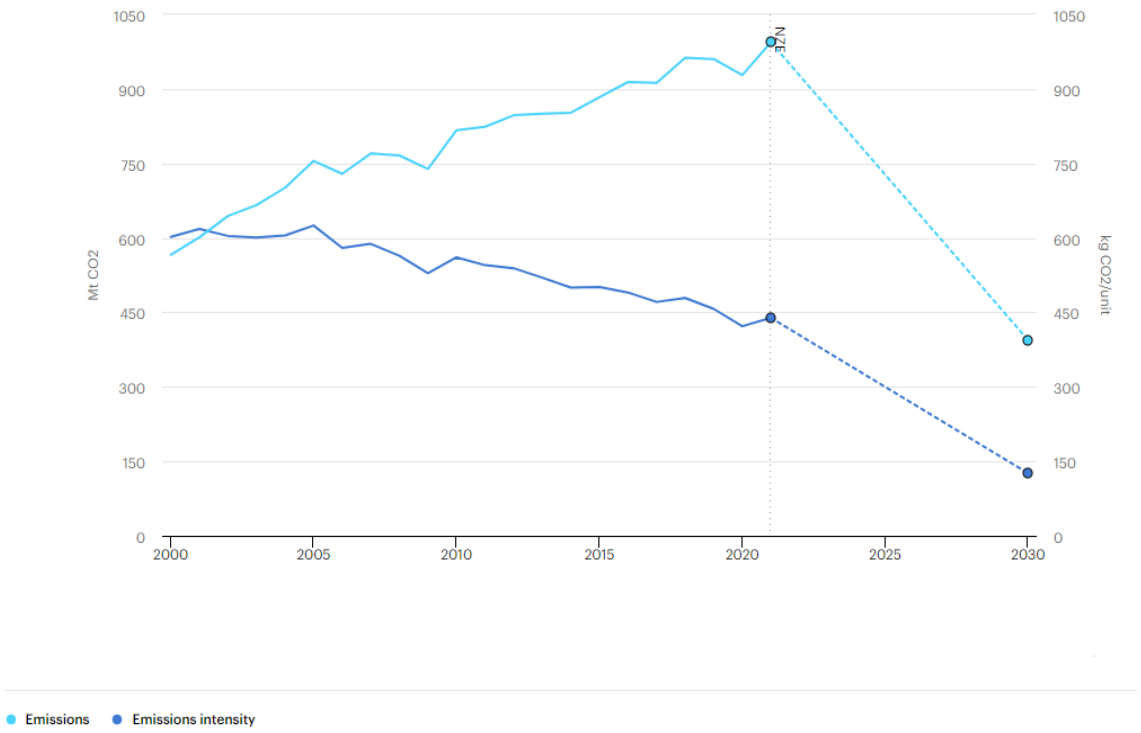

Figure 3: CO2 emission from space cooling and a single unit

To summarize, it is therefore fundamental for the building sectors to invest in other areas and particularly in more sustainable technologies if it is to reduce its global final energy consumption and energy sector emissions.

Geothermal energy is a valid alternative that could help to reduce the greenhouse gas emissions from the building sector. There are many possibilities to exploit the heat from the ground for heating and cooling purposes. Boreholes and groundwater heat pumps are well-known technologies. Seasonal thermal storages like the Aquifer Thermal Energy Storage (ATES) are also an interesting options already adopted for large scale building or district heating and cooling in Central Northern Europe countries.

Common ATES models are usually developed using complex fluid dynamics simulations, which require long computational times and have low interoperability in building and district energy tools.

The following thesis is the continuation of a research paper[1] and aims to describe the development of a simple and flexible ATES model in *MATLAB* and its integration with energy data from a simulation, performed with *EnergyPlus*, in order to have a first "planning" tool for these systems.

[1] Elisa Scalco, Angelo Zarrella, Alessandro Maccarini, Alireza Afshari, *"An aquifer thermal energy storage model for efficient simulations of district systems"*

1. Geothermal system and ATES

Geothermal energy is the energy stored in the form of heat beneath the surface of the solid earth. It comes from the earth's crust thanks to the radioactive decay of naturally occurring radioactive elements inside rocks. Going more deeper in the ground, the average temperature gradient is 30°C/km.

The geothermal resources can be subdivided in three general categories [2], high temperatures application, intermediate temperature and low temperature or low enthalpy application.

The high temperature resources (>150°C) find application in power production; these resources can be steam or water dominant and can be used with direct plant, flash plant o binary plant. The intermediate resources (<150°C, >90°C) refer to systems which use heat directly from the ground or in the production of power with an organic Rankine cycle. Both these categories require particular conditions, large perforation of the ground (figure 4) and appropriate location with high geothermal gradient and moreover these geothermal sources are not spread uniformly on the earth.

1.1 Low enthalpy technology

Low enthalpy resources consist of systems which extract heat from the upper layers of the ground and, in most of the applications, require a heat pump, to reach the heating and cooling purpose; this technology is called Ground-Source Heat Pump (GSHP). Unlike the high or intermediate resources, the low ones can be used more easily because they use the ground as a heat source and sink, and not specific deeper zones.

Generally, the ground is an excellent source due to its constant temperature as opposed to air.

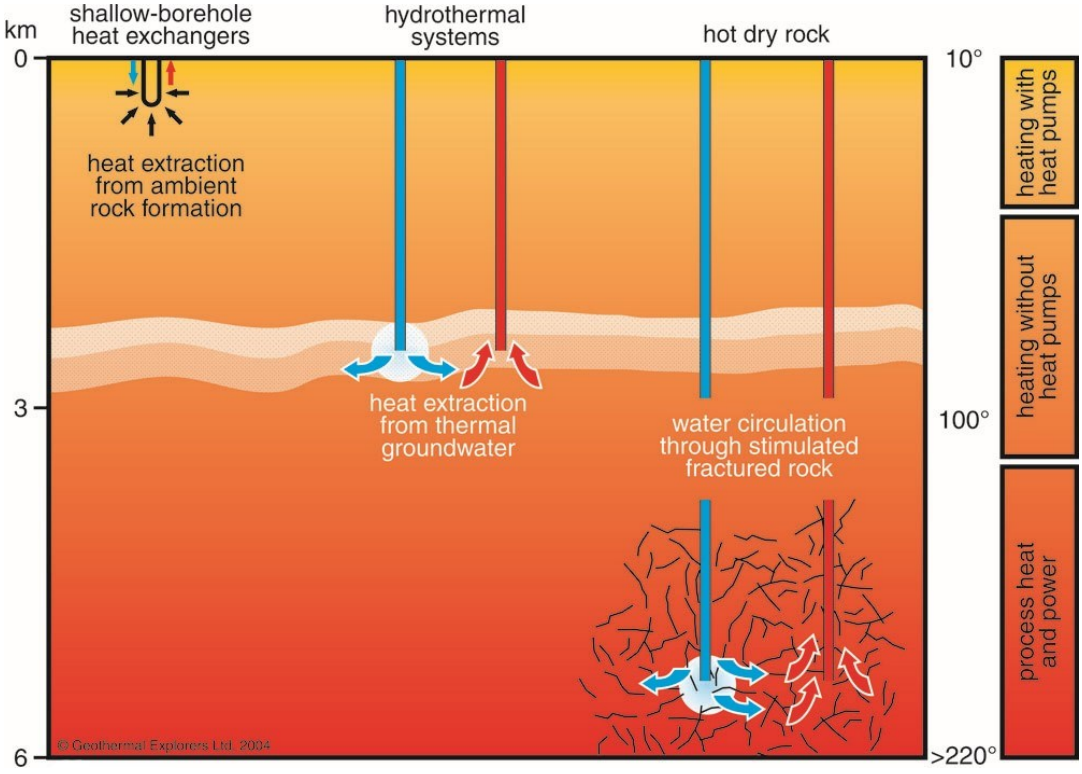

Figure 4: Geothermal System

The ground-source heat pump systems includes:

- Ground Coupled Heat Pump (GCHP), a reversible vapour compression cycle linked to a closer ground heat exchanger buried in soil (borehole heat exchanger). Inside the pipes in the borehole, a water solution circulates in a closed loop, acting as an evaporator during heating mode or condenser during cooling. Alternately, heat pump refrigerant could directly circulate inside. The possible configurations are vertical, horizontal or slinky configuration (figure 5). In case of soft soil or for high structural load, the geothermal probes can be installed in piles (energy piles technology).
- Ground Water Heat Pump (GWHP), systems which extract water from the ground in a well and use it for the heat pump; after initial use, water is

injected in another well or in a lake, pond or river. They are open loop technologies. Usually they cost less and require less space than GCHP and have an excellent heat transfer due to the open loop. The main disadvantages of the GWHP are the availability of ground water and the local environmental regulation which may be restrictive.

- Surface Water Heat Pump (SWHP), plants that use local surface reserves of water such as a lake, pond or river. They could be indirect, i.e. closed loop where a heat exchanger is immersed in water or direct (open loop), with withdrawal and injection of water.

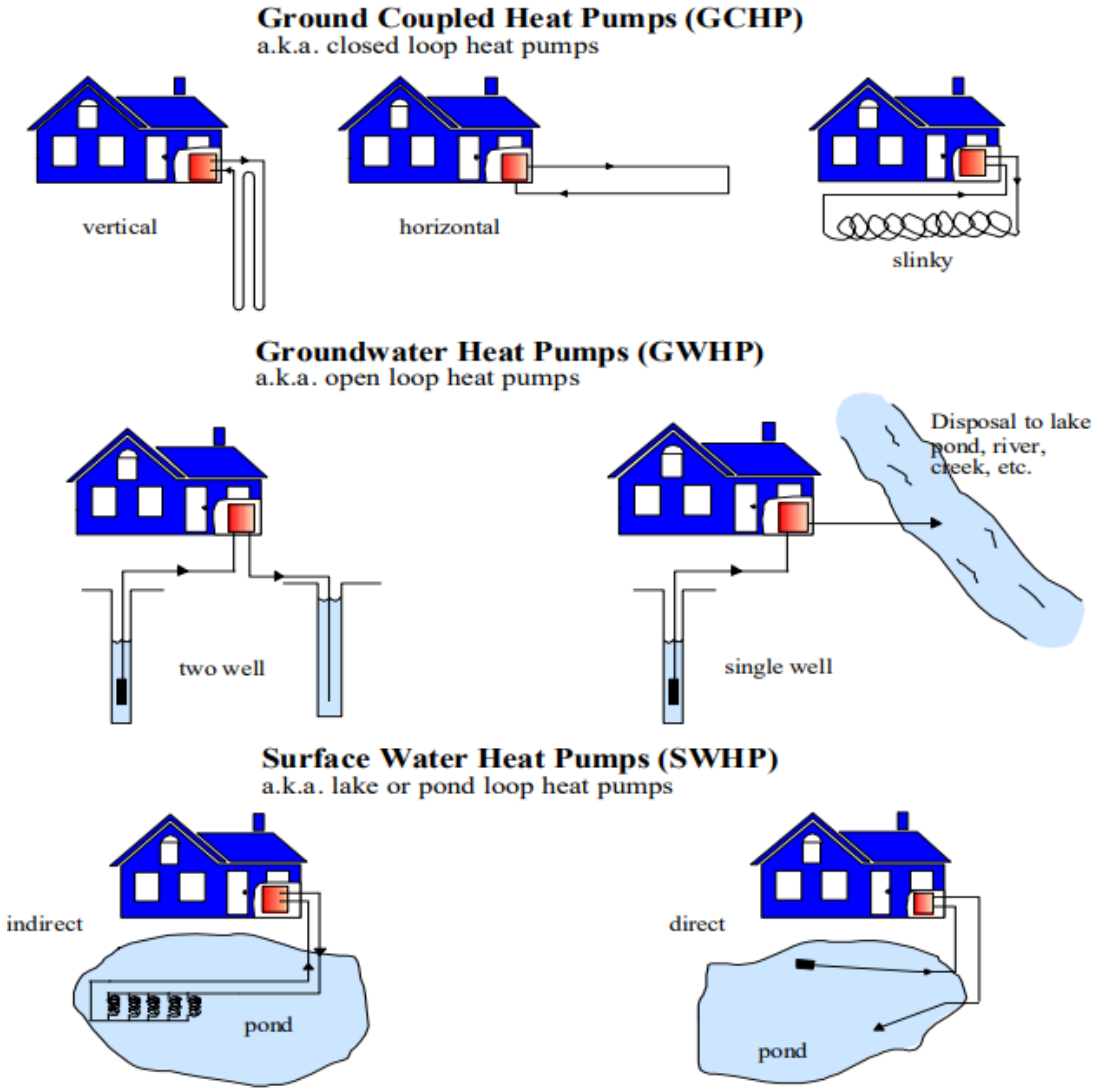

Figure 5: Ground Source Heat Pump

1.2 Underground Thermal Energy Storage

The Underground Thermal Energy Storage system (UTES) are technologies that form a part of the low temperature resources. In many cases, the energy demand of a building does not coincide in time with the supply; this seasonal mismatch could be tackled with thermal storage. The ground can store heat or cold energy for a future use. There are many typologies of UTES system (figure 6)

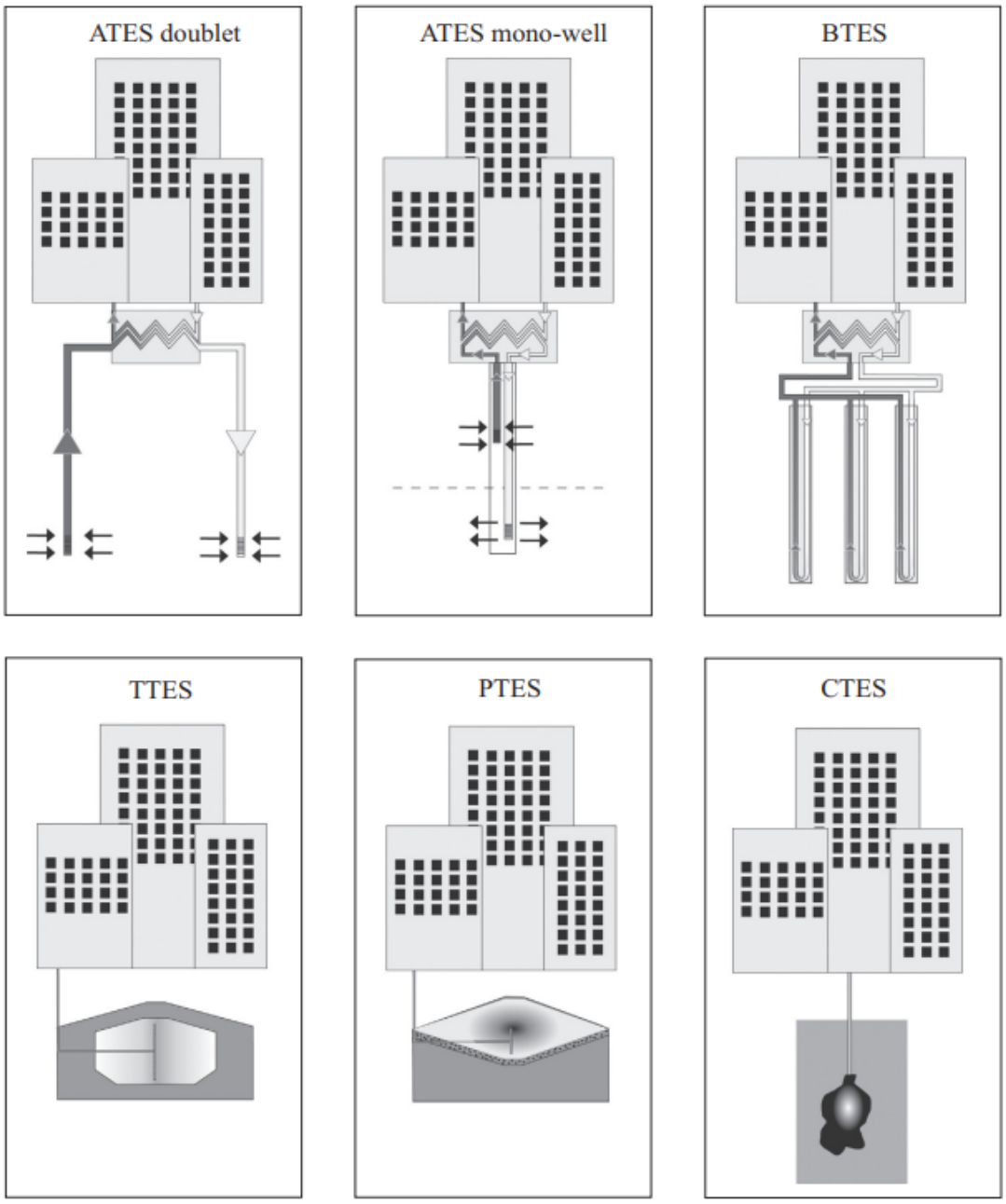

Figure 6: Underground Thermal Energy Storage typologies

The main typology of UTES system are:

- ATES (Aquifer Thermal Energy Storage);
- BTES (Borehole Thermal Energy Storage);
- TTES (Tank Thermal Energy Storage);
- PTES (Pit Thermal Energy Storage);
- CTES (Cave Thermal Energy Storage).

1.3 Aquifer Thermal Energy Storage

ATES is a system where the storage and recovery of thermal energy is achieved by the extraction and injection of water from aquifers using groundwater wells. ATES could be mono-well or doublet; across Europe the doublet is the mainly used.

In the case of an ATES doublet, during the winter months, water is extracted from a well (warm well), used in a heat pump or heat exchanger, and injected at lower temperature in the second well (cold well). During summer, the water is extracted from the cold well and after using it, injected at higher temperature into the warm well.

The presence of the heat pump or heat exchanger depends on the available aquifer temperature and the building plants demand temperature. Usually, as illustrated in figure 7, during cooling mode the systems uses a heat exchanger.

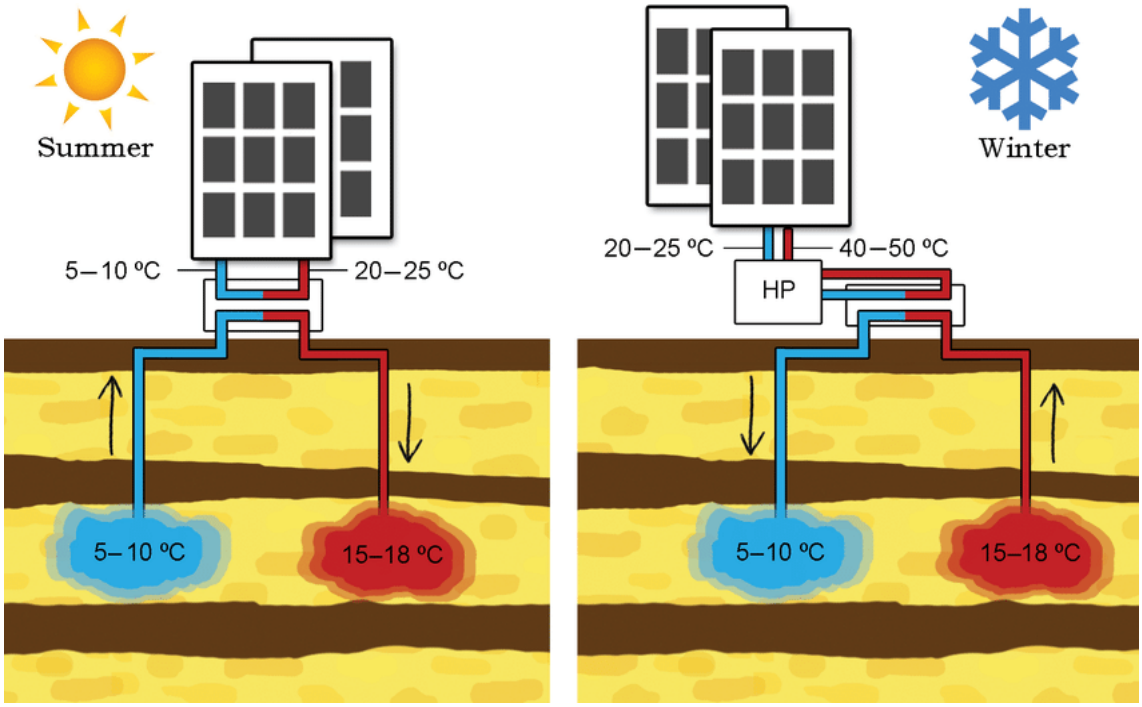

Figure 7: ATES working principle example

ATES can be either low temperature (<40°C), which are the most commonly used systems, or high temperature (>40°) [3];

ATES can be classified according to:

- energy source[2],
- layout of the well,
- application,
- ground type,
- aquifer characteristics and,
- size,

as shown in figure 8.

[2] ATES systems can implement energy both for the heat and cold source in different way: commonly from the internal excessive heat or cold of the building, but there are also ATES which implement waste heat from industry, combined and heat power plant or renewable energy such as solar thermal collectors or geothermal energy.

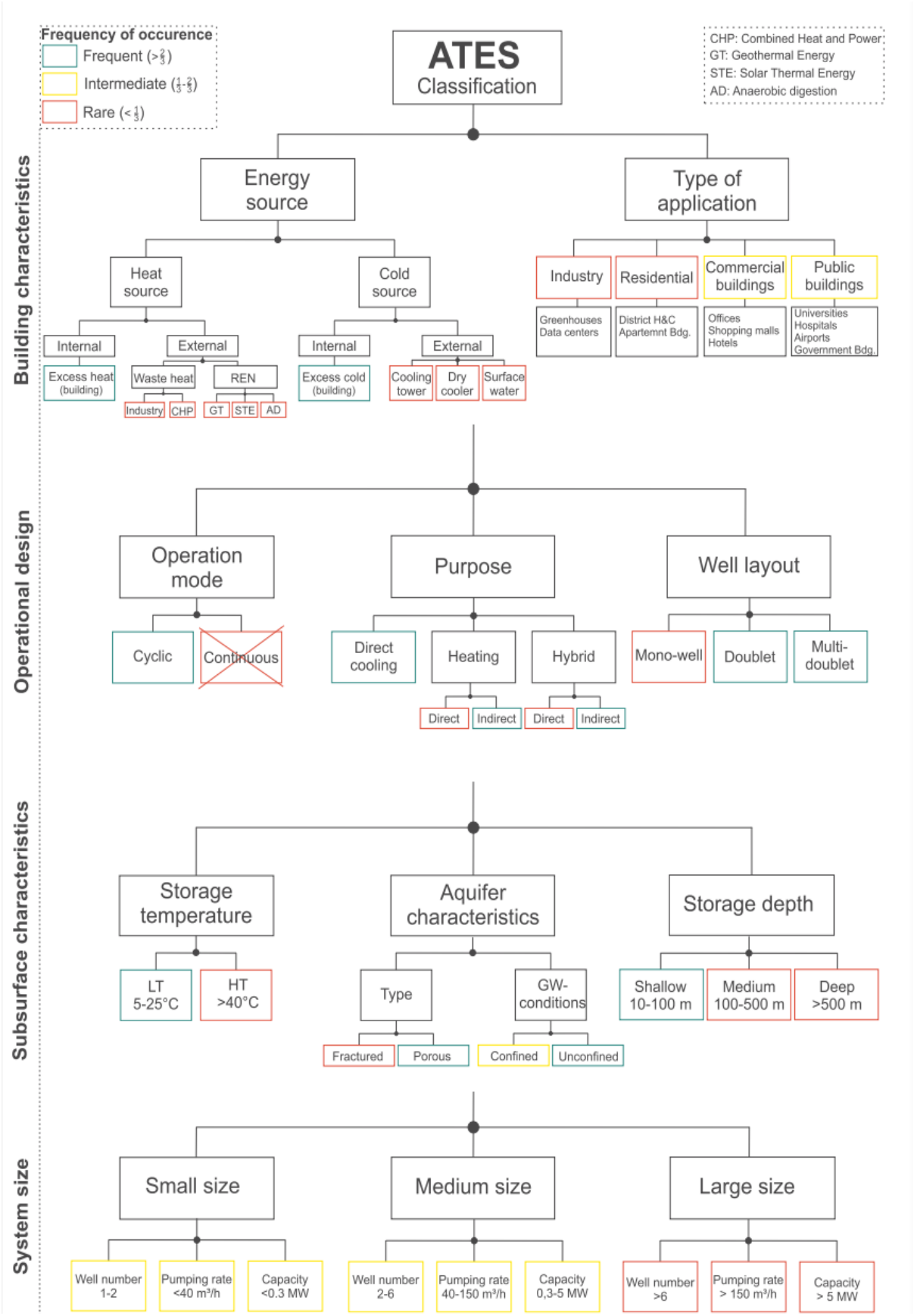

Figure 8: ATES classification

1.3.1 State of art

As reported in Paul F. et al. [4], the first prototype of an ATES system dates back in mid-1960s in Shanghai the system was used for cooling in textiles industries.

In this first generation of ATES there were a lot of problems including: clogging of the heat exchanger, corrosion of the well, strong imbalance between hot and cold loads, and swelling of clay material surrounding the aquifers.

With the beginning of the oil crisis in the mid-1970, the research into and development of energy storage were intensified, and the idea of storing thermal energy in aquifers started to be developed in North America and Europe. Over the years, ATES systems have overcome the main issues and have continued to be an interesting technology for heating and cooling for same regions/countries.

Nowadays, more of 2800 ATES are implemented worldwide with 85% of installations in the Netherlands and 10% in other Central North Europe countries (such as Sweden, Belgium and Denmark), which together provide about 2.5 TWh of heat and cold energy per year[3] [4], mainly used for large buildings like hospitals, airports or universities and also for district heating and cooling networks.

As it shown in figure 9, ATES systems are not spread worldwide in industrialized countries, which have great demand for sustainable heat and cold, not just for geological feasibility or climatic condition, but also due to market barriers.

[3] Equal to 150000 households in Central Europe.

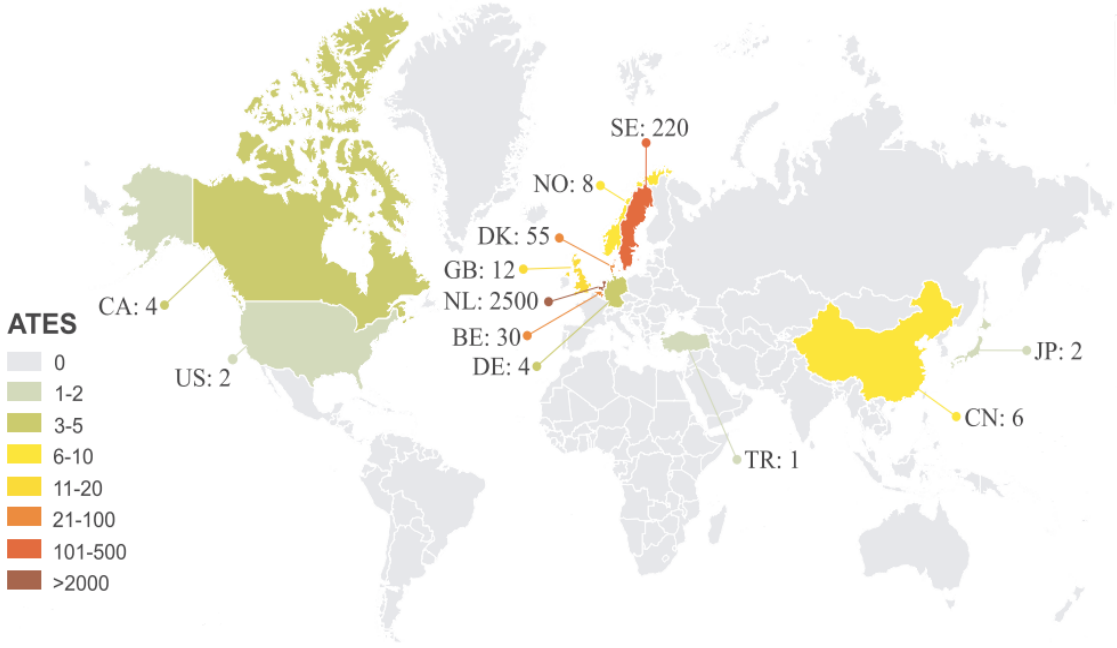

Figure 9: Implemented ATES worldwide

These limitations are of different natures, socio-economic, regulatory, technical and political which vary with a dynamic process of three different phases.

The first phase, an emerging market phase, is where the main barriers depend on the lack of awareness and mistrust in technology in addition to the technical feasibility[4]. People in charge and plant installers do not consider the use of ATES, and the public does not know about the technology and could have prejudices about the economic and technical feasibility. One way to overcome this obstacle is the active promotion of ATES, but it is often not sufficient. For example, for more of 20 years, the *Reichstag* building in Berlin has been heated and cooled with an aquifer thermal energy storage, but Germany, as it shown in figure 10, is still in the emerging phase and have only a few ATES implemented.

[4] In case of low temperature storage <40°C, there are no unsolved technical problem [5], high temperature storages usually have more well corrosion issues.

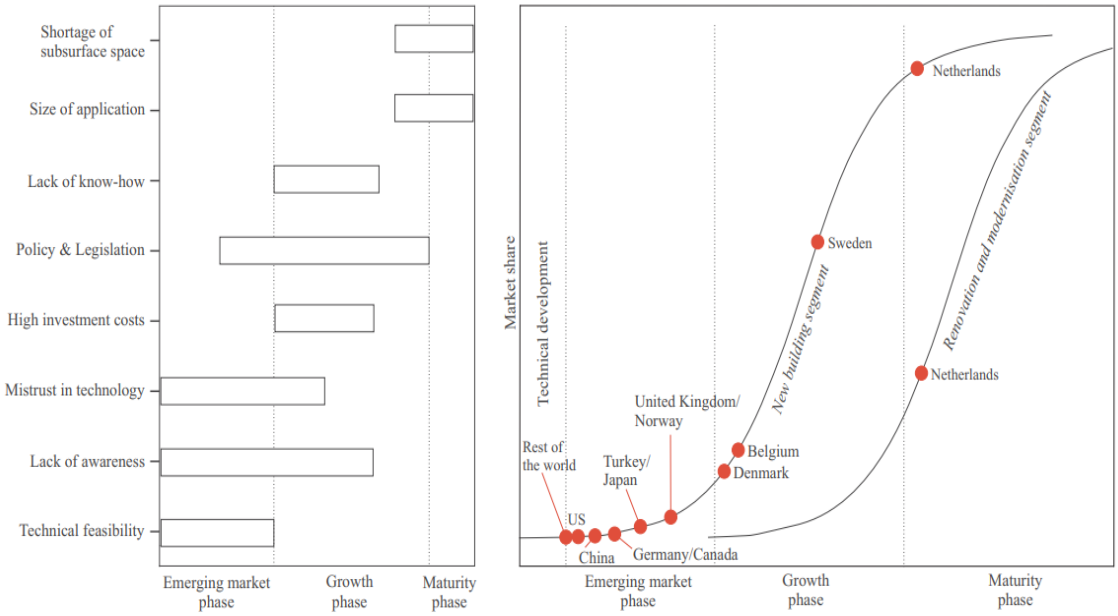

Figure 10: On left: market barriers; on right: countries in the phases

ATES has high initial costs compared to conventional systems, especially for drilling, that requires investments risks in order to explore the suitability for an ATES, resulting in lack of economic trust for clients, despite ATES having low payback times.

In the second phase, a growth phase that corresponds with commercialization, the main market barriers are due to regulatory issues. These aspects analyse the environmental risks about the geothermal resources, subdivided in hydrogeological, chemical, thermal and microbiological impacts. Important considerations for an ATES system are: groundwater injection temperature in the aquifer, maximum drilling depth, minimum distance between the wells[5] or other geothermal application and contaminated sites. More barriers during the growth phase are the lack of ATES installation know-how amongst local companies and the high investment cost. Large consultancies often do not risk harming their

[5] To avoid thermal interference, wells are located at a safety distance depending the aquifer/operation properties multiplied by a coefficient . Usually each country has his own coefficient. See Chapter 4.3.

reputation with an unknown new technology [4] while smaller ones are not able to manage the large projects that an ATES needs.

The maturity phase is the third and final stage. It is mainly influenced by the shortage of space and size of the application. The Netherlands, the leading country for ATES technologies for new buildings and renovated ones (mentioned figure 10), have problems due to the high demand of energy from ATES exceeding the available space. The size of the application is another barrier. A key aspect for an ATES is the thermal storage, if the building loads are not enough to reach the seasonal storage as in case of low energy demand buildings, the system is useless. For this reason, ATES plants could be integrated in district heating/cooling network in case of residential zones or large buildings. In old buildings, the size influences the replacing of old terminal units and HVAC applications also, which are not always usable with the temperature extracted from the wells.

1.3.2 ATES modelling software

There are different versions of fluid dynamics software in circulation that are used for ground-water system modelling and simulation and they are commonly adopted for ATES.

One of the most widely used is the modular finite-difference groundwater flow model known as *MODFLOW*, developed by the U.S. Geological Survey. *MODFLOW*, which is based on finite-difference method, is able to simulate aquifers in which the saturated flow condition exists[6], Darcy's law for fluids flowing through porous medium applies, density of ground water is constant

[6] Water flow caused by gravity's pull.

throughout the aquifer, and the main directions of the hydraulic conductivity do not vary within the system [6]. In short, the software divides the aquifer in rectangular blocks (cells) by a grid in three dimension organized in rows, columns and layers (figure 11).

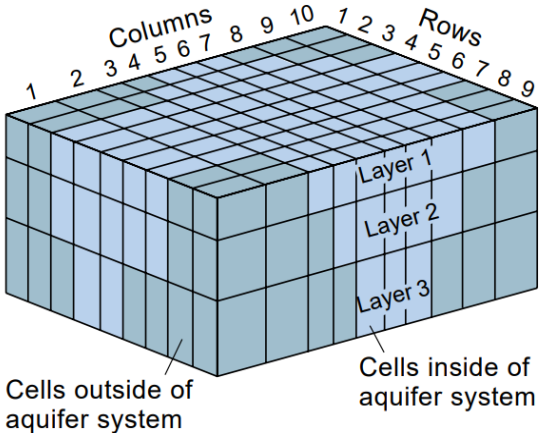

Figure 11: Example of model grid for simulating three-dimensional groundwater flow

For each cell, aquifer properties must be specified along with other information concerning wells, rivers, other inflow or outflow. In this way, ground-water equations are solved for each cells.

Other similar software commonly use are: Finite Element subsurface FLOW system - *FEFLOW*, Simulator for HEat and MAss Transport - *SHEMAT* and Modular Three-Dimensional Multispecies - *MT3DMS*.

As stated in Basar B. et al. [7], these fluid dynamics software systems have limited capability to integrate dynamic building/district simulation tools such as *EnergyPlus, TRNSYS* and *Modelica.* The paper [7] lists various models which can be used for ATES evaluation, including the description of one using a combination of *COMSOL* and *MATLAB* to facility the interconnection of building/district energy simulations. *COMSOL* is able to study and solve the ground-water flow problem, however this is not the aim of the following thesis work, which is limited specifically to the aquifer temperature calculation.

1.4 Aim of the thesis

The main goal of the following thesis is the development of a tool for the "early planning" of an ATES system.

ATES are, commonly, such highly complex system to plan, design and analyse they would benefit from a simple development tool. A big issue comes from the thermohydraulic simulation where fluid dynamics software are usually used (chapter 1.3.2) which are very accurate, but require large computing times and have low interoperability with energy tools.

In order to overcome this issue, the model written in *MATLAB*, should be able to calculate the water temperature in the aquifer in a simple way without pressure calculation after injection and extraction of groundwater. It should also determine how much water flow is required by the building/district, which depends on the energy demands calculated with the energy simulation performed in *EnergyPlus*.

Users should be able to add input parameters easily by loading the aquifer or system properties and its energy data in *Excel* files. The goal is to calculate the thermal performance of the ATES as accurately as possible with low computation effort, given the assumptions of calculation without hydraulic simulation of the aquifer. Furthermore, the model should also be flexible, so to be easily adaptable in case of necessity of adding or modifying data and equations about the aquifer or system choices.

2. Model description

The following chapter will describe the model with the assumptions and equations used to calculate the temperature inside the aquifer. The model was initially conceptualized in Elisa S. et al. [8]. In this thesis, the model has been further developed including additional features (e.g. leakage consideration), verified against other software tools, and fully validated with measured data.

2.1 General overview

Two wells were considered inside the aquifer. Both are represented as independent cylinders (figure 12) with height coinciding with the aquifer thickness. Initially the model has been studied and developed as a one-dimensional with heat conduction and advection along the "x" axis without the contribution of possible upper and lower layers.

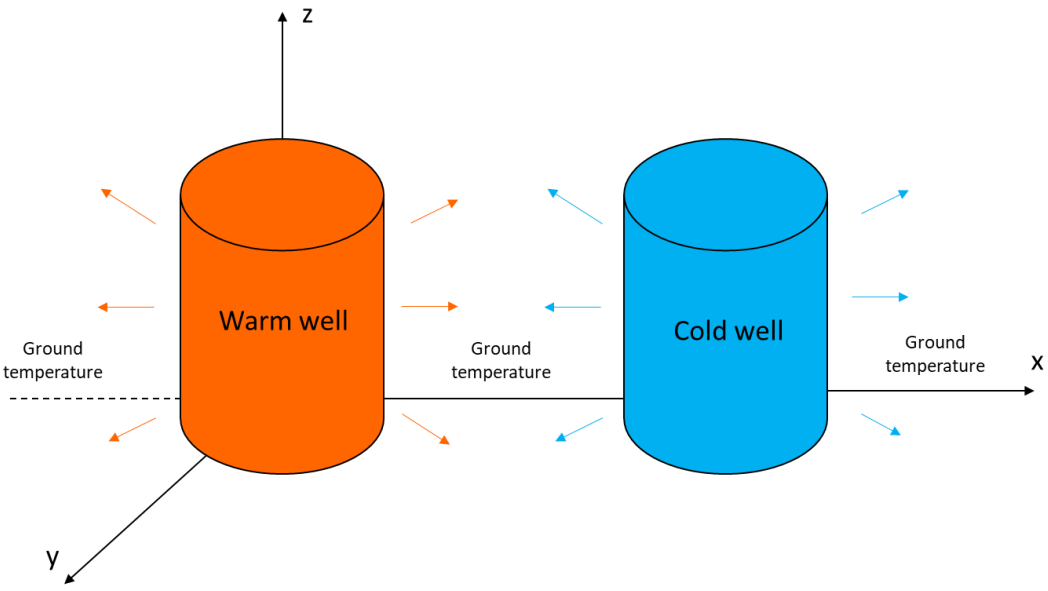

Figure 12: Wells representation

The main assumptions are:

- calculation of time and spatial variation of the temperature on the radial direction;

- axial symmetry for both wells;
- no water velocity inside the aquifer;
- constant temperature along the height of the wells;
- the discretization of the aquifer has been made with an increasingly extended concentric circular crown starting from the radius of the well this requires the maximum radius to be fixed to stop subdivision;
- the transient heat and mass equation in aquifer porous media has been solved with a finite-difference approach;
- to evaluate the behaviour of the aquifer, a simple lumped-parameter system, similar to an electrical network, was used where in each active node has its own thermal resistance and capacitance.

2.2 Finite difference method for heat conduction

The Finite Difference Methods (FDM) are numerical techniques used to solve differential equations through the approximation of the derivatives.

In the FDM, derivatives are replaced by differences as an example below:

$$\frac{df(x)}{dx} \approx \frac{f(x+\Delta x)-f(x)}{\Delta x} = \lim_{\Delta x \to 0} \frac{\Delta f(x)}{\Delta x}$$

Quite accurate results can be obtained by making small changes to the differential quantities.

FDMs can be used to solve heat conduction problems. Considering the one-dimensional heat conduction equation without internal energy generation, where the parameter α is called thermal diffusivity:

$$\frac{\partial T}{\partial \tau} - \alpha \cdot \frac{\partial^2 T}{\partial x^2} = 0, \qquad \alpha = \frac{\lambda}{\rho c_p} \left[\frac{m^2}{s}\right]$$

For a time instant p (time) and generic node i (space) the derivates are approximated, in explicit time stepping method, as follows:

$$\left.\frac{\partial T}{\partial \tau}\right|_{i,\ p+\frac{1}{2}} \simeq \frac{T_{i,p+1} - T_{i,p}}{\Delta\tau};\ \left.\frac{\partial T}{\partial x}\right|_{i+\frac{1}{2},\ p} \simeq \frac{T_{i+1,p} - T_{i,p}}{\Delta x}$$

$$\left.\frac{\partial^2 T}{\partial x^2}\right|_{i,p} \simeq \frac{\left.\frac{\partial T}{\partial x}\right|_{i+\frac{1}{2},\ p} - \left.\frac{\partial T}{\partial x}\right|_{i-\frac{1}{2},\ p}}{\Delta x} \simeq \frac{T_{i-1,p} - 2T_{i,p} + T_{i+1,p}}{\Delta x^2}$$

Or as alternative, in implicit time stepping method:

$$\left.\frac{\partial^2 T}{\partial x^2}\right|_{i,p+1} \simeq \frac{T_{i-1,p+1} - 2T_{i,p+1} + T_{i+1,p+1}}{\Delta x^2}$$

The implicit method, used in the model, differs from the explicit method because the spatial derivates are calculated in the new time step. This method is slower and it requires the linear system to be solved at each time step to calculate the temperature at p+1 instant.

By substituting the implicit solution into the heat conduction equation, we obtain

$$\frac{T_{i,p+1} - T_{i,p}}{\Delta\tau} - \alpha \cdot \frac{T_{i-1,p+1} - 2T_{i,p+1} + T_{i+1,p+1}}{\Delta x^2} = 0$$

That is equal to:

$$\frac{T_{i-1}^{p+1} - T_i^{p+1}}{R_{i,i-1}} + \frac{T_{i+1}^{p+1} - T_i^{p+1}}{R_{i,i+1}} = C_i\left(\frac{T_i^{p+1} - T_i^{p}}{\Delta\tau}\right)$$

Where R and C are respectively the thermal resistance and capacitance.

2.3 Porous medium

An important assumption has been made for considering the real behaviour of the aquifer.

In aquifers water flows in a porous medium made of sandy/rock material which influences the heat transfer. The parameter φ, which is the porosity, indicates in percentage how much empty space there is inside the aquifer where water can flow. As the porosity increases more water flows and is able to hold heat. It determines the thermal capacity of a volume of aquifer.

According to these equation, from Basar B. et al. [7], the effective volumetric heat capacity and thermal conductivity of the aquifer, are function of the porosity:

$$C_{s,aq} = \left(\rho c_p\right)_{aq} = \left(\rho c_p\right)_{water} \cdot \Phi + \left(\rho c_p\right)_{sand} \cdot (1 - \Phi)$$

$$\lambda_{aq} = \lambda_{water} \cdot \Phi + \lambda_{sand} \cdot (1 - \Phi)$$

2.4 Lumped discretization

In figure 13, an example of the lumped discretization for a 3 node system is shown, which are defined "active" and have an associated lumped thermal resistance *R* and thermal capacitance *C*.

Nodes *0* and *Tg*, instead, represent respectively the well radius, where R_{10} is the bore thermal resistance, and the undisturbed ground at ground temperature.

About the active nodes, the parameters are placed into the barycentric medium radius of the considered crown.

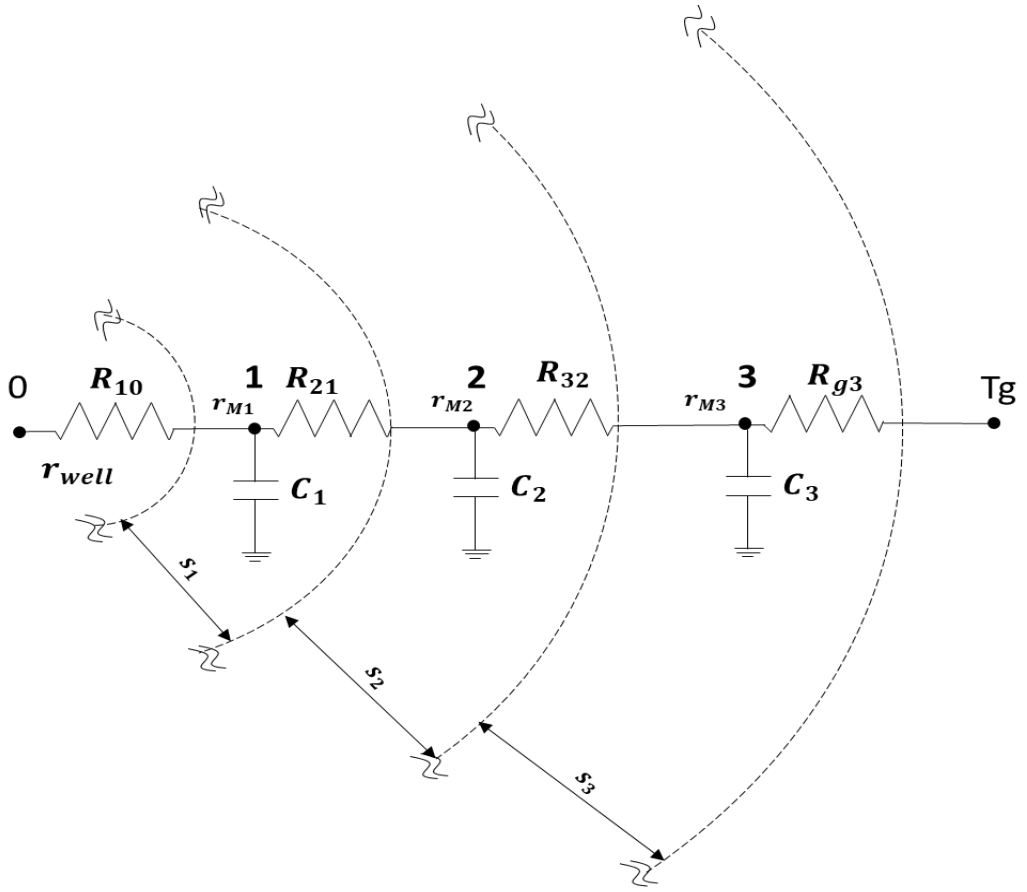

Figure 13: 3-node lumped system example

Each annulus is spaced according to an expansion coefficient (c_{exp}), an arbitrary value between 1.1 and 1.2, required at the simulation starting together with the maximum radius where the subdivision ends. This number is used to increase the thickness *s* of the annulus staring from the bore as it is shown in the following example for the first active node:

$$s_1 = c_{exp} \cdot r_{well}$$

$$r_{ext,1} = r_{well} + s_1$$

$$r_{M1} = \sqrt{\frac{r_{ext,1}^2 + r_{well}^2}{2}}$$

Then, for the generic *i* node:

$$s_i = \left(c_{exp}\right)^i \cdot r_{well}$$

$$r_{ext,i} = r_{internal} + s_i$$

$$r_{Mi} = \sqrt{\frac{r_{ext,i}^2 + r_{int,i}^2}{2}}$$

The lumped parameters for *i* node have been calculated in analytical way:

Radial Thermal Resistance of the cylindrical layer:

$$R_{i,i-1} = \frac{\log\left(\frac{r_{Mi}}{r_{Mi-1}}\right)}{2\pi \cdot \lambda_{aq} \cdot h} \left[\frac{K}{W}\right]$$

Thermal Capacitance:

$$C_i = C_{aq} \cdot Vol_i \left[\frac{J}{K}\right]$$

For each active node, they are reported the energy balance equation considering only the heat conduction as the final equation shown in chapter 2.2.

Node 1:

$$\frac{T_0^p - T_1^p}{R_{10}} + \frac{T_2^p - T_1^p}{R_{21}} = C_1\left(\frac{T_1^p - T_1^{p-1}}{\Delta\tau}\right)$$

Node 2:

$$\frac{T_1^p - T_2^p}{R_{21}} + \frac{T_3^p - T_2^p}{R_{32}} = C_2\left(\frac{T_2^p - T_2^{p-1}}{\Delta\tau}\right)$$

Node 3:

$$\frac{T_g^p - T_3^p}{R_{g3}} + \frac{T_2^p - T_3^p}{R_{32}} = C_3\left(\frac{T_3^p - T_3^{p-1}}{\Delta\tau}\right)$$

The left side of the equation represents the contribution of heat conduction, the right side the contribution of storage heat expressed through the thermal capacitance.

The superscripts in the temperature indicate the time dependence, because the approach to the finite-difference restricts temperature to discrete points as the

nodes in space and also time. Therefore, a time step is required, $\Delta\tau$, set at the start of the simulation, which separates the successive calculations.

The calculation starts at time ”p-1”, with input known temperature “p-1” to find temperature at current time “p” .

2.5 One-dimensional model

For the sake of simplicity, a one-dimensional model is presented with heat conduction and advection. In an ATES system there are three distinct phases: injection, storage and withdrawal of groundwater.

During injection, water, coming from the building/district plant, goes to the bore grout in the warm/cold well depending on cooling/heating mode, while during the withdrawal phase, water is extracted from the opposite well and sent to the plant. In the storage period, there is no flow of water and the aquifer temperature is only influenced by conduction between annulus and ground.

2.5.1 Injection and storage equations

Figure 14 shows the equations, during the injection phase, where the contribution on the left side of the volumetric flow takes into account the advection.

For storage, the equations are the same, but without water flow.

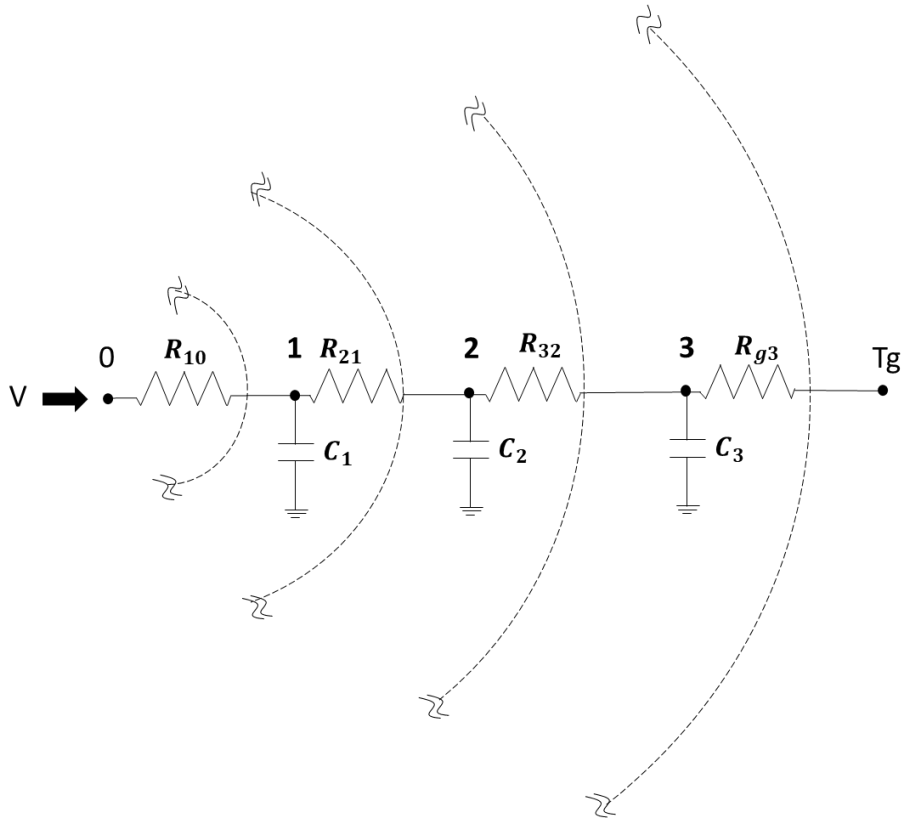

Figure 14: 3-node system during injection

Node 1:

$$\frac{T_0^p - T_1^p}{R_{10}} + \frac{T_2^p - T_1^p}{R_{21}} + \rho c_p V(T_0^p - T_1^p) = C_1\left(\frac{T_1^p - T_1^{p-1}}{\Delta\tau}\right)$$

Node 2:

$$\frac{T_1^p - T_2^p}{R_{21}} + \frac{T_3^p - T_2^p}{R_{32}} + \rho c_p V(T_1^p - T_2^p) = C_2\left(\frac{T_2^p - T_2^{p-1}}{\Delta\tau}\right)$$

Node 3:

$$\frac{T_g^p - T_3^p}{R_{g3}} + \frac{T_2^p - T_3^p}{R_{32}} + \rho c_p V\left(T_2^p - T_3^p\right) = C_3\left(\frac{T_3^p - T_3^{p-1}}{\Delta\tau}\right)$$

The equations are inserted, in *MATLAB,* in the following linear matrix system:

$$\begin{Bmatrix} -\frac{1}{R_{10}} - \frac{C_1}{\Delta\tau} - \frac{1}{R_{21}} - \rho c_p V; & \frac{1}{R_{21}}; 0 \\ \frac{1}{R_{21}} + \rho c_p V; & -\frac{1}{R_{21}} - \frac{1}{R_{32}} - \frac{C_2}{\Delta\tau} - \rho c_p V; & \frac{1}{R_{32}} \\ 0; & \frac{1}{R_{32}} + \rho c_p V; & -\frac{1}{R_{g3}} - \frac{1}{R_{32}} - \frac{C_3}{\Delta\tau} - \rho c_p V \end{Bmatrix} x \begin{Bmatrix} T_1^p \\ T_2^p \\ T_3^p \end{Bmatrix} = \begin{Bmatrix} \frac{-T_0}{R_{10}} - \frac{C_1 T_1^{p-1}}{\Delta\tau} - \rho c_p T_0 V \\ \frac{-C_2 T_2^{p-1}}{\Delta\tau} \\ \frac{-T_g}{R_{g3}} + \frac{-C_3 T_3^{p-1}}{\Delta\tau} \end{Bmatrix}$$

Where the solution is the temperature vector at time "p".

2.5.2 Withdrawal equation

In the extraction phase (figure 15), the system works in reverse to the injection phase with water flow coming from the other direction. In this case, the extracted temperature "T_0" is unknown then it was necessary to add an extra equation (node 0).

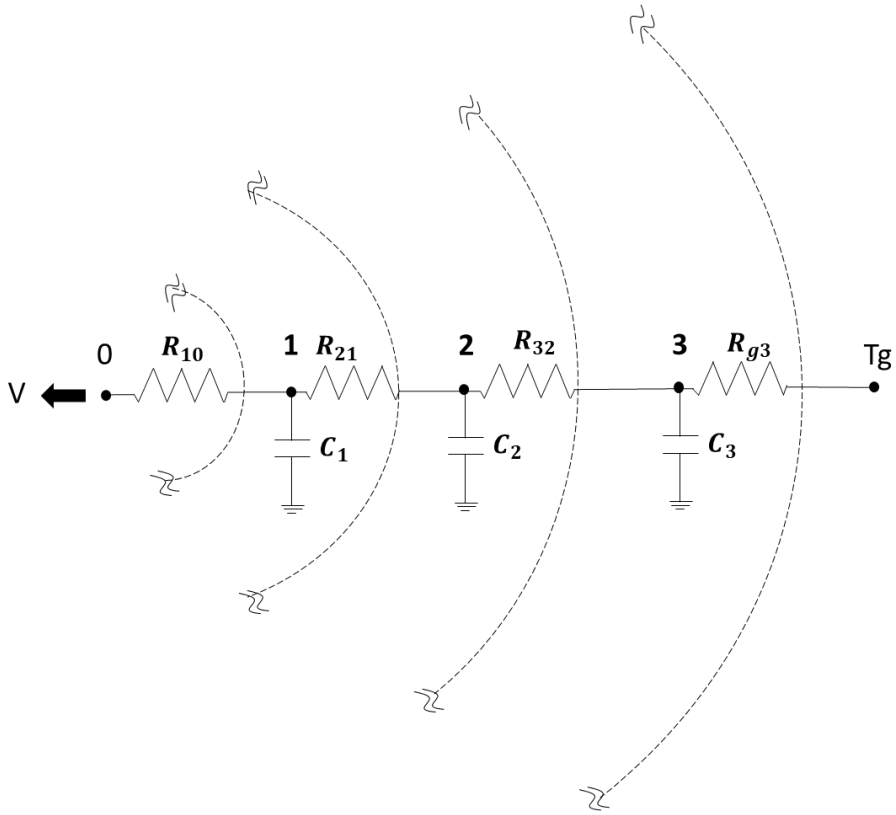

Figure 15: 3-node system during withdrawal

Node 0:

$$\frac{T_1^p - T_0^p}{R_{10}} + \rho c_p V(T_1^p - T_0^p) = 0$$

Node 1:

$$\frac{T_0^p - T_1^p}{R_{10}} + \frac{T_2^p - T_1^p}{R_{21}} + \rho c_p V(T_2^p - T_1^p) = C_1\left(\frac{T_1^p - T_1^{p-1}}{\Delta\tau}\right)$$

Node 2:

$$\frac{T_1^p - T_2^p}{R_{21}} + \frac{T_3^p - T_2^p}{R_{32}} + \rho c_p V(T_3^p - T_2^p) = C_2\left(\frac{T_2^p - T_2^{p-1}}{\Delta\tau}\right)$$

Node 3:

$$\frac{T_g^p - T_3^p}{R_{g3}} + \frac{T_2^p - T_3^p}{R_{32}} + \rho c_p V(T_g - T_3^p) = C_3\left(\frac{T_3^p - T_3^{p-1}}{\Delta\tau}\right)$$

Linear matrix system:

$$\begin{Bmatrix} -\frac{1}{R_{10}} - \rho c_p V; \frac{1}{R_{10}} + \rho c_p V; 0; 0 \\ \frac{1}{R_{10}}; -\frac{1}{R_{10}} - \frac{1}{R_{21}} - \rho c_p V - \frac{C_1}{\Delta\tau}; \frac{1}{R_{21}} + \rho c_p V; 0 \\ 0; \frac{1}{R_{21}}; -\frac{1}{R_{21}} - \frac{1}{R_{32}} - \frac{C_2}{\Delta\tau} - \rho c_p V; \frac{1}{R_{32}} + \rho c_p V \\ 0; 0; \frac{1}{R_{32}}; -\frac{1}{R_{g3}} - \frac{1}{R_{32}} - \frac{C_3}{\Delta\tau} - \rho c_p V \end{Bmatrix} x \begin{Bmatrix} T_0^p \\ T_1^p \\ T_2^p \\ T_3^p \end{Bmatrix} = \begin{Bmatrix} 0 \\ \frac{-C_1 T_1^{p-1}}{\Delta\tau} \\ \frac{-C_2 T_2^{p-1}}{\Delta\tau} \\ \frac{-T_g}{R_{g3}} + \frac{-C_3 T_3^{p-1}}{\Delta\tau} - \rho c_p T_g V \end{Bmatrix}$$

2.6 Two-dimensional model

In order to improve the model, upper and lower layers of the ground have been added. To keep the model simple enough, both for upper and lower layers, two nodes with axial thermal resistance and thermal capacitance associated have been inserted to account for heat conduction along the vertical axis.

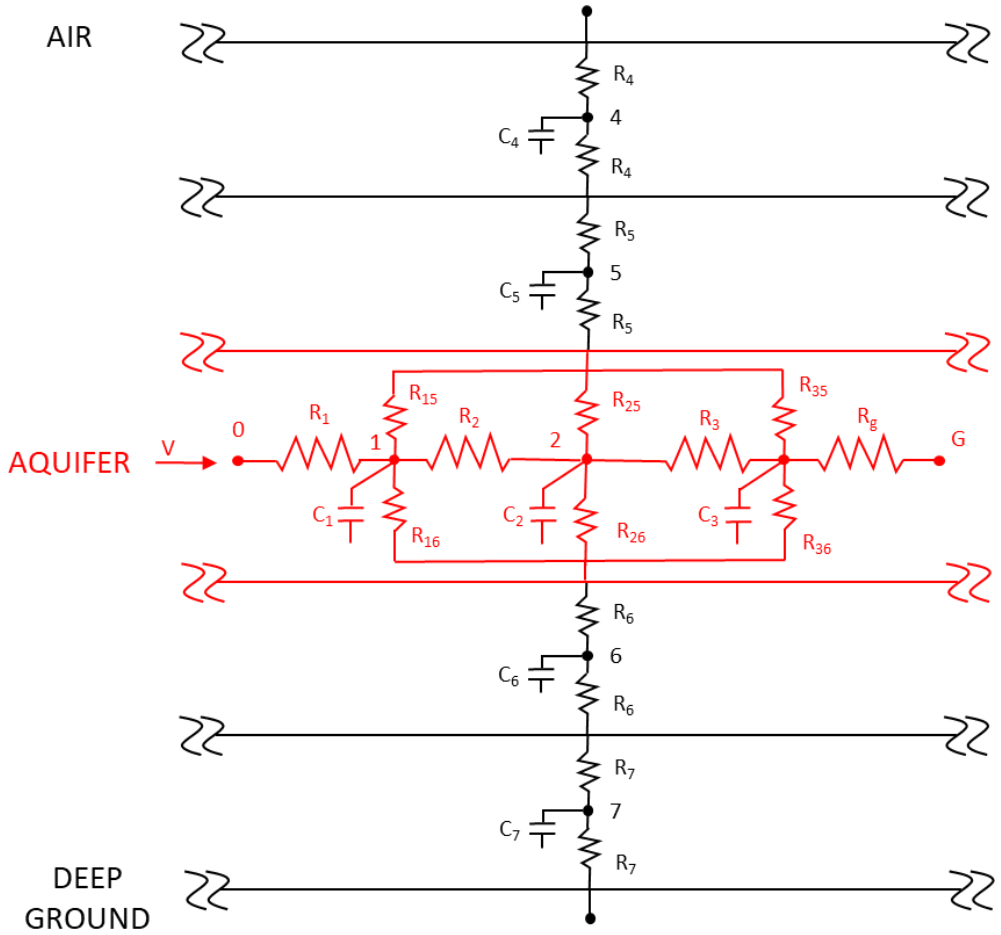

Figure 16: final 2D discretized ground, injection phase

The new discretization also takes into account the outside air temperature, as a boundary condition, although it does not have much influence on aquifer temperature. The other boundary condition is the deep ground.

The thermal resistances for the ground layers (in above figure 16, nodes 4, 5, 6, 7) have been calculated:

$$R_i = \frac{h_i}{2\lambda_i \cdot (\pi r_{max}^2)} \left[\frac{K}{W}\right]$$

While the axial thermal resistances for the aquifer are:

$$R_{i,ax} = \frac{h_{aq}}{\lambda_{aq} \cdot (2\pi(r_{ext}^2 - r_{ext-1}^2)} \left[\frac{K}{W}\right]$$

With reference to the above mentioned figure 16, starting from the upper node, the new thermal balance equation in each node is listed, as an example during the injection/storage phase:

Node 4:

$$\frac{T_{air}^{p} - T_{4}^{p}}{R_4} + \frac{T_{5}^{p} - T_{4}^{p}}{R_4 + R_5} = C_4 \left(\frac{T_{4}^{p} - T_{4}^{p-1}}{\Delta\tau} \right)$$

Node 5:

$$\frac{T_{5}^{p} - T_{4}^{p}}{R_4 + R_5} + \frac{T_{1}^{p} - T_{5}^{p}}{R_{15} + R_5} + \frac{T_{2}^{p} - T_{5}^{p}}{R_{25} + R_5} + \frac{T_{3}^{p} - T_{5}^{p}}{R_{35} + R_5} = C_5 \left(\frac{T_{5}^{p} - T_{5}^{p-1}}{\Delta\tau} \right)$$

Node 1:

$$\frac{T_{0}^{p} - T_{1}^{p}}{R_1} + \frac{T_{2}^{p} - T_{1}^{p}}{R_2} + \rho c_p V \left(T_{0}^{p} - T_{1}^{p} \right) + \frac{T_{5}^{p} - T_{1}^{p}}{R_{15} + R_5} + \frac{T_{6}^{p} - T_{1}^{p}}{R_{16} + R_6} = C_1 \left(\frac{T_{1}^{p} - T_{1}^{p-1}}{\Delta\tau} \right)$$

Node 2:

$$\frac{T_{1}^{p} - T_{2}^{p}}{R_2} + \frac{T_{3}^{p} - T_{2}^{p}}{R_3} + \rho c_p V \left(T_{1}^{p} - T_{2}^{p} \right) + \frac{T_{5}^{p} - T_{2}^{p}}{R_{25} + R_5} + \frac{T_{6}^{p} - T_{2}^{p}}{R_{26} + R_6} = C_2 \left(\frac{T_{2}^{p} - T_{2}^{p-1}}{\Delta\tau} \right)$$

Node 3:

$$\frac{T_{2}^{p} - T_{3}^{p}}{R_2} + \frac{T_{g}^{p} - T_{3}^{p}}{R_3} + \rho c_p V \left(T_{2}^{p} - T_{3}^{p} \right) + \frac{T_{5}^{p} - T_{3}^{p}}{R_{35} + R_5} + \frac{T_{6}^{p} - T_{3}^{p}}{R_{36} + R_6} = C_3 \left(\frac{T_{3}^{p} - T_{3}^{p-1}}{\Delta\tau} \right)$$

Node 6:

$$\frac{T_{7}^{p} - T_{6}^{p}}{R_6 + R_7} + \frac{T_{1}^{p} - T_{6}^{p}}{R_{16} + R_6} + \frac{T_{2}^{p} - T_{6}^{p}}{R_{26} + R_6} + \frac{T_{3}^{p} - T_{6}^{p}}{R_{36} + R_6} = C_6 \left(\frac{T_{6}^{p} - T_{6}^{p-1}}{\Delta\tau} \right)$$

Node 7:

$$\frac{T_{g}^{p} - T_{7}^{p}}{R_7} + \frac{T_{6}^{p} - T_{7}^{p}}{R_7 + R_6} = C_7 \left(\frac{T_{7}^{p} - T_{7}^{p-1}}{\Delta\tau} \right)$$

So, for the node 1, 2 and 3 of the aquifer, there is the contribution of conduction due to upper layers (node 5) and lower (node 6).

For the withdrawal phase, there will be an additional equation relative to node 0 (chapter 2.5.2).

The bidimensional model achieves better results, as it shown in paper [8], validated with data from Carotenuto A. et al. [9], where an experimental groundwater well has been built in order to measure the real temperatures after periods of injection, storage and withdrawal.

2.7 Water leakages

In the model, groundwater leakages within the domain which influence the heat transfer process and therefore the overall result have been analyzed.

Usually, all aquifers are surrounded by impermeable layers of clay which limit water losses outside the domain. However, in considering the hypothesis of constant temperature along the aquifer thickness, resulting in no thermal stratification, it may be interesting to consider that a part of the water flow injected or extracted is not involved in the heat transfer process. Since the model proposed does not require fluid dynamics simulation, it is hard to study the accurate behaviour of water losses.

As it is shown in figure 17, in the node 0 which corresponds to the well, the volumetric flow has been set as required one for the ATES/building system, but in the further nodes (the circular crowns), during the injection phase, the water flow is lower reaching the minimum in the last node of the domain. In contrast, during the withdrawal phase, from the last node the flows reach their maximum level, reducing as it gets closer to the well node, where the flow is request one.

So summarizing, with *Vol* the volume of the aquifer annulus, the flow in the generic i are: for injection $V_i = V \cdot (1 - l) \cdot Vol_i$, while for withdrawal $V_i = V \cdot (1 + l) \cdot Vol_i$

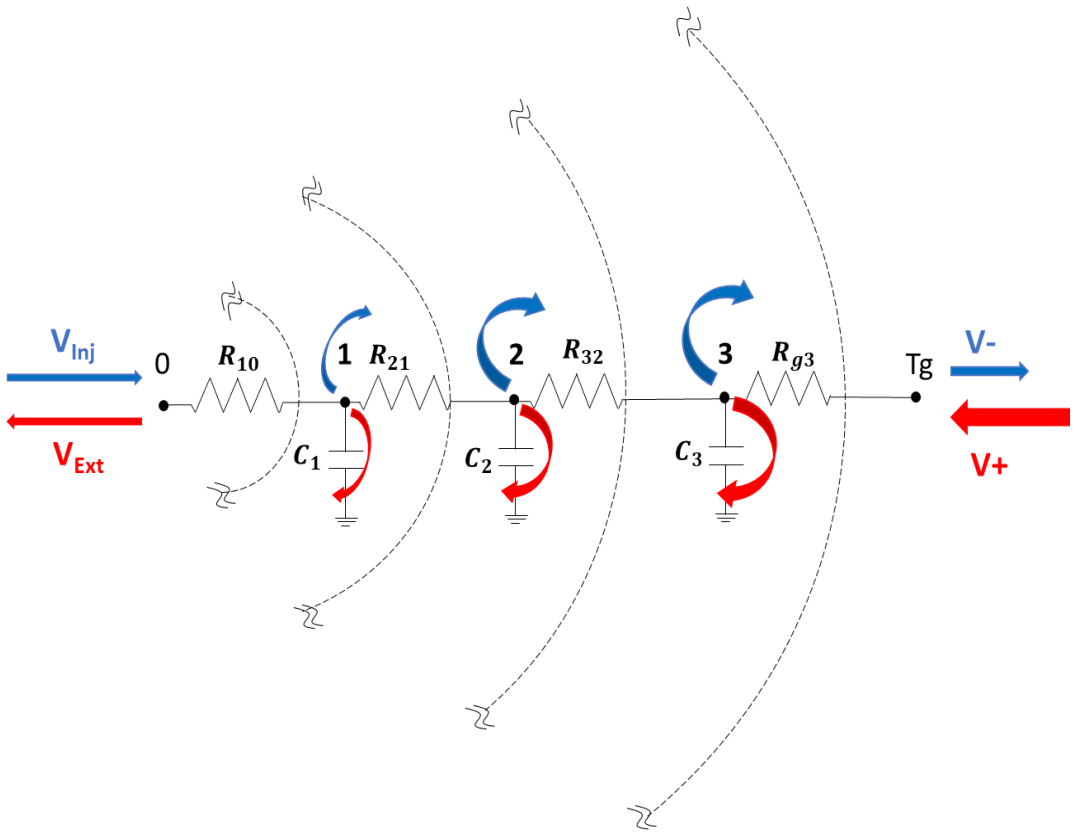

Figure 17: Example of the leakages for a 3 node system

3. Model validations

After completing the model for the aquifer, two validations have been conducted, the first with the research paper Julian E. et al. [10] from the journal *Geothermics* while the second from real data from an ATES system.

3.1 Validation with *Geothermics*

Paper [10] is a benchmark study for thermo-hydraulic modelling simulations of low enthalpy geothermal process for high temperature ATES. Each simulators[7], with different licensing and characteristics, have been tested in four synthetic cases in order to create a comparative test suit:

- Case 1, transient pressure validation.
  It has been simulated the injection of water in a testing well idealized as a reservoir with homogenous properties into a cylinder with radial and cartesian meshing, focused on analyse of the pressure response;
- Case 2, injection-falloff-drawdown-build up well test.
  The testing well has been simulated during all the three phase of injection, storage and withdrawal;
- Case 3, experimental heat transport validation test.
  This case is aimed at studying the unidimensional, unsteady heat and mass transport in the aquifer porous media, focus on the evolution of the thermal front.
- Case 4, *Horton-Rogers-Lapwood* problem.
  It has been modelled the natural convection into porous mediums.

The results from case 2 were chosen for the validation of this work. It has been analysed with three different scenarios, called variants; the first one, chosen for

[7] For information on simulators, check report [11].

the comparison, defines the aquifer as a homogenous cylinder (figure 18) with radial mesh.

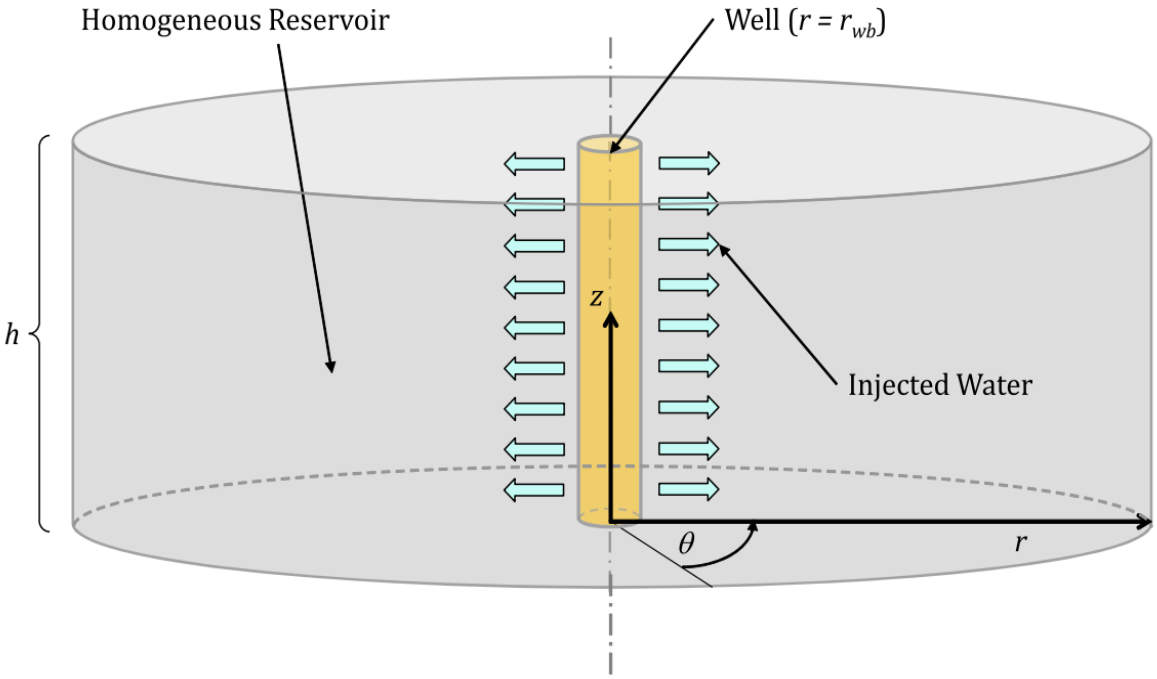

Figure 18: Homogeneous aquifer model

The other two variants, not analysed in this work, introduce respectively a region of higher uniform rock permeability and porosity around the well and a fracture zone at a specific distance from the well which change the material properties.

In the homogenous variant, buoyancy effects have been neglected, while the top and bottom boundary have been set to adiabatic and no flow. Practically, the data has been compared with the result of a one-dimensional simulation (chapter 2.5)

The input properties used in the *MATLAB* code are reported in table 1.

Rock properties have been combined with water in order to use "effective" properties as already explained on chapter 2.3.

Parameter	Value
Water density ϱ_w	994.75 kg/m^3
Water specific heat c_{pw}	4186 J/kgK
Water[8] thermal conductivity λ_w	0.6 W/mK
Rock density ϱ_r	2680 kg/m^3
Rock specific heat c_{pr}	833 J/kgK
Rock thermal conductivity λ_r	2.8 W/mK
Aquifer thickness h	200 m
Well radius r_{wb}	0.1 m
Porosity φ	20%
Ground/Initial temperature T_g	34°C
Time step Δt	3600 s
Domain radius r_{max}	2400 m

Table 1: Geothermics properties for validation

The well has been simulated for one year with the following water flow and temperature in the following order:

- **Injection:** water is pumped at 0.001 m^3/s at 120 °C for 120 days (2880 hours);
- **Storage** ("falloff phase"): no water flow for 60 days (1440 hours);
- **Withdrawal** ("drawdown"): water is extracted with 0.001 m^3/s of flow rate for 120 days (2880 hours);
- **Storage** ("build-up phase"): no flow for 65.25 days (1566 hours);

[8] In paper [9] simulations, fluid properties are calculated as function of pressure and temperature, because in a high temperature ATES, temperature range is about 25°C-90°C. For the comparison they have been chosen constants values as the difference is not that relevant.

As the *Geothermics* paper does not provide any information about water leakages, they have been neglected for the *MATLAB* simulation.

The data carried on with thermo-hydraulic simulators and the comparison with the result of the model simulations are illustrated below.

In the *Geothermics* results (figure 19), only the temperature values corresponding to 0, 50, 100, 150, 200, 250, 310 and 365.25 days are reported; for this reason, the model results are presented both with their own time steps (3600 s) and only with the previous days highlighted.

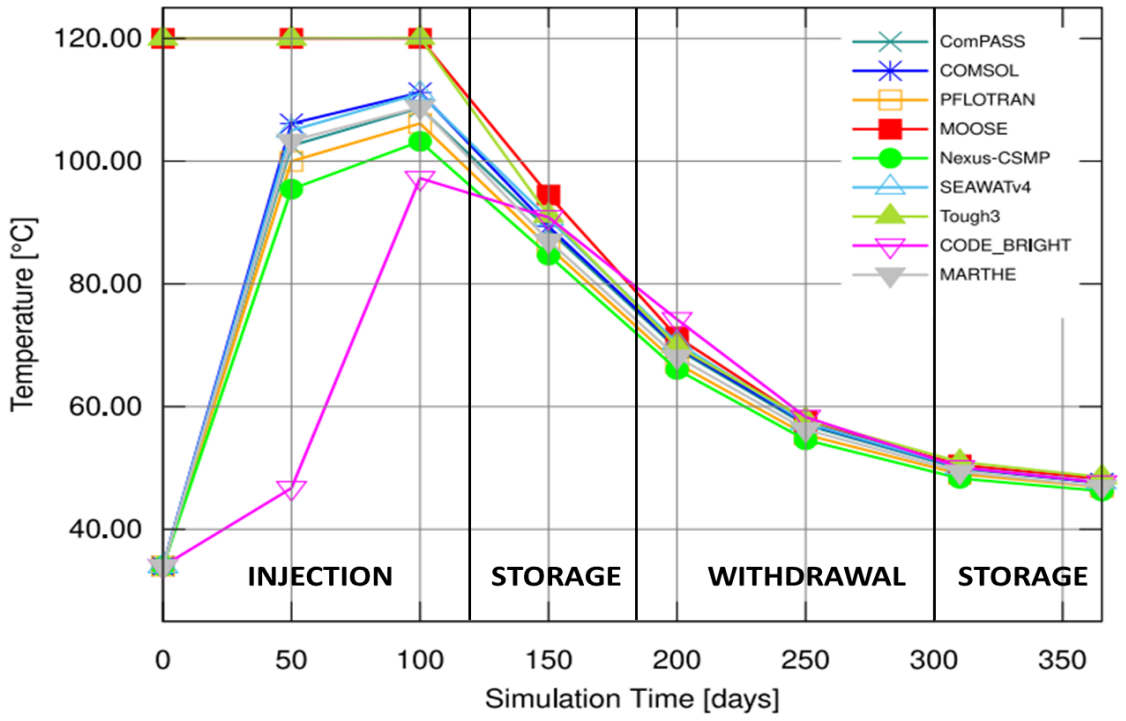

Figure 19: Simulators results, distance 1m from the well

As stated in [10], the discrepancy between the initial value for *Tough3*, *MOOSE* and the other simulators is due to the different injection condition. These simulators do not use an enthalpy source-type or rare-type condition but they use a Dirichlet boundary condition for temperature; this is evident from the fixed

nature of the temperature evolution for the first 120 days, the injection period. *CODE_BRIGHT* presents a considerable time delay not specified in the paper.

For comparison, it has been chosen to simulate the model for different expansion coefficient, which determines the mesh and the number of active nodes in aquifer and they have been taken the result of *SEAWATv4*, because it uses a finite difference method for space discretization, that is the same as the model and the results are average for all the others.

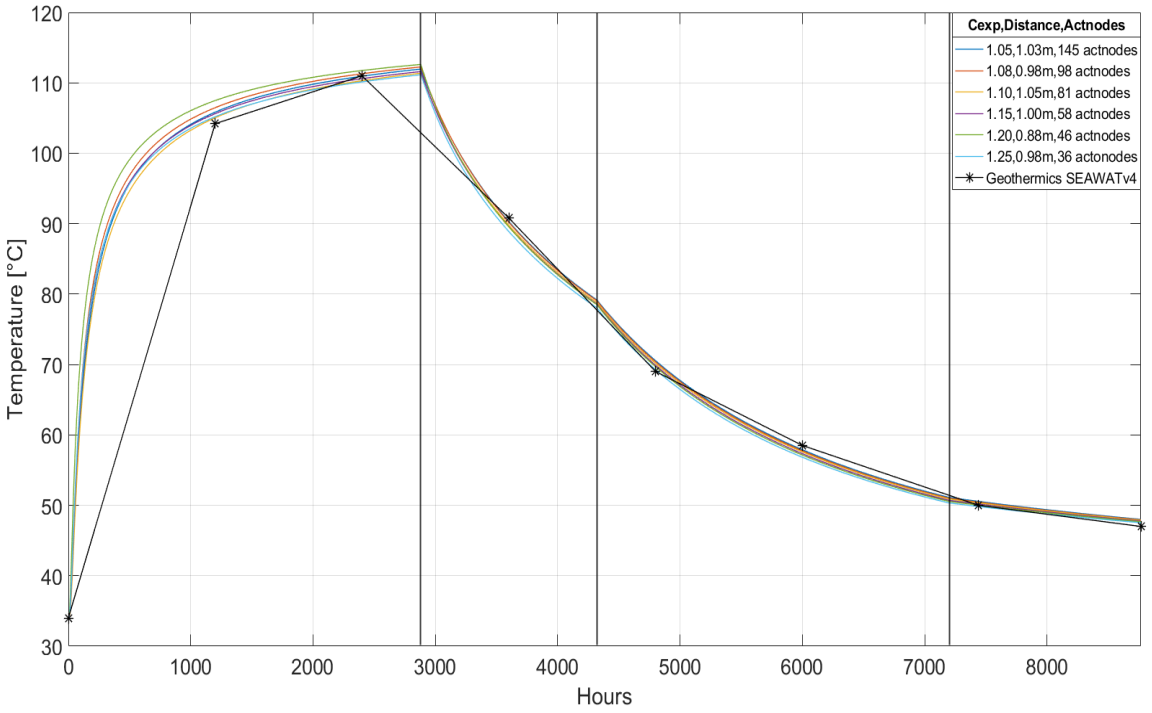

Figure 20: Comparison Geothermics/Model, at distance 1m from the well

As shown in figure 20 and 21, the data from *SEAWATv4* (black line) is in good agreement with the results obtained from the model. The model results represent the aquifer temperature at the node closer to 1m from the well.

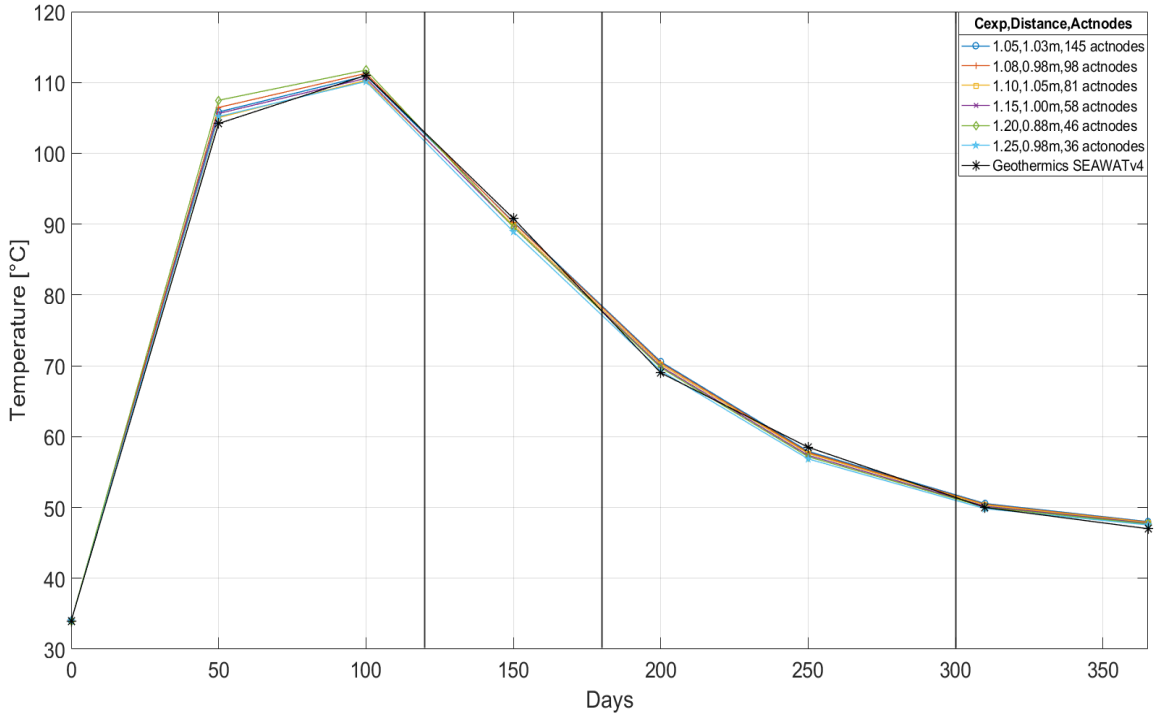

Figure 21: Comparison Geothermics/Model, at distance 1m from the well, only 50, 100, 150, 200, 250, 310, 365.25 days

The results at 10m from the well are also reported (figure 22).

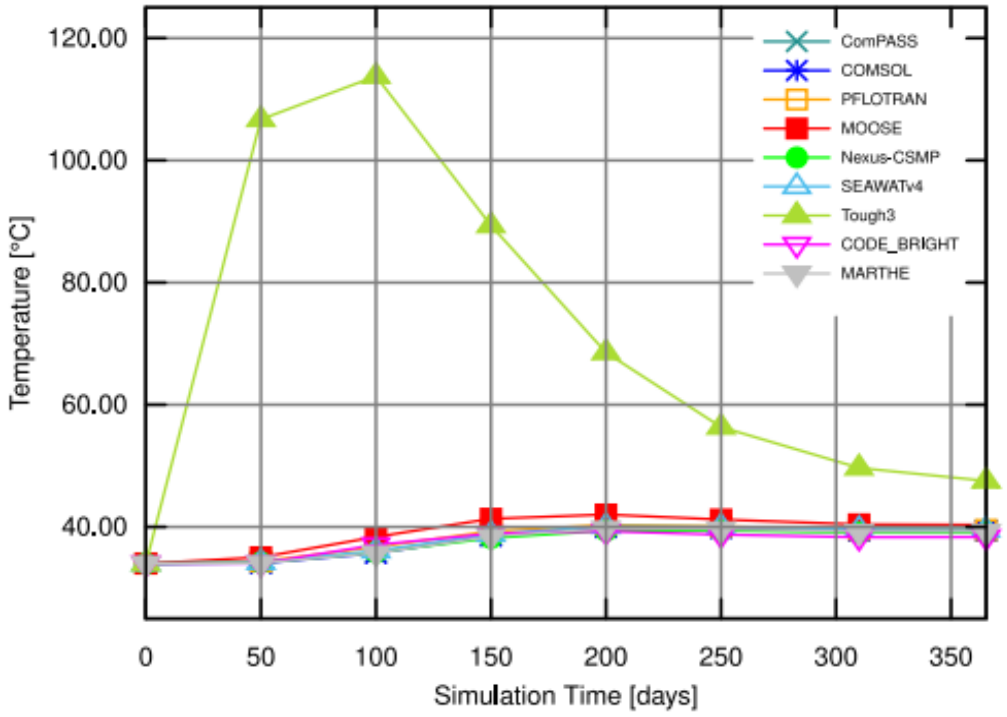

Figure 22: Geothermics results at 10m from the well

In figure 23, it is reported the comparison between *Geothermics* and the model.

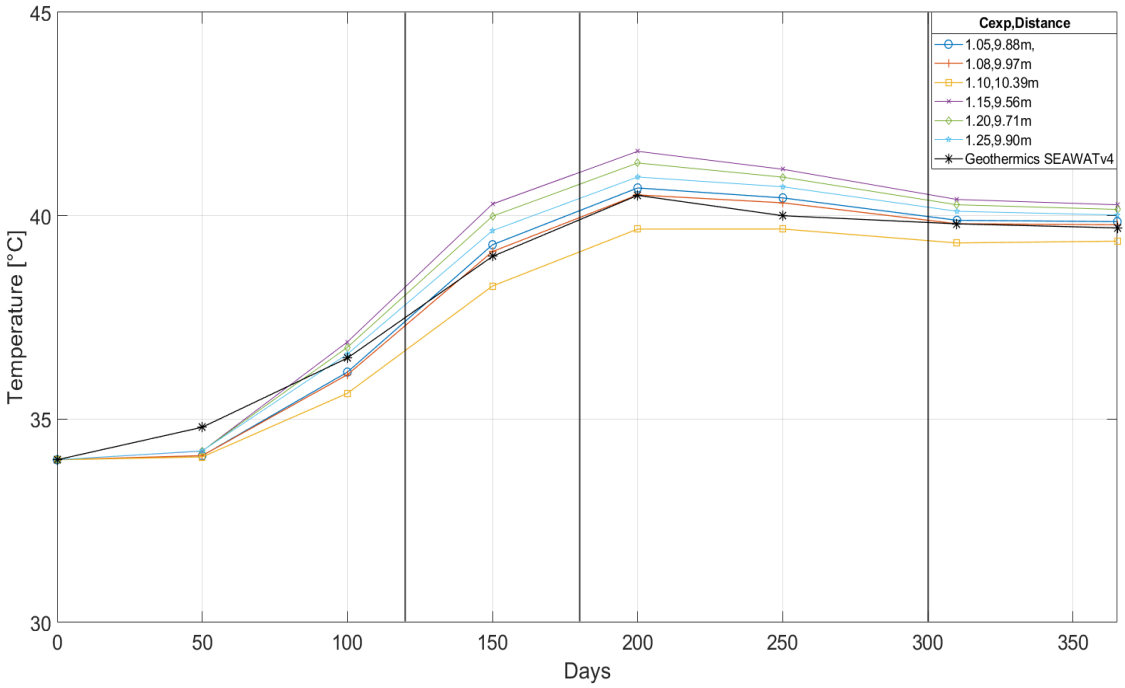

Figure 23: Comparison Geothermics/Model, at distance 10m from the well

Possible errors could be due to the inaccuracy of the well distance. The model is not able to calculate the result precisely at a fixed distance from the aquifer because it depends on the number of nodes and expansion coefficient. For this reason, the result for C_{exp} equal to 1.1, the yellow curve, appears lower because the closer node to 10 m is at 10.39 m.

3.2 Validation with Delft ATES data

This paragraph introduces a validation of the model with measured data obtained from an ATES system located in Delft, Netherlands. Unlike the previous one, in this validation there is the analysis of two wells of the aquifer thermal energy storage, the warm well and the cold one. The periods of injection and withdrawal are not separated, but one contemporary to the other. During the cooling mode, there is a withdrawal from the cold well but, at the same time, the

injection into the warm well, also; vice versa for the heating mode. The storage periods represent the ATES shutdown where the building does not demand energy.

In the plant there are respectively a heat pump with a peak boiler for heating and a heat exchanger for cooling. The well are about 150 m apart with a radius of about 500 mm.

Prof. Martin Bloemendal of the University of Technology of Delft has given his contribution for this work, allowing the use the measurements and information of the plant.

As shown in figure 24, the ATES has a sandy aquifer with 30 m in thickness surrounded by two 40 m layers of impermeable clay.

Figure 24: Delft ATES representation

In table 2, ground and layer properties used are recorded.

Parameter	Value
Aquifer	
Water density ϱ_w	1000 kg/m^3
Water specific heat c_{pw}	4186 J/kgK
Water thermal conductivity λ_w	0.5 W/mK
Sand density ϱ_r	1300 kg/m^3
Sand specific heat c_{ps}	833 J/kgK
Sand thermal conductivity λ_s	2.8 W/mK
Aquifer thickness h	30 m
Well radius r_{wb}	0.5 m
Porosity φ	30%
Undisturbed ground temperature T_g	11.5°C
Initial well temperature[9]	8.9 °C (cold well), 13.7 °C (warm well)
Ground Layers	
Clay volumetric specific heat	2.3x10^6 J/ m^{3}K
Clay thermal conductivity	0.8 W/mK
Layers thickness	40 m

Table 2: Delft simulation properties

While the model discretization properties are:

Parameter	Value
Time step	480 s
Maximum domain radius	180 m
Expansion coefficient	1.1

Table 3: Delft simulation discretization properties

[9] Corresponding to the first timestep temperature.

The time step has been chosen since all the ATES measurement, for 2 years, have been taken every 8 minutes, 480 seconds.

For the simulation, a leakage coefficient has been considered, as the one presented in chapter 2.7, equal to 2.5×10^{-7} m^3_w/m^3_{aq} which corresponds to 16% of losses of water flow in the last node for the injection phase (for the withdrawal phase, in the last node there is an increase of 16%).

In addition to water volumetric flow measurements (figure 25), positive in case of cooling and negative for heating, the warm and cold well temperatures (figure 26) have been provided.

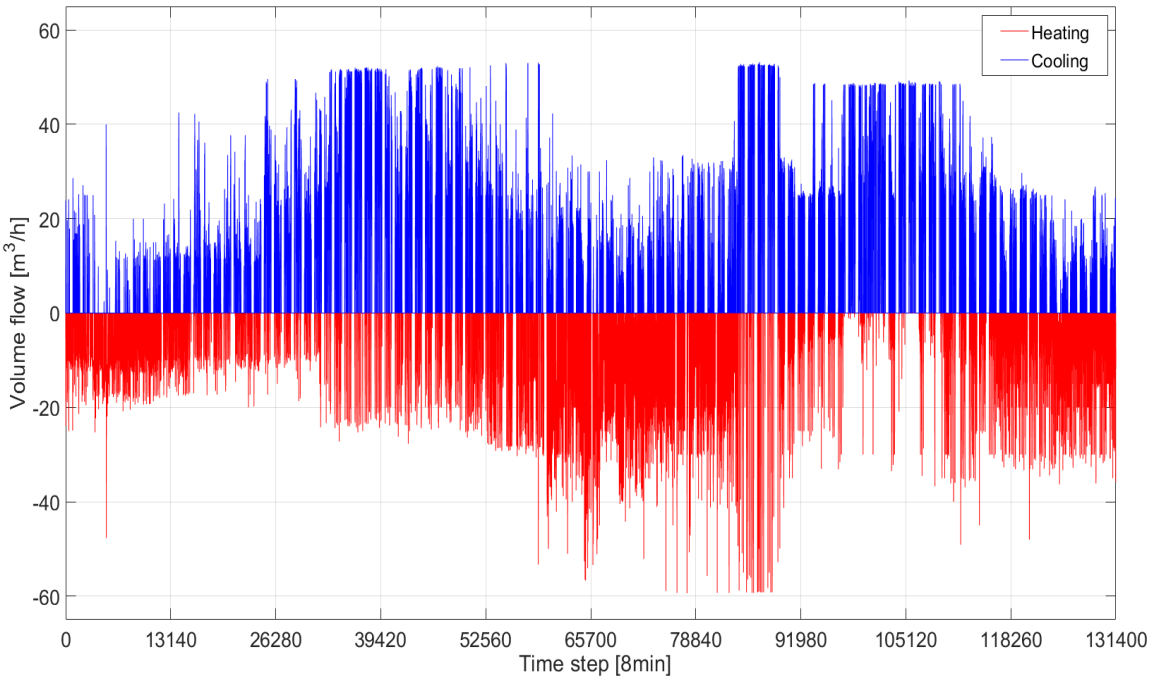

Figure 25: Water flow during 2 years, 131400 time steps

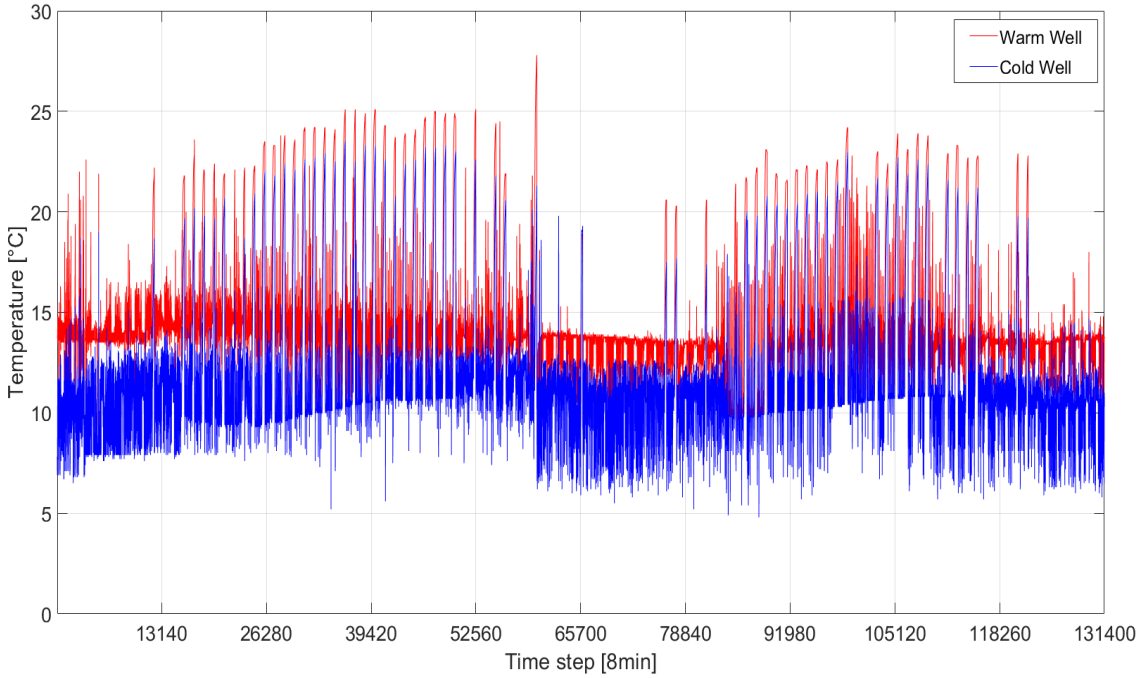

Figure 26: Measured well temperature

In figure 27, the outside air temperature[10] has also been reported, due to the two-dimensional model needs to know this value for a more precise simulation.

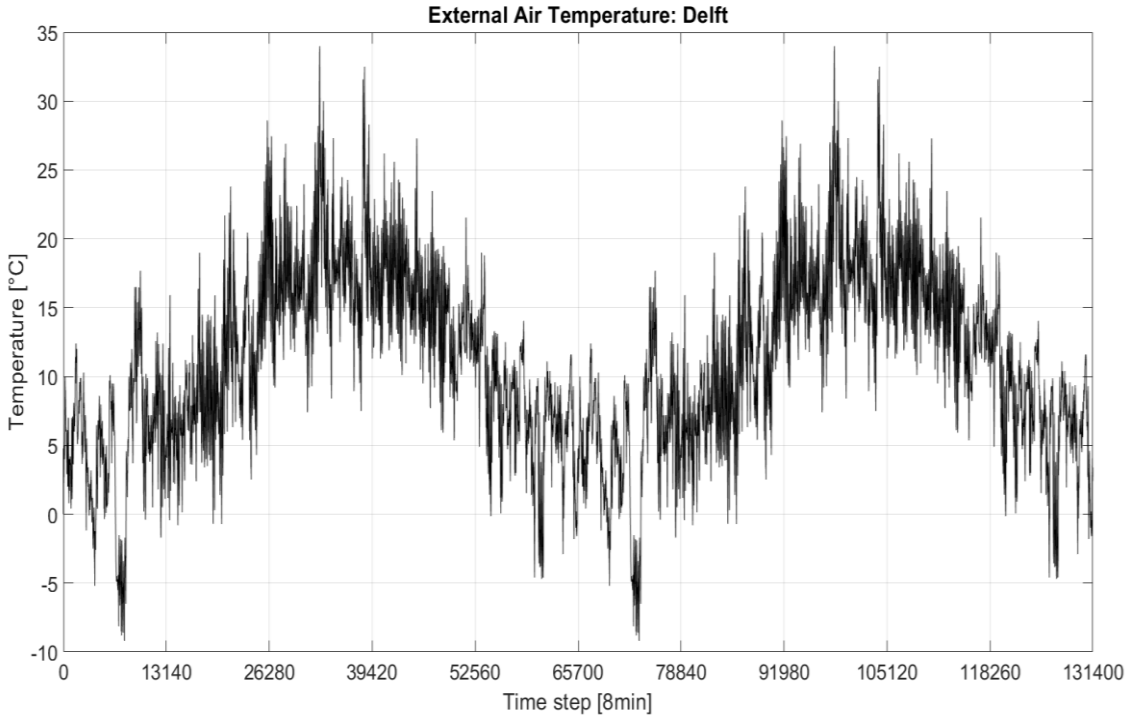

Figure 27: Delft air temperature

[10] Air temperatures *EnergyPlus* weather data, https://climate.onebuilding.org/default.html.

The temperature difference ΔT (figure 28) between warm temperature and the cold one, which varies within 0.1 and 9.9, has been used as input value. The calculated injected temperature is equal to the well temperature plus or minus the ΔT depending on cooling or heating mode.

$$T_{injection} = T_{extraction} \; +/- \; \Delta T$$

Considering the following equation for each time step, the extracted energy for heating and injected for cooling are calculated:

$$E_{extracted\backslash injected} \; = V \rho c_{pw} \, \Delta T$$

The total energy extracted, injected and the total volume of water during the 2-year simulation are reported in the following table 4:

$E_{extracted}$ [MWh]	$E_{injected}$ [MWh]	$Vol_{heating}$ [m^3]	$Vol_{cooling}$ [m^3]
288.890	424.440	71960	123580

Table 4: Energy and volume of water extracted and injected in Delft case

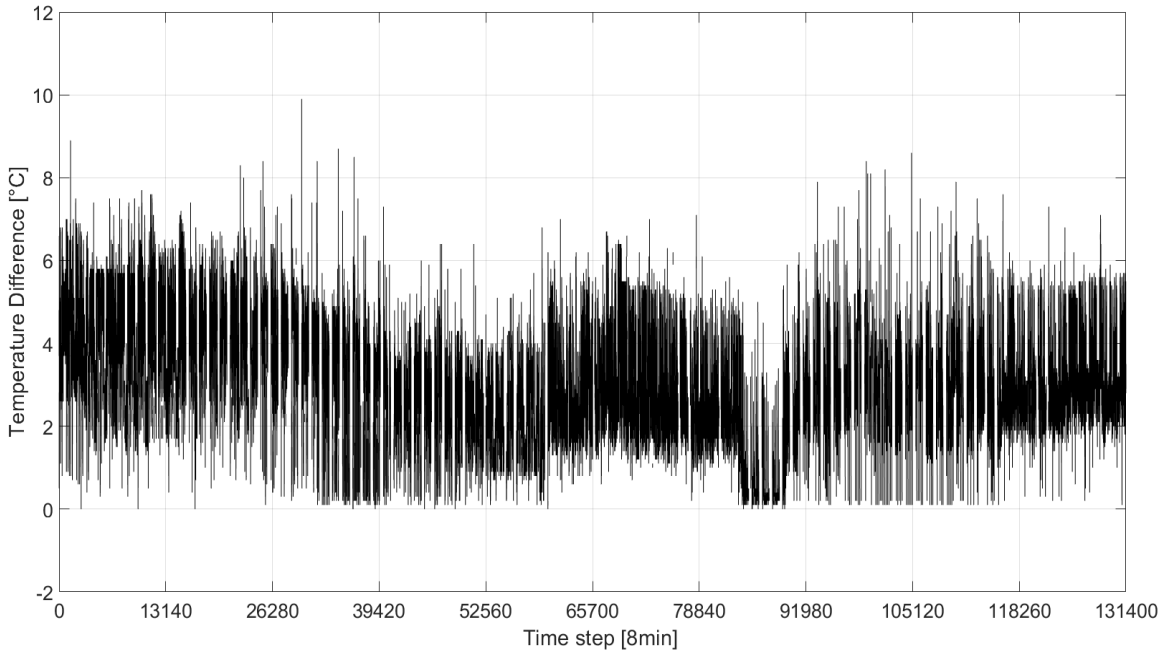

Figure 28: Temperature difference

The calculated temperature of the two groundwater wells is reported in the following page in comparison with the measured data.

The Root Mean Square Error (RMSE) has been calculated, in order to evaluate differences between the model's calculated temperatures and the measurements, with the following formula:

$$RMSE = \sqrt{\sum_{p}^{Tot} \frac{\left(T_{calculated,p} - T_{measured,p}\right)^2}{Tot}} \ [°C]$$

Where *p is* the time instant and *Tot* the total number of the time steps.

In table 5, RMSE values are reported.

RMSE, warm well	0.7135 °C
RMSE, cold well	0.7141°C

Table 5: RMSE values for 8 minutes time step

In figure 29 and 30, well temperature comparison between measurements and model results are plotted for the warm well and cold well respectively.

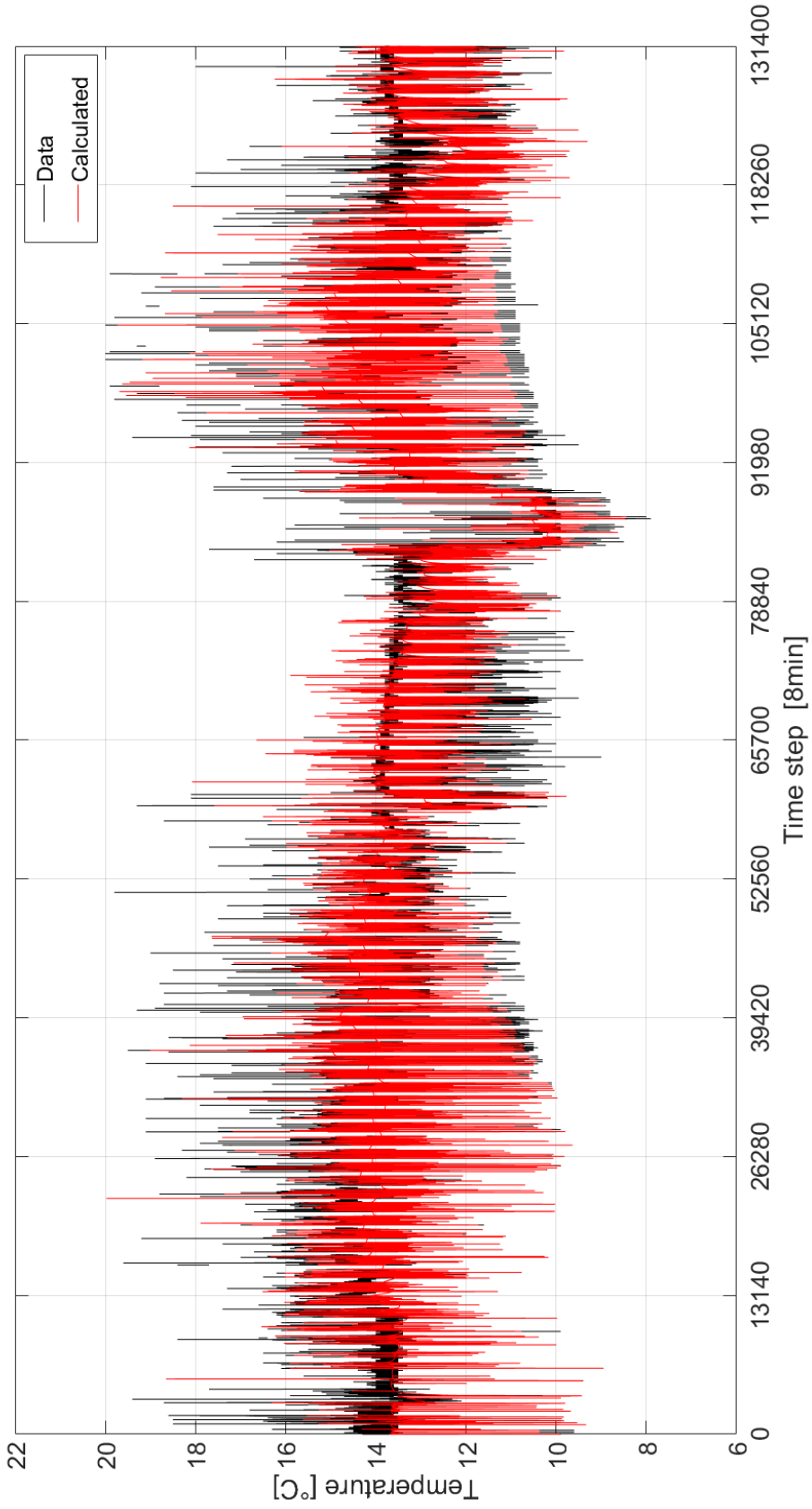

Figure 29: Warm temperature comparison

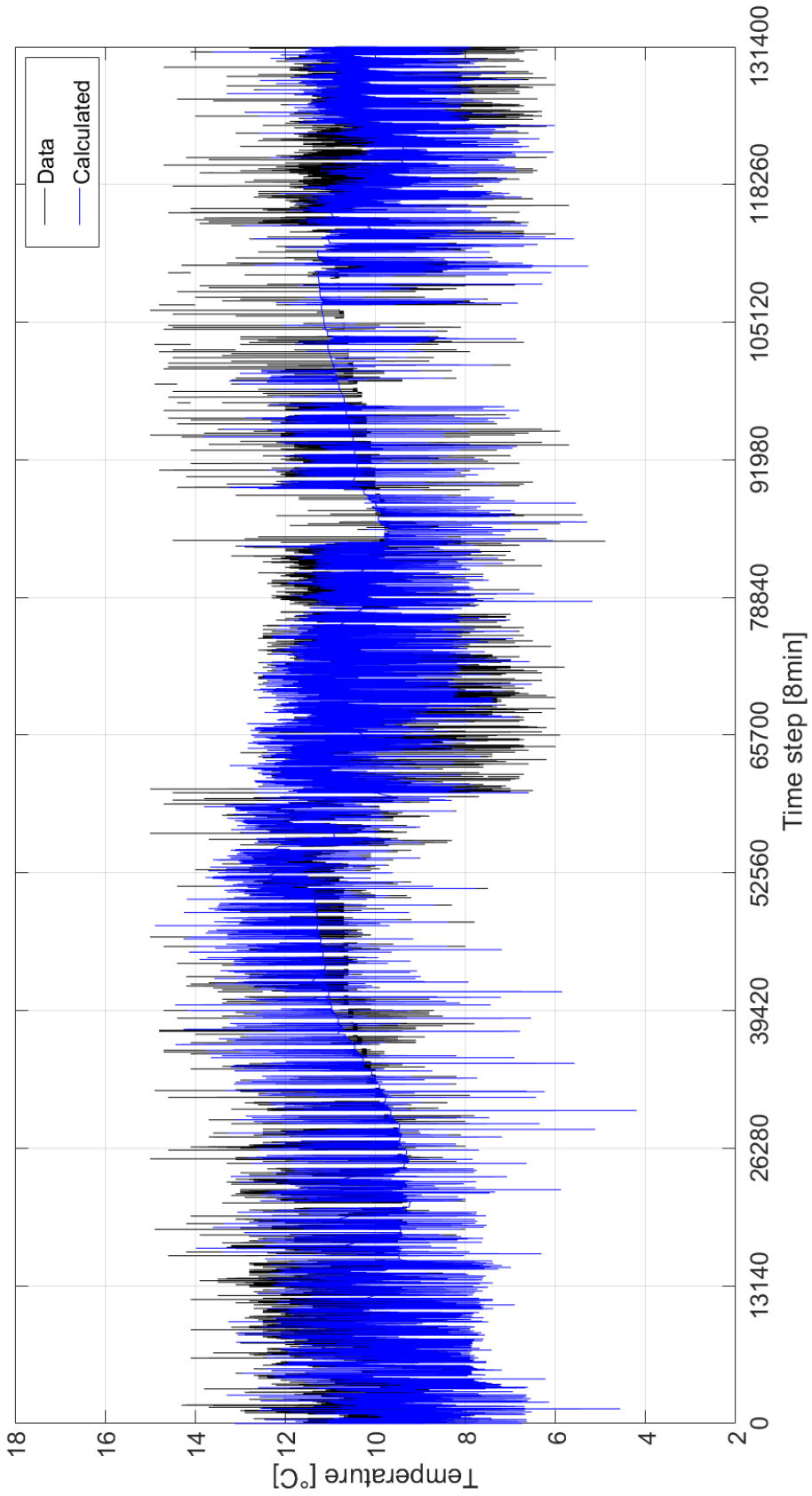

Figure 30: Cold well temperature comparison

Based on the RMSE, the model generates quite similar results to those measured; further confirmation comes from figures 31 and 32 which report zoomed section of the temperature plots.

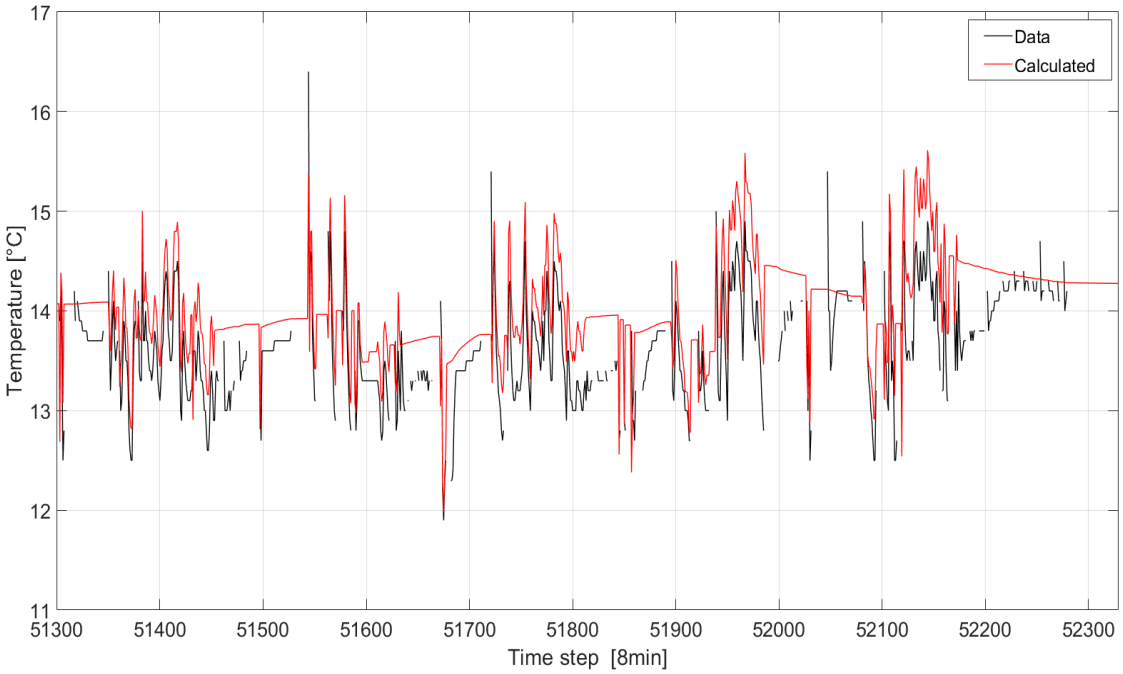

Figure 31: Zoomed warm well graph

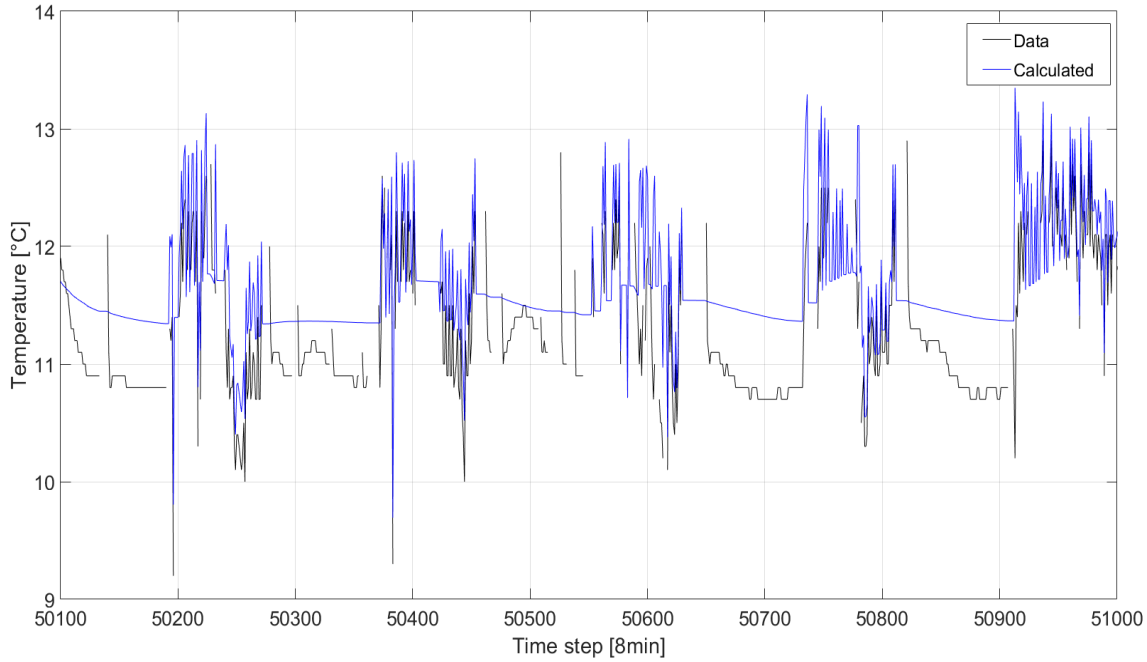

Figure 32: Zoomed cold well graph

As it is shown in the previous figures, the model trend follows the measured one results, however it was decided not to report the data measured during the storage periods due to the real measurements presented a high value during the storage phases, when there is no water flow. The temperature detector reveals the temperature of the technical room where there are the supply and return of wells, reaching even temperature >20 °C. The same situation happens in the time steps immediately after long storage periods also; the detector may fail to reveals the correct water temperature in just 8 minutes due to its technical limits.

In order to decrease the still high temperature values, it was decided to increase the time step to 48 minutes (2880 seconds). An average of six values (6 times 8 minutes) was taken for all the measures i.e. the wells temperatures and the flow rate.

The plots of temperature comparisons for 48 minute time steps are reported in figure 33 and 34.

The comparison results appear slightly better than the 8 minutes case and the RMSE calculated is marginally lower:

In table 6, RMSE values are reported.

RMSE, warm well	0.7090 °C
RMSE, cold well	0.7096 °C

Table 6: RMSE values for 48 minutes timestep

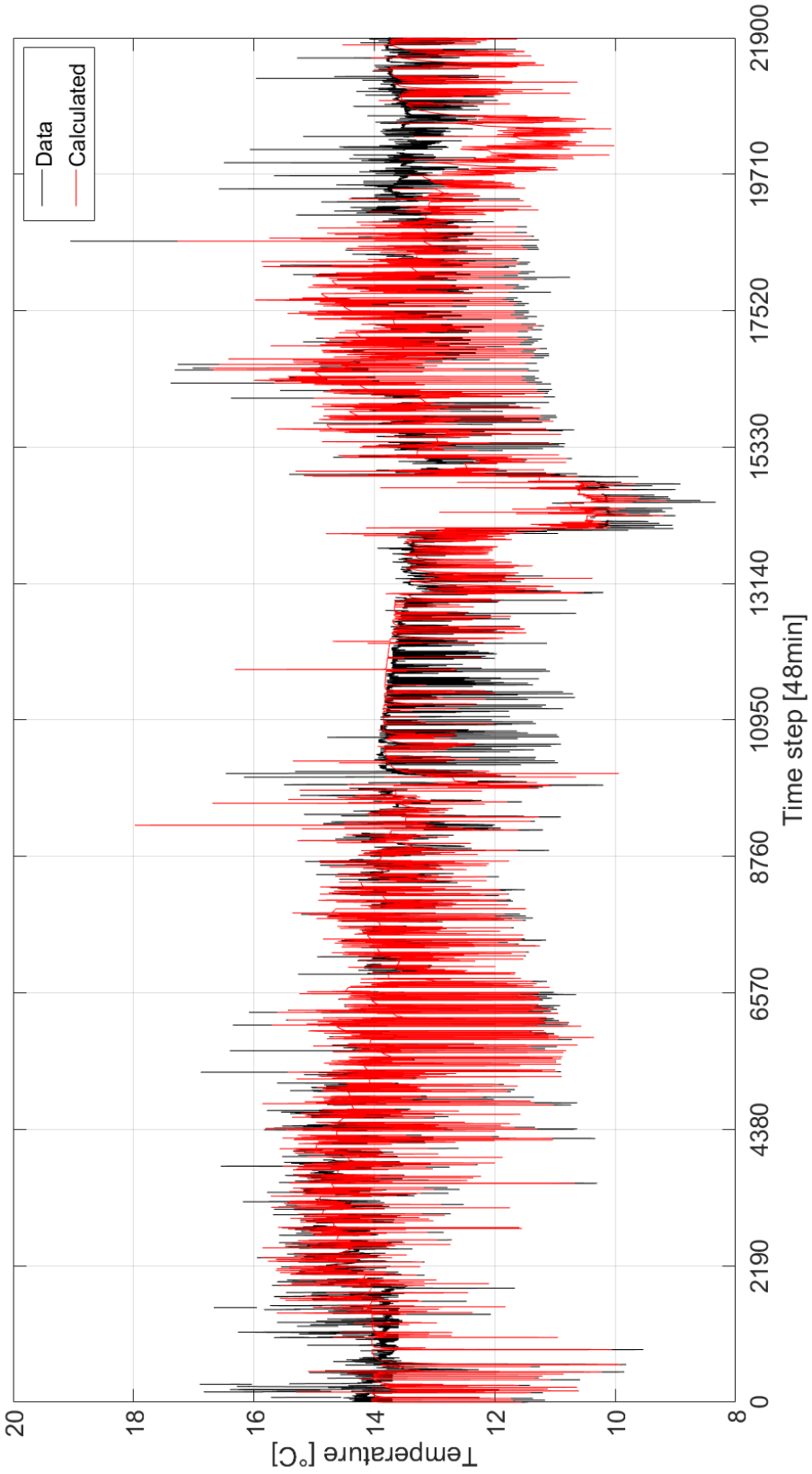

Figure 33: Warm temperature comparison (48 minutes)

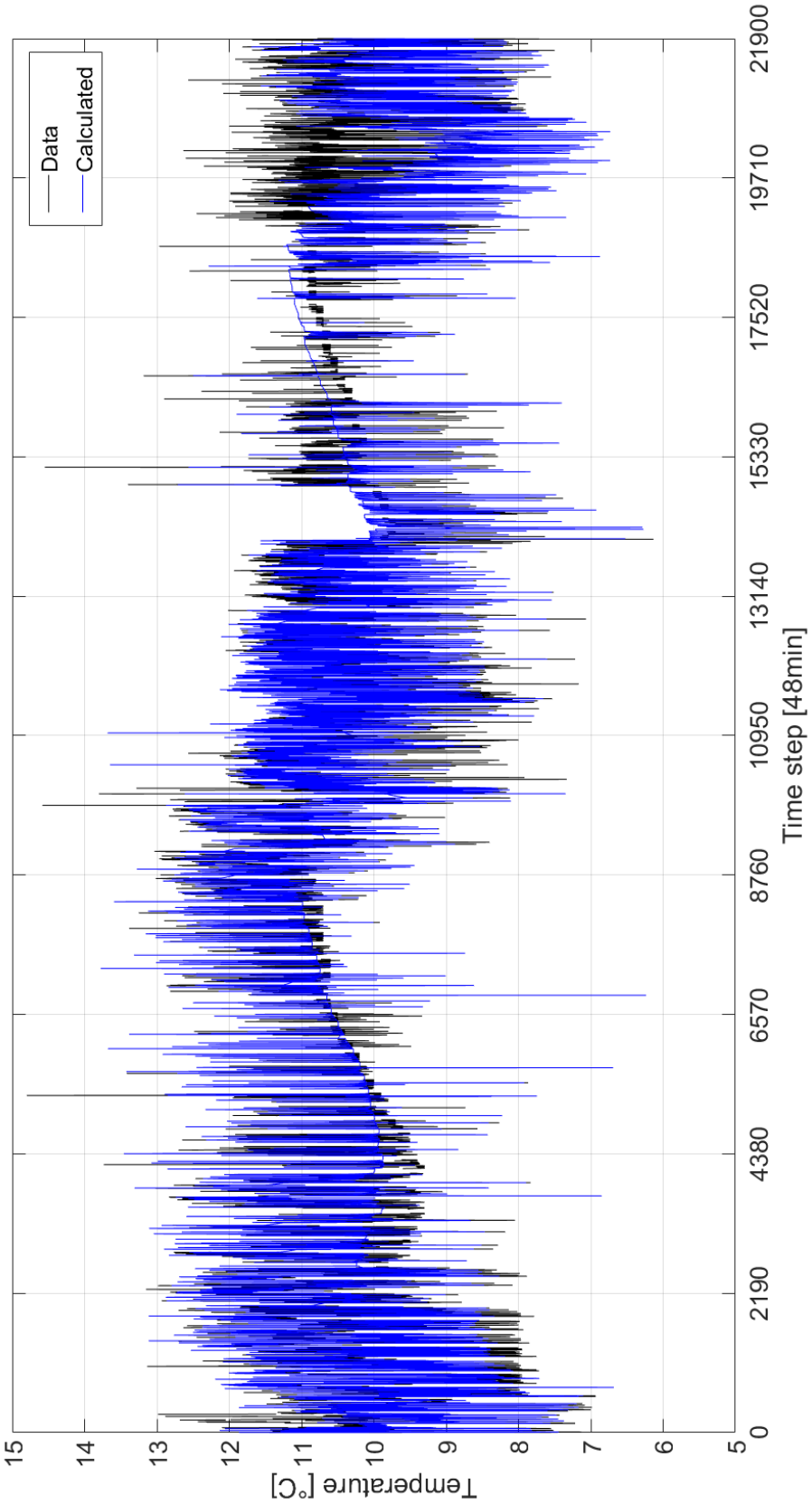

Figure 34: Cold temperature comparison (48 minutes)

4. Building simulation integration

In this last chapter, the integration of a building energy simulation in the aquifer model will be presented and analysed with some applications. Three case studies were performed, each with different energy demands and location.

In figure 35, a schematic diagram of the overall operation of model is reported:

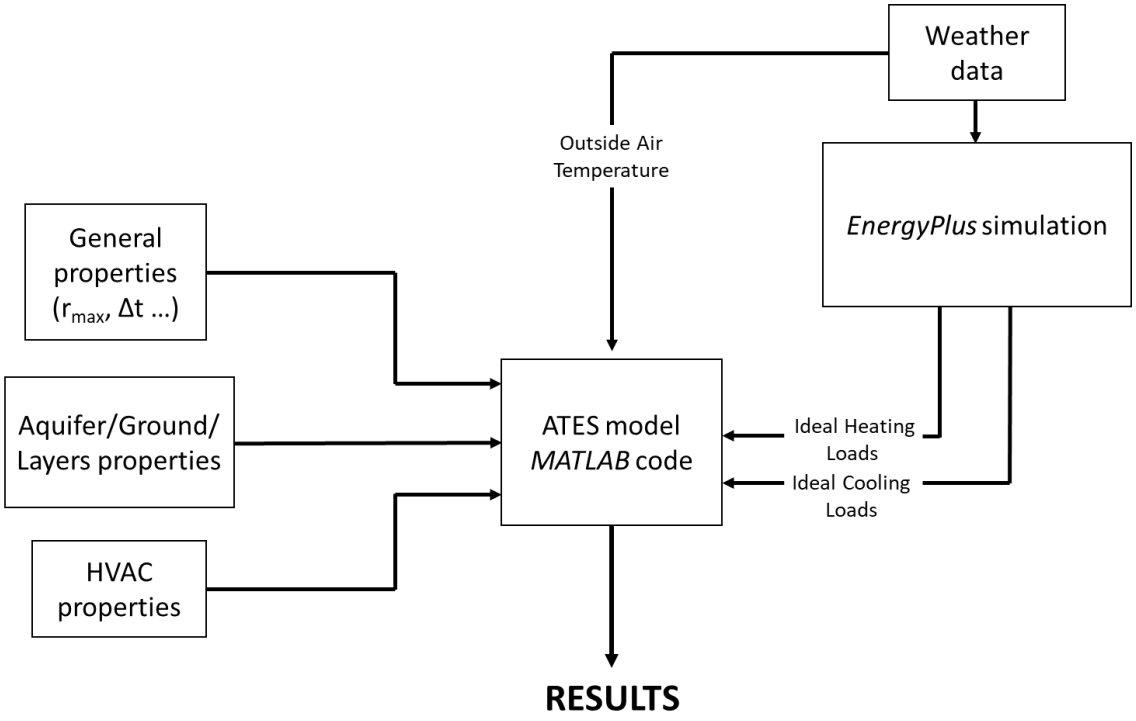

Figure 35: Model diagram

The main steps are:

- An *EnergyPlus* simulation is carried out. It requires the weather data in order to calculate the ideal heating and cooling demands, which are then loaded in the model together with the outside air temperature.
- A hypothetical HVAC system is linked to the ATES, from which it is possible to estimate the ground-water volume flow required for the energy demand.

- The general discretization properties, such as the time steps, radius of domain and the properties of the aquifer and the ground layers are inserted in the model.

4.1 *EnergyPlus* simulation

The energy tool used for building simulation is the software *EnergyPlus™*, developed by the U.S Department Of Energy (DOE).

The case analysed is a large office building[11] (figure 36) of the early 2000s; the main information about the building are reported in table 7.

Total area	46230 m^2
Total volume	178146 m^3
Gross wall area	11590 m^2
Window area	4636 m^2
Aspect Ratio	1.5
Number of floors	12+basament
External wall U-value	0.85
Roof U-value	0.36
Windows U-value	3.24
Solar Heat Gain Coef.	0.39

Table 7: Building main information

[11] More information on the building simulation can be found on the U.S. Department of Energy, website *https://www.energy.gov/eere/buildings/new-construction-commercial-reference-buildings;* office building in Baltimora.

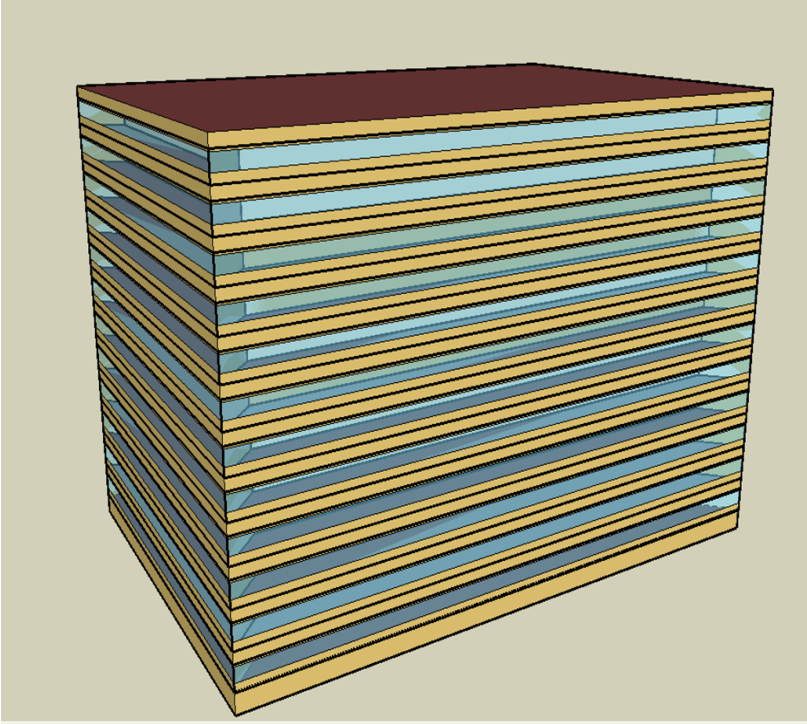

Figure 36: Building representation

In the energy tool simulation, the hourly ideal heating and cooling loads are calculated for a year.

The heating and cooling schedules have been modified from those commonly used on the DOE website [note 11]; the updated ones are shown below in table 8:

Cooling Setpoint temperature °C															
Hours	**7**	**8**	**9**	**10**	**11**	**12**	**13**	**14**	**15**	**16**	**17**	**18**	**19**	**20**	**21**
Workdays	25	25	25	25	25	25	25	25	25	25	25	25	25	25	25
Saturday	25	25	25	25	25	25	25	/	/	/	/	/	/	/	/
Heating Setpoint temperature °C															
Hours	**7**	**8**	**9**	**10**	**11**	**12**	**13**	**14**	**15**	**16**	**17**	**18**	**19**	**20**	**21**
Workdays	21	21	21	21	21	21	21	21	21	21	21	21	21	21	21
Saturday	21	21	21	21	21	21	21	/	/	/	/	/	/	/	/

Table 8: Cooling/heating setpoint temperature

The plant is switched off all day Sunday, from 14.00 on Saturday and every workday night from 22.00 to 7.00 the following morning.

4.2 Plant characteristic

For the HVAC linked to the aquifer thermal energy storage doublet, a heat exchanger (figure 37) and a ground-water heat pump (figure 38) have been chosen for cooling and heating purposes respectively.

The choice of using a heat exchanger directly for cooling is mainly for economic, environmental and feasibility reasons; in fact, for all three cases analysed, the temperatures of the cold well are less than 15 °C. With that temperature range it is possible to use low temperature cooling terminals such as active beams, which require water from about 16 °C to 19 °C or floor cooling.

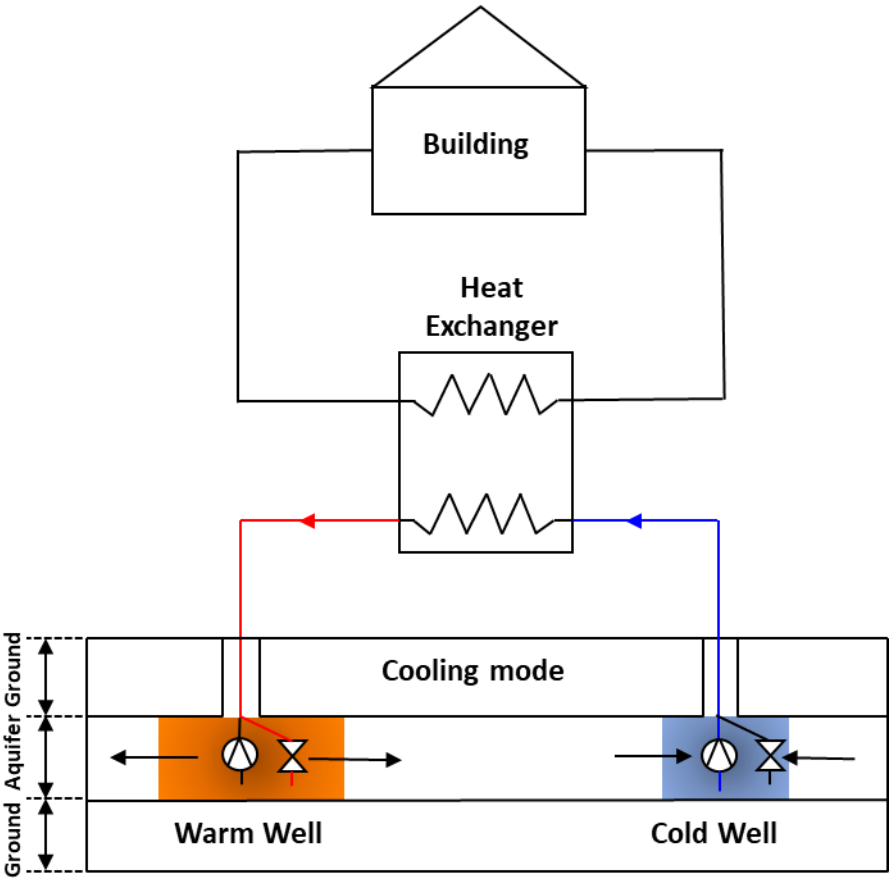

Figure 37: ATES, cooling mode

The water volumetric flow rate extracted from the cold well is calculated as follows:

$$V_C = \frac{Q_{building}}{\rho_w c_{pw}(T_{inj} - T_{ext})} \left[\frac{m^3}{s}\right]$$

Regarding the heating mode, a ground-water to water heat pump produces hot water at 40 °C (T_{WLC}) at the condenser; with this range it is possible to use the same terminals, such as active beams or floor heating.

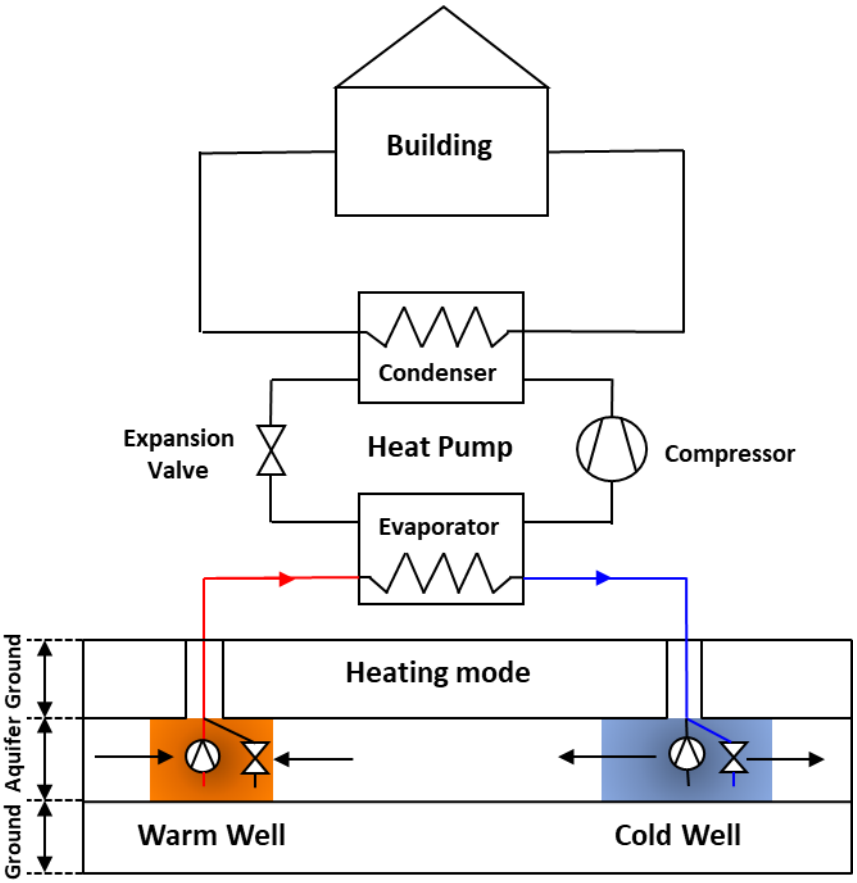

Figure 38: ATES, heating mode

The Coefficient Of Performance (COP) of the heat pump has been modelled according to the following formula:

$$COP_H = \eta_{carnot} \cdot \frac{T_{WLC} + \Delta T_{pp}}{(T_{LWC} + \Delta T_{pp}) - (T_{LWE} - \Delta T_{pp})} \; [-]$$

where all the temperatures are in Kelvin and the water temperature leaving the evaporator T_{WLE} is the injected water temperature in the cold well. This model[12] for a heat pump considers the changes in the COP with temperatures in the same way as the Carnot efficiency changes (usually a value between 30%-40%). Moreover, a pinch-point temperature difference was considered to account for the heat exchange on the heat pump condenser and evaporator.

The thermal load on the ATES side, i.e. on the evaporator of the heat pump, and the volumetric water flow required, have been calculated as follows:

$$Q_{evap} = Q_{cond} \cdot (1 - \frac{1}{COP_H}) \quad [W]$$

$$V_H = \frac{Q_{evap}}{\rho_w c_{pw}(T_{ext} - T_{inj})} \quad \left[\frac{m^3}{s}\right]$$

where the thermal load on the condenser side is the heat required by the building.

In the model developed, the temperature difference ΔT_H and ΔT_C between extracted and injected water temperatures have been considered constant.

Another important consideration has been assumed regarding the simultaneity of thermal loads. Given the large size of the building and its function, it is common to have simultaneous demand for heating and cooling; for this reason an ideal heat recovery system was assumed to be used. Ideally, during winter, if a room needs to be cooled, excessive heat would be used for heating elsewhere; vice versa during summer.

[12] This COP model used in *Modelica* software for modelling complex system; see *Modelica* library *https://simulationresearch.lbl.gov/modelica/releases/v8.0.0/help/Buildings_Fluid_HeatPumps.html*.

4.3 Thermal radius

When designing ATES systems, attention must be paid to the installation distance between the warm well and the cold well. The thermal front could influence the temperatures of the two wells, so they must be installed at a minimum distance from each other to avoid such thermal interference.

Assuming the homogeneity of the ground, neglecting the vertical infiltration and the natural ground-water velocity (as stated in Basar B. et al. [7]), during the injection in aquifer well, the fluid forms a theorical cylindrical volume of warm/cold water (as reported in S. Beernink et al. [12]). The radius of this cylinder is called thermal radius.

The thermal radius R_{th} of an ATES well depends on the seasonal injected water volume, aquifer thickness, volumetric heat capacities of water and aquifer which are assumed constant along the radial and vertical directions.

$$R_{th} = \sqrt{\frac{C_{s,w} \cdot Vol_{inj}}{C_{s,aq} \cdot \pi \cdot h}}$$

As it is shown in figure 39, in the case of different type wells, the minimum distance to avoid thermal interference is given by the product between a coefficient D_o and the thermal radius, similarly in case of the same type of wells the product is between the coefficient D_s; in case of different thermal radii, the distance is calculated based on the average thermal radius of the two wells.

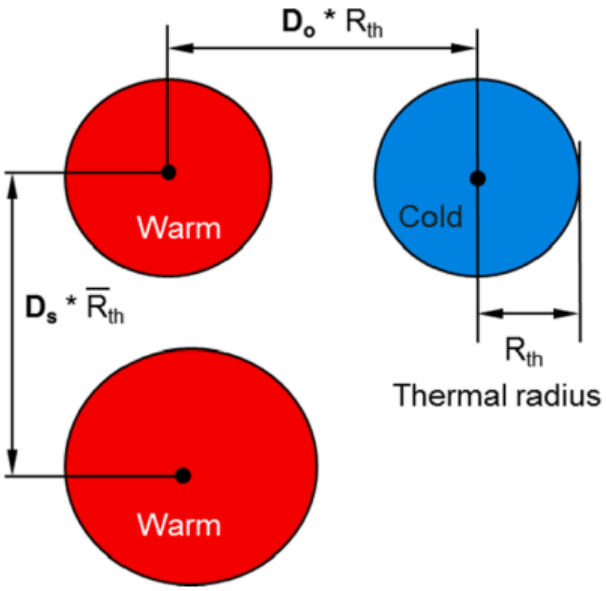

Figure 39: Schematic overview of distances

The *D* coefficients usually depend on local policies; for safety reasons, the values given by Dutch authorities are used: D_o equal to 2 and D_s equal to 3.

An example is reported below in table 9, which report the thermal radii of the Delft ATES presented in Chapter 3.2.

Thermal radius, warm well	**Thermal radius, cold well**	**Average thermal radius**
29.45 m	21.23 m	25.34 m

Table 9: Delft thermal radius

The yearly seasonal total injected volume in the Delft case are 35980 m^3 and 61790 m^3 respectively for cold well (during heating mode) and warm well (during cooling mode).

As shown in figures 40 and 41, considering three times the average thermal radius equal to 75 m, already over 42 m away there are temperatures corresponding to Delft's undisturbed ground temperature of 11.5 °C, so there is no more thermal interference. Furthermore, as far as the cold well is concerned, given the unbalanced load, it receives less water flow, and after a distance from the injection site of 30 m, there is no more interference.

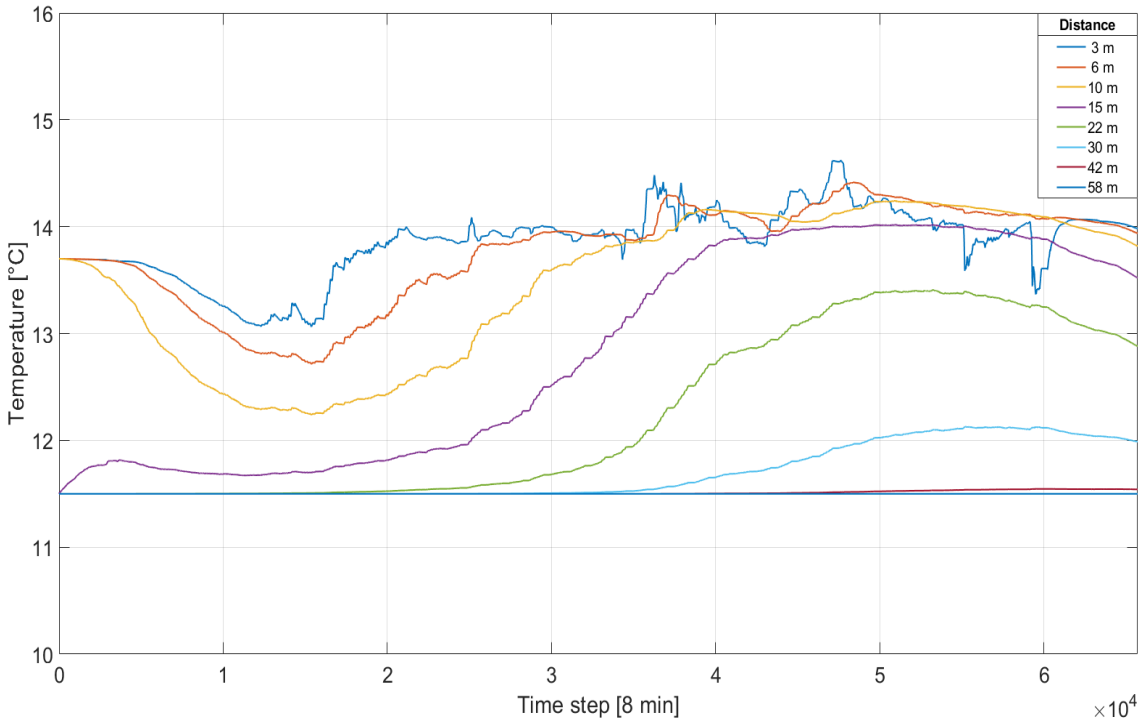

Figure 40: Delft warm well at different distance

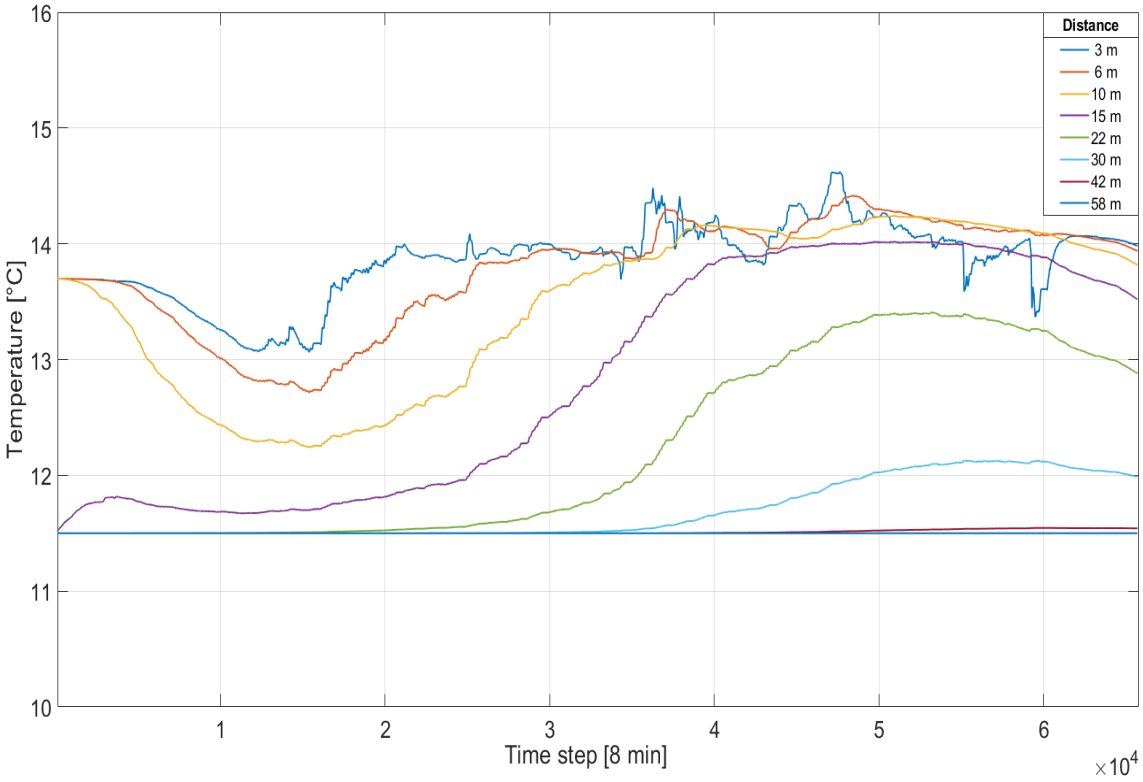

Figure 41: Delft cold well at different distance

4.4 Case studies

The cases studies reported represent three different situations; each case has been analysed in different location[13] Verona (IT), Frankfurt (DE) and Helsinki (FI) in order to have a cooling dominant case, a balanced case and a heating dominant case.

In addition to the locations, the values of the internal loads, internal mass, number of people, light and electrical equipment were modified with the *EnergyPlus* multiplier in such a way as to highlight the different load cases.

Table 10 shows the common input values for all cases, while figure 42 shows the common stratigraphic section adopted:

[13] Weather file *.epw* for *EnergyPlus* on https://climate.onebuilding.org/default.html.

Parameter	Value
General Properties	
Expansion coefficient	1.1
Time step Δt	3600 s
Domain radius r_{max}	200 m
Aquifer	
Water density ϱ_w	1000 kg/m^3
Water specific heat cp_w	4186 J/kgK
Water thermal conductivity λ_w	0.5 W/mK
Sand density ϱ_s	1300 kg/m^3
Sand specific heat cp_s	2000 J/kgK
Sand thermal conductivity λ_s	2.5 W/mK
Aquifer thickness h	25 m
Well radius r_{wb}	0.5 m
Porosity φ	30 %
Leakages coefficient	2.5x10^{-7} m^3_w/ m$^3_{aq}$
Ground layers	
Clay volumetric specific heat C_s	2.3x10^6 J/ m^{3}K
Clay volumetric specific heat C_s	2.3x10^6 J/ m^{3}K
Layers thickness	40 m
HVAC data	
T_{WLC}	40 °C
ΔT_H	5 °C
ΔT_C	5 °C
η_{carnot}	40 %
ΔT_{PP}	2 K

Table 10: Common input properties

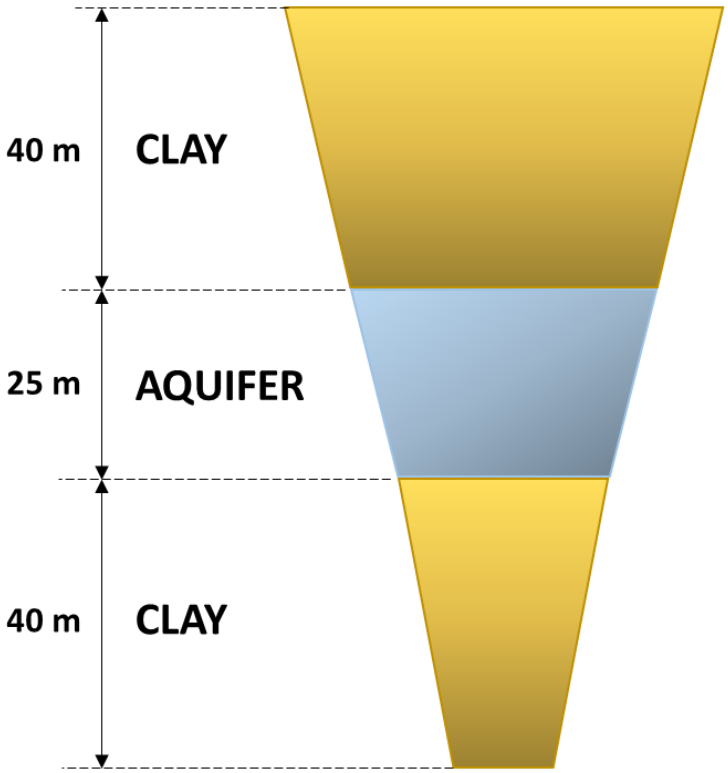

Figure 42: Stratigraphic section

4.4.1 Verona: cooling dominant case

The first case reported is a cooling dominant one located in Verona. Some information such as ground temperature, the loads multiplier and yearly energy demands are recorded in table 11.

Undisturbed Ground Temperature/ Initial Temperature	13.5 °C
***EnergyPlus* multiplier**	
Internal Mass	70 %
People	70 %
Light	50 %
Electrical equipment	70 %

Yearly energy demands	
Heating	431.66 MWh
Cooling	1739.9 MWh

Table 11: Cooling dominant case, data

In figure 43, thermal loads and outdoor air temperature are reported, while in figure 44, monthly energy histograms for heating energy at condenser (building side) and evaporator (ATES side) are shown. About the cooling, for both sides, only a single histogram has been reported due to the presence of an ideally heat exchanger.

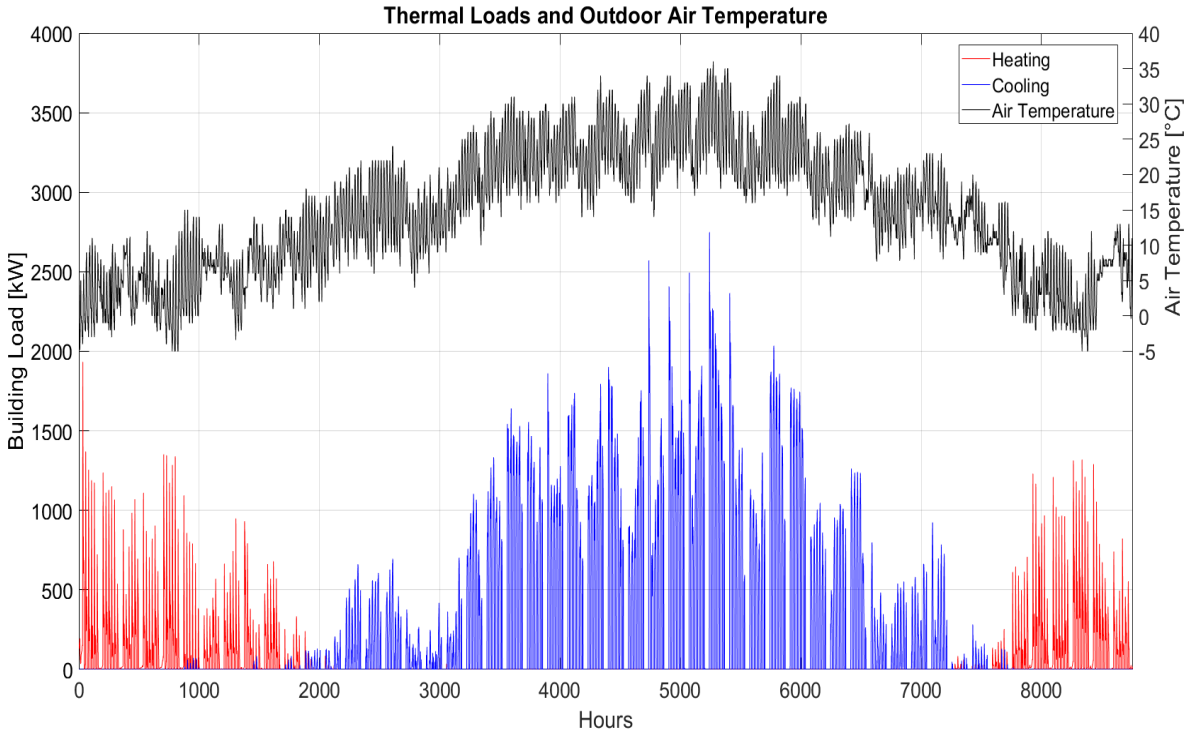

Figure 43: Cooling dominant case, thermal loads and air temperature

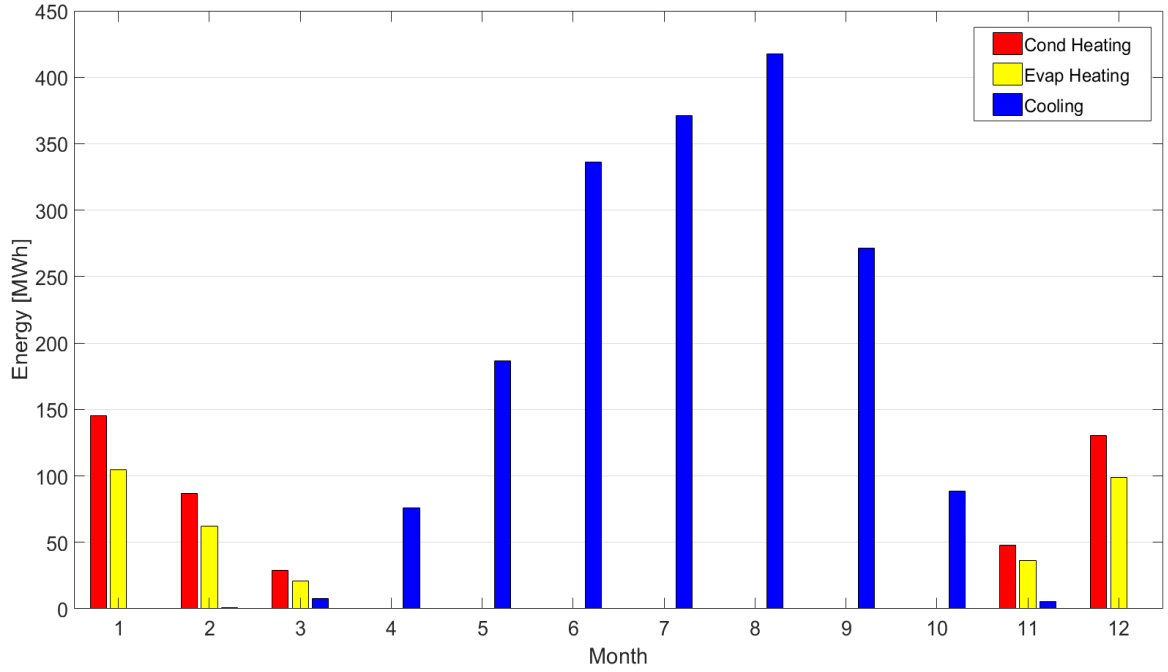

Figure 44: Cooling dominant case, energy histogram

The water volumetric rate are reported in figure 45.

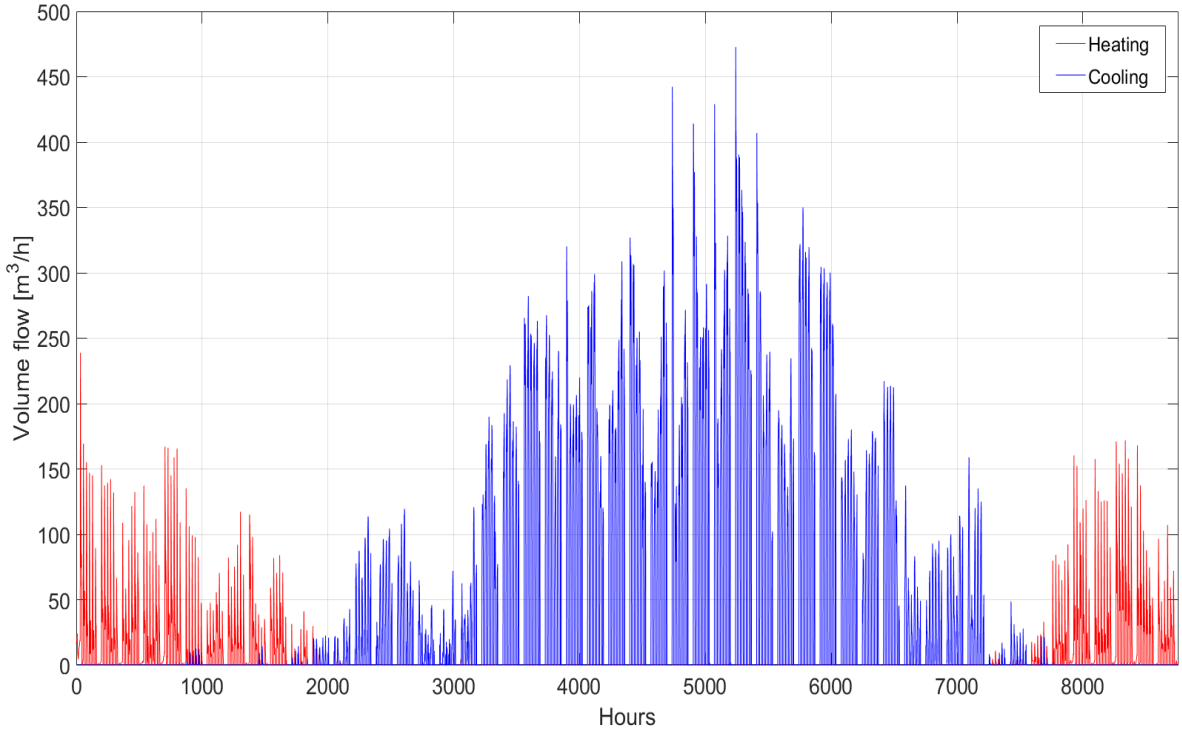

Figure 45: Cooling dominant case, volumetric flow rates

In order to show the temperature trends of the wells, the results for 20 years of simulation[14] are reported in figure 46.

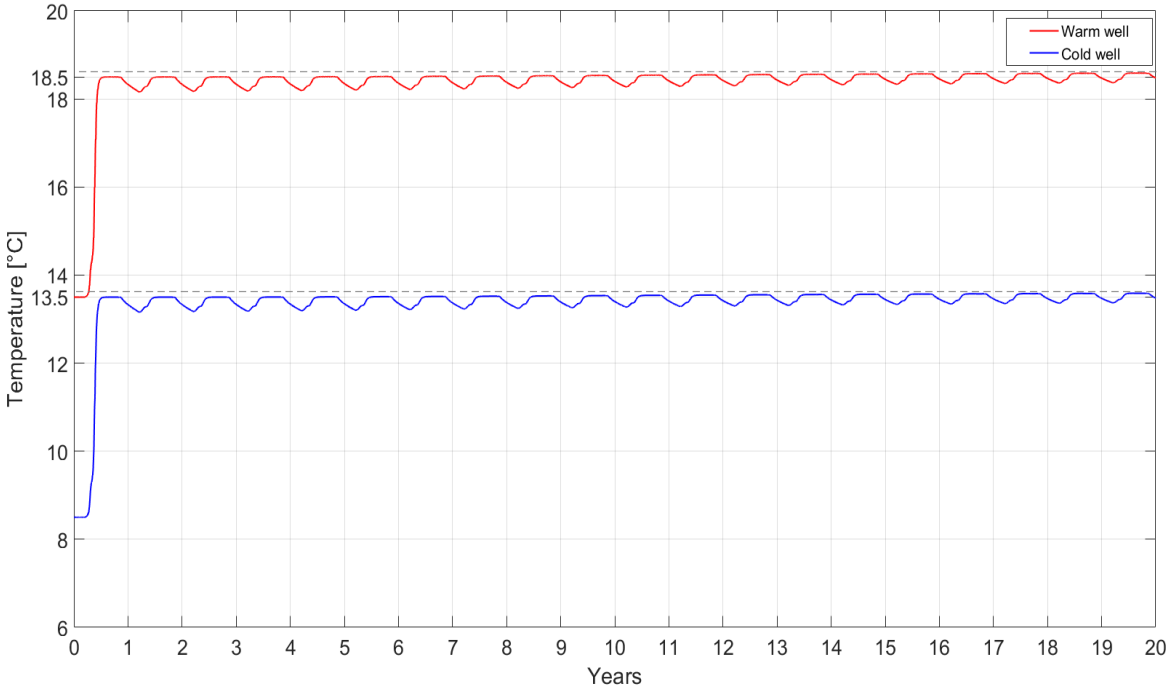

Figure 46: Cooling dominant case, wells temperatures 20 years

As can be seen from the previous graph, in the first time steps at the heating season starting, the temperature of the warm well remains unchanged (equal to the undisturbed temperature) while the cold well temperature is reduced from 13.5 °C to 8.5 °C (ΔT is fixed). The next increase is due to the cooling phase where water is withdrawn from about 8.5 °C and injected at 13.5 °C. This significant increase is due to the loss of cold water in well and, of course, the higher ground temperature. The temperature of the cold well stops at around 13.5 °C, while for the hot well it stops at 18.5 °C. They remain constant until the beginning of the heating period, where they drop together.

[14] The simulation of 20 years (175200 hours) requires about 35-40 minutes of computational time to run the script reported in Appendix. Of course the value depends on the graphs plotted, maximum radius and number of active nodes for the discretization. The calculator performances influence the time.

Another peculiarity that is noticeable is that over the 20 years, there is a slight temperature rise for both wells of about 0.09 °C (grey dotted line in the above mentioned figure 46), due to the cooling dominant case with very unbalanced loads between the heating and cooling energy extracted. Another possible cause could be performed by the temperature of the topmost ground layer in contact with the outside air. This influence is so minimal.

In figure 47, the heat pump COP is reported, obviously only for the heating mode.

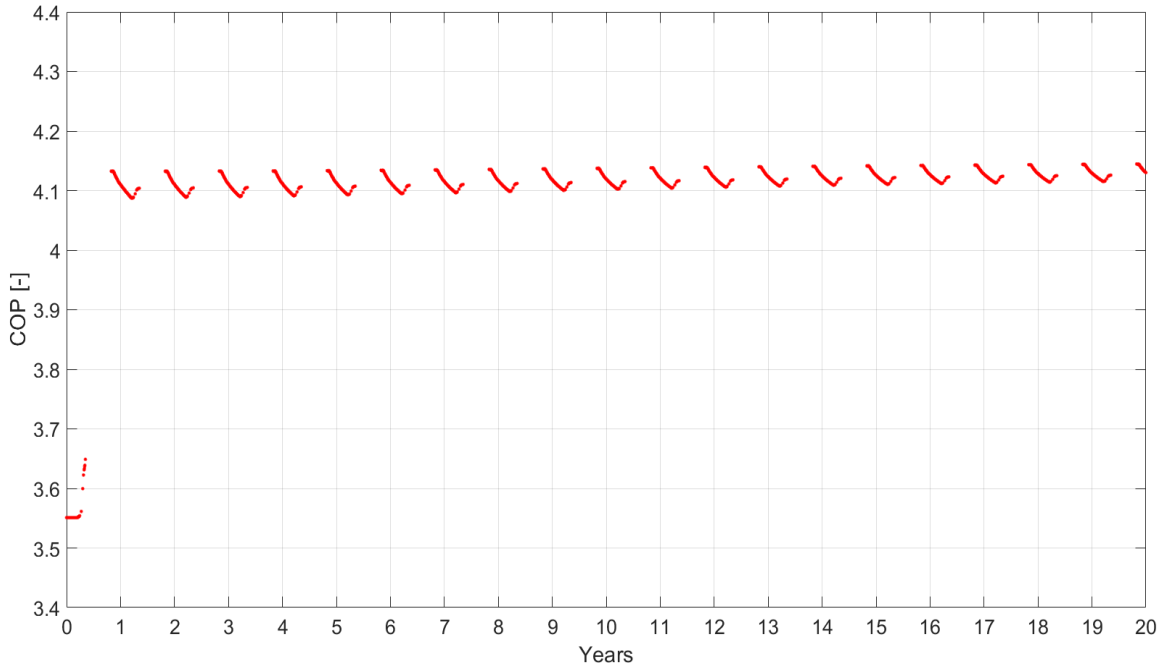

Figure 47: Cooling dominant case, COP

The COP is influenced by the injected temperature in the cold well (water leaving the evaporator), for this reason in the first time steps COP is about 3.55÷3.65, while it reaches values around 4.1 when the injected temperatures are about 13.5 °C. Furthermore, the Carnot efficiency was fixed at 40%.

The COP calculated does not take into account the system with all the auxiliaries, such as the ground-water submersible pumps.

The yearly operation hours of the heat pump are 2253 h.

In the next graphs (figure 48 and 49) there are reported the injected and extracted water temperature for both wells.

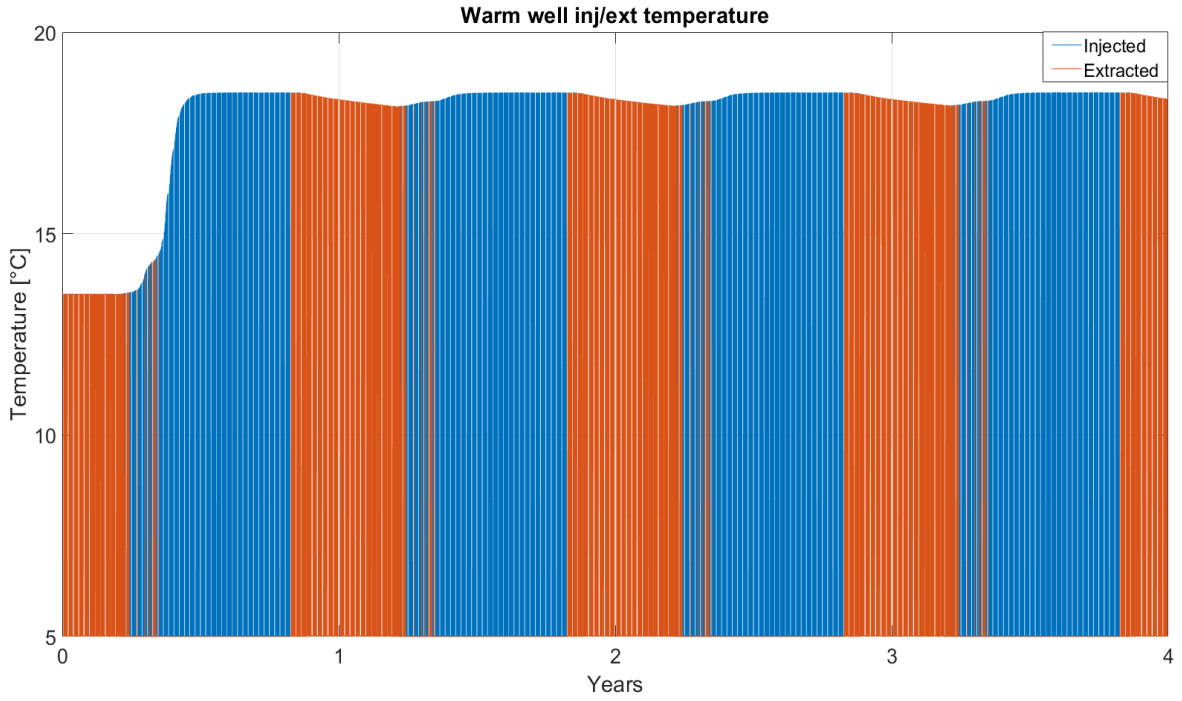

Figure 48: Cooling dominant case, warm well inj/ext temperature

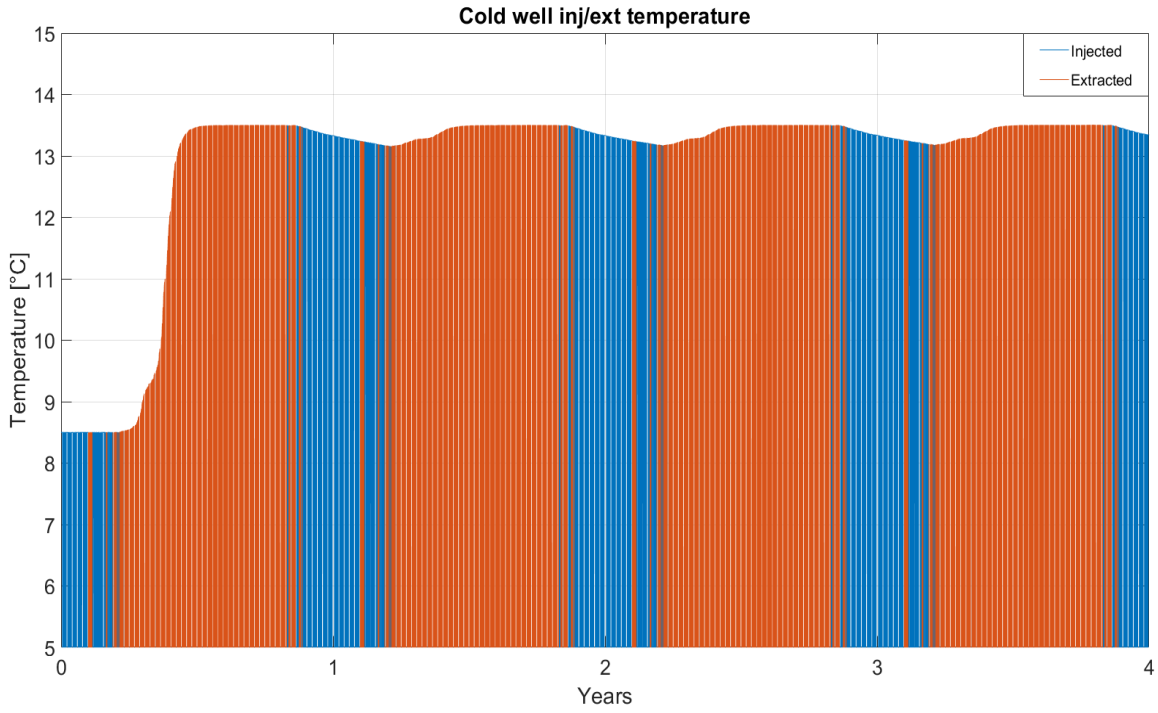

Figure 49: Cooling dominant case, cold well inj/ext temperature

Regarding the installation distance between the wells, the calculation of the thermal radius has been done avoiding thermal interference.

The total injected volume and thermal radii are shown in table 12.

Yearly Vol_{inj} warm well	**Yearly Vol_{inj} cold well**	**R_{th}, warm well**	**R_{th}, cold well**	**3 x Average R_{th}**
302940 m^3	55560 m^3	72.5 m	31 m	155 m

Table 12: Cooling dominant case, thermal radii

As confirmed by the calculated thermal radii and the following figures 50 and 51, the distance must be at least 155 m.

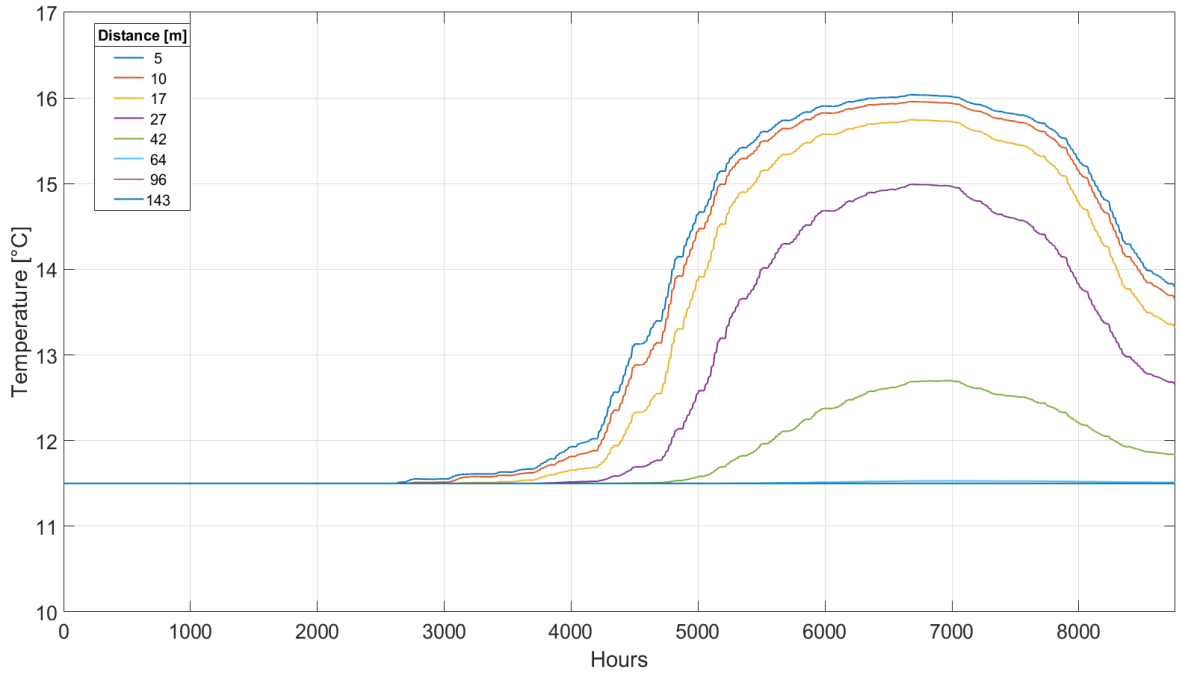

Figure 50: Cooling dominant case, warm temp at different distance, 8760 h

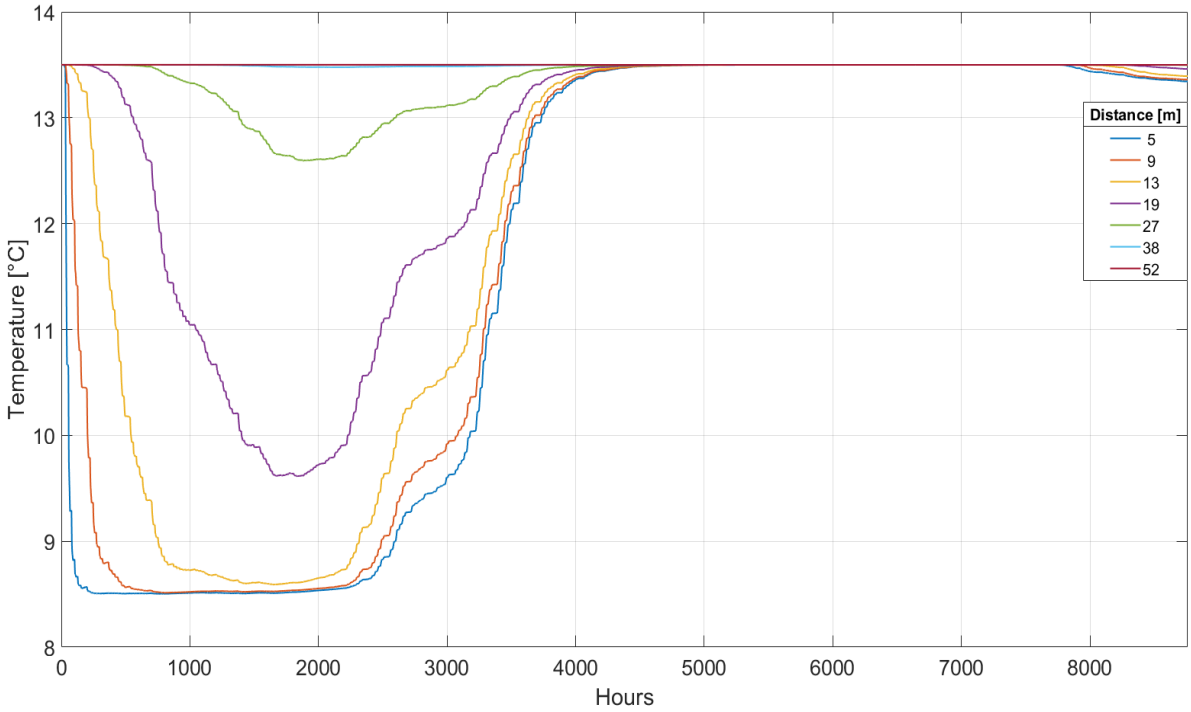

Figure 51: Cooling dominant case, cold temp at different distance, 8760 h

4.4.2 Frankfurt: balanced case

The second case reported is a balanced one located in Frankfurt. The table 13 reports ground temperature, loads multiplier and yearly energy demands.

Undisturbed Ground Temperature/ Initial Temperature	11.5 °C
***EnergyPlus* multiplier**	
Internal Mass	70 %
People	70 %
Light	50 %
Electrical equipment	65 %
Yearly energy demands	
Heating	1103.57 MWh
Cooling	963.26 MWh

Table 13: Balanced case, data

Figure 52, 53 and 54 show thermal loads and air temperature, monthly energy histogram and flow rate respectively.

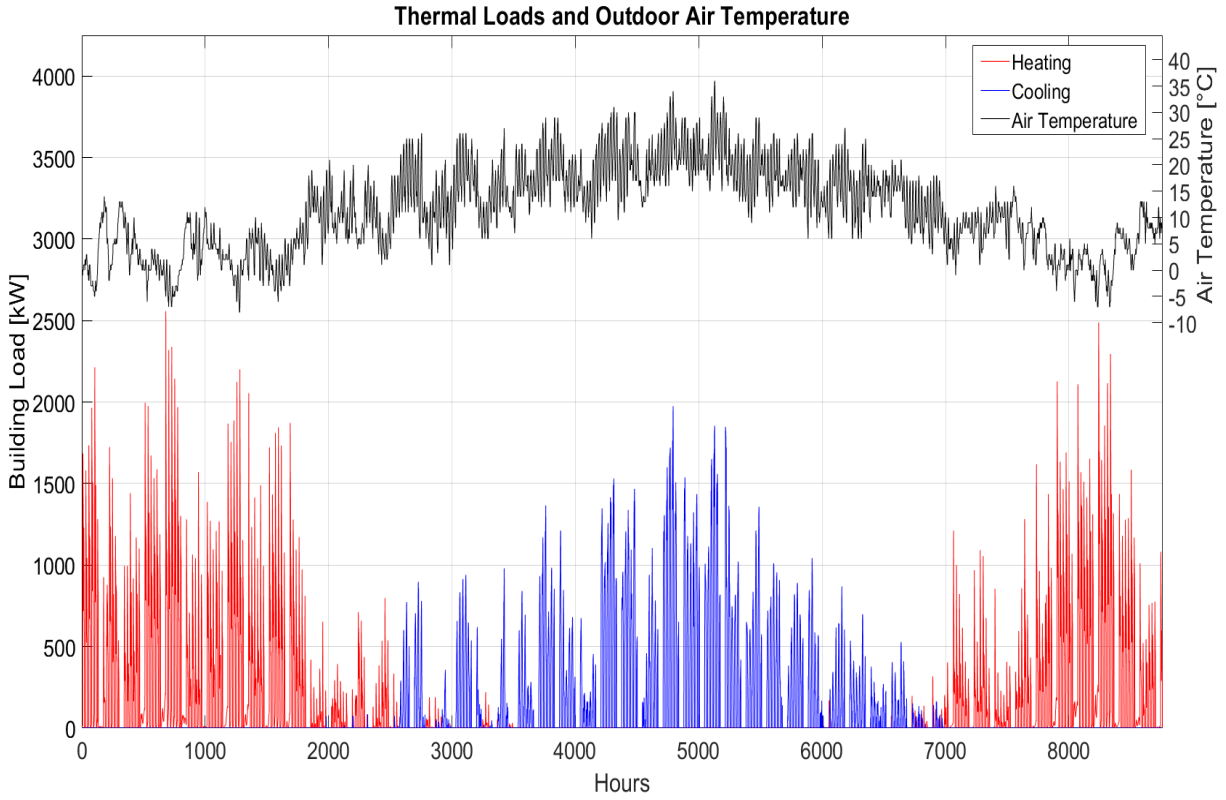

Figure 52: Balanced case, thermal loads and air temperature

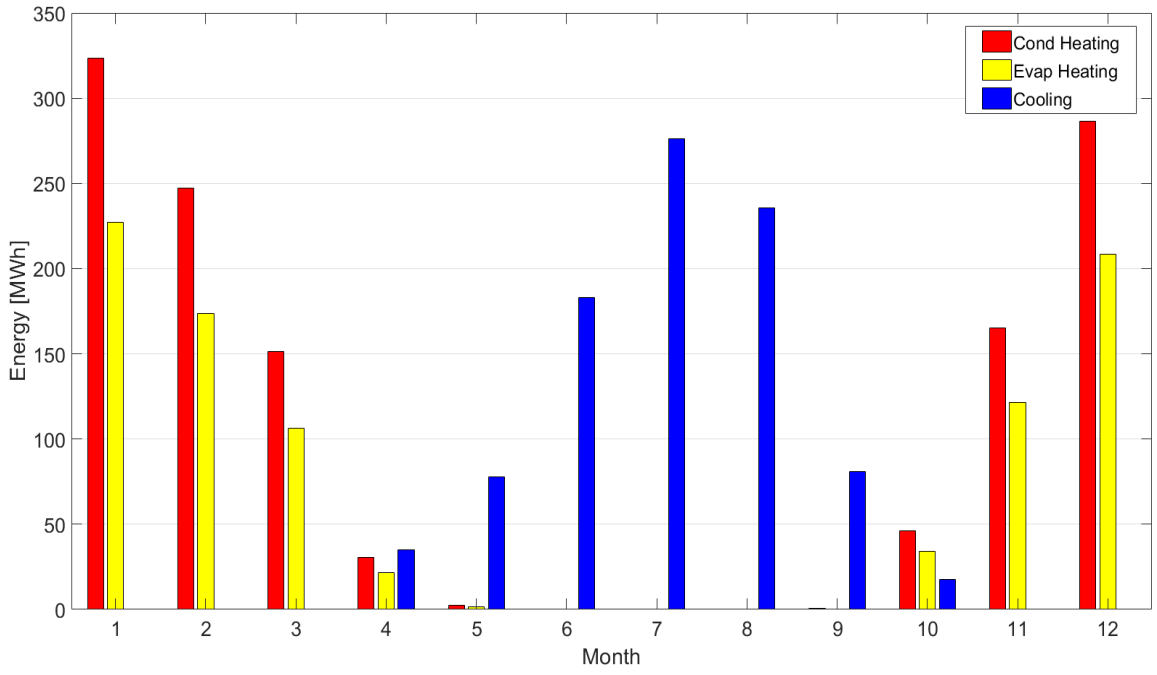

Figure 53: Balanced case, energy histogram

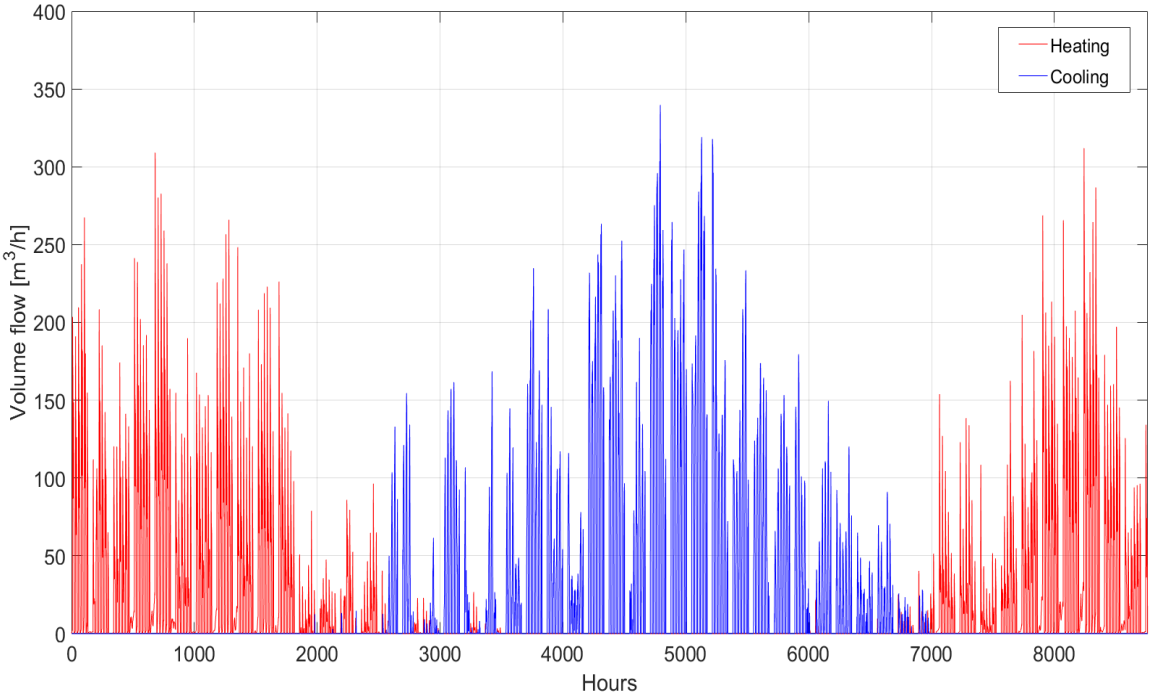

Figure 54: Balanced case, volumetric flow rates

As it is illustrated in figure 55, compared to the cooling dominant case, the balanced one has a different trend due to the lower cooling loads.

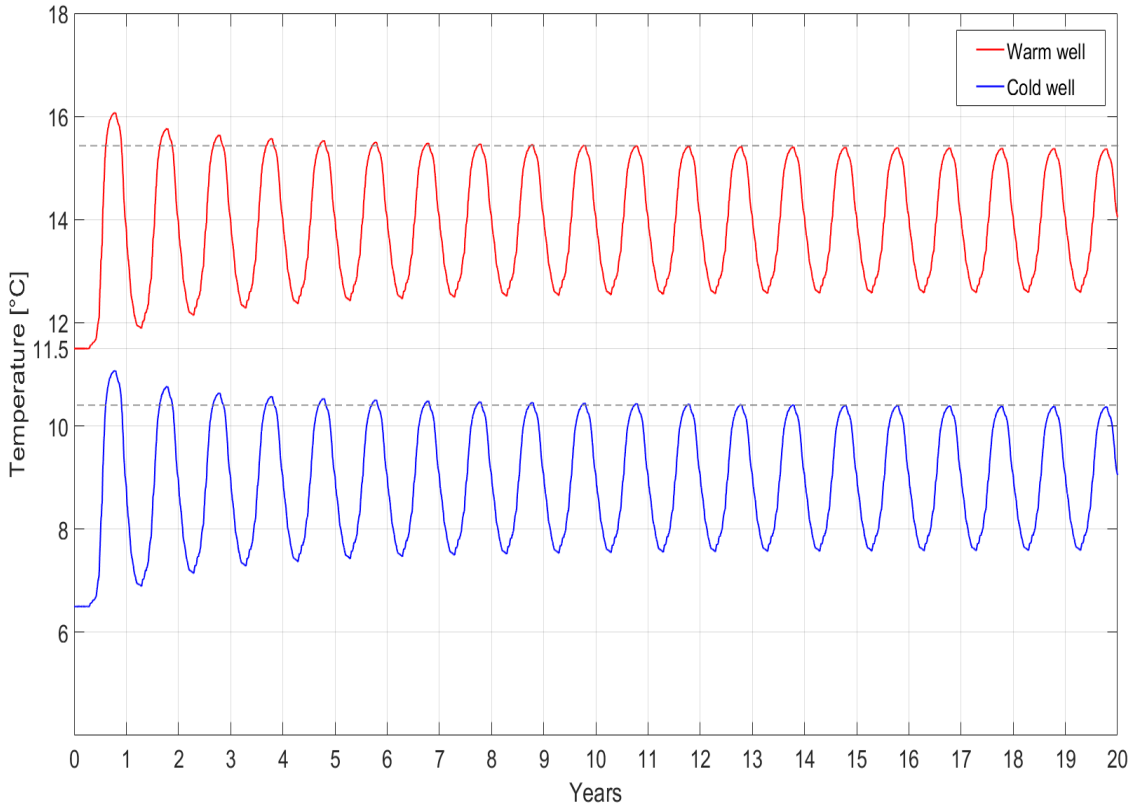

Figure 55: Balanced case, wells temperatures 20 years

In the previous mentioned figure 55, the temperature of the cold well does not reach the undisturbed ground temperature of 11.5 °C. After about the 7th year, the peak temperatures are around 15.5 °C and 10.5 °C for the hot and cold wells respectively, which corresponds to the end of the cooling season and the beginning of the heating season. This trend remains constant for the remainder of the 20-year simulation with oscillations of amplitude of 3°C.

Regarding the coefficient of performance, the range is about 3.3÷3.85 (figure 56), while the yearly operation hours are 3415 h.

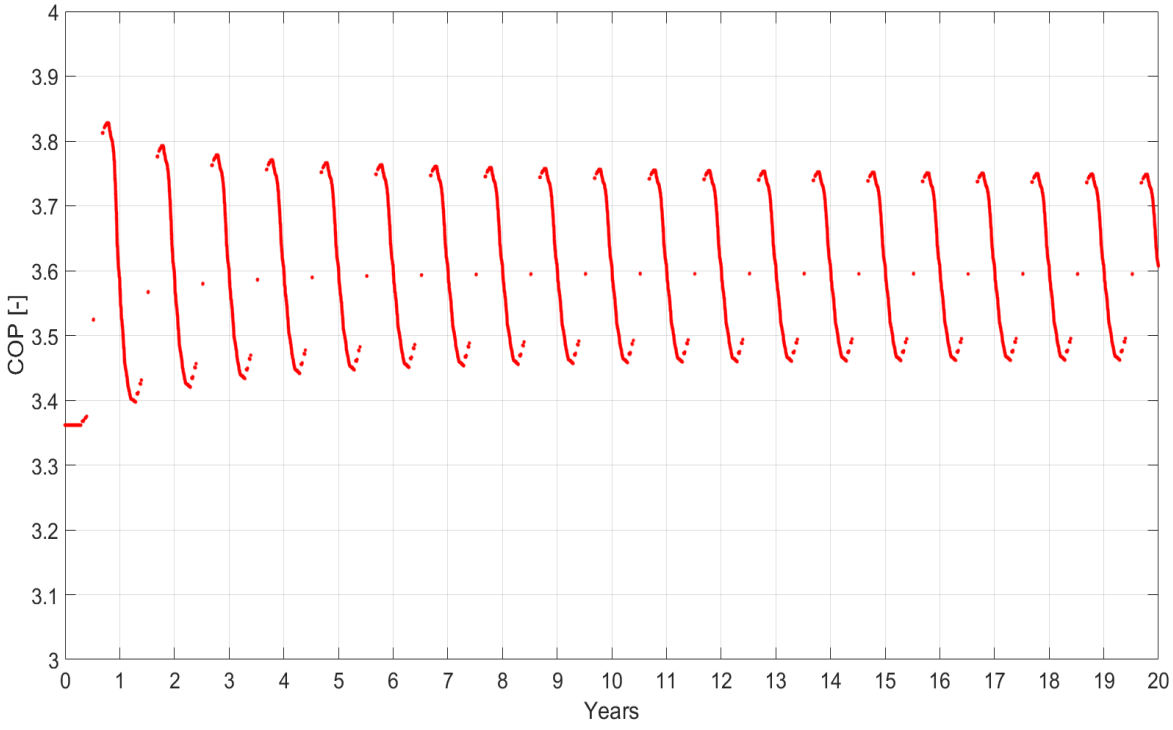

Figure 56: Balanced case, COP

The injected and extracted temperatures are reported as follows in figure 57 and 58.

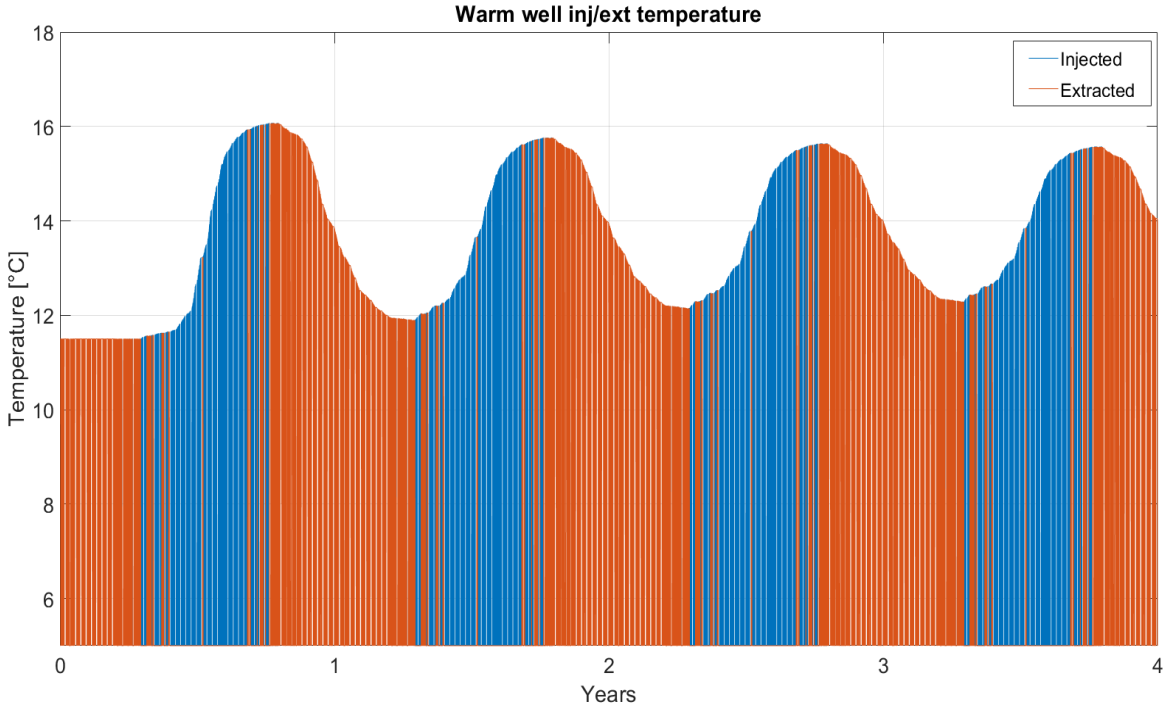

Figure 57: Balanced case, warm well inj/ext temperature

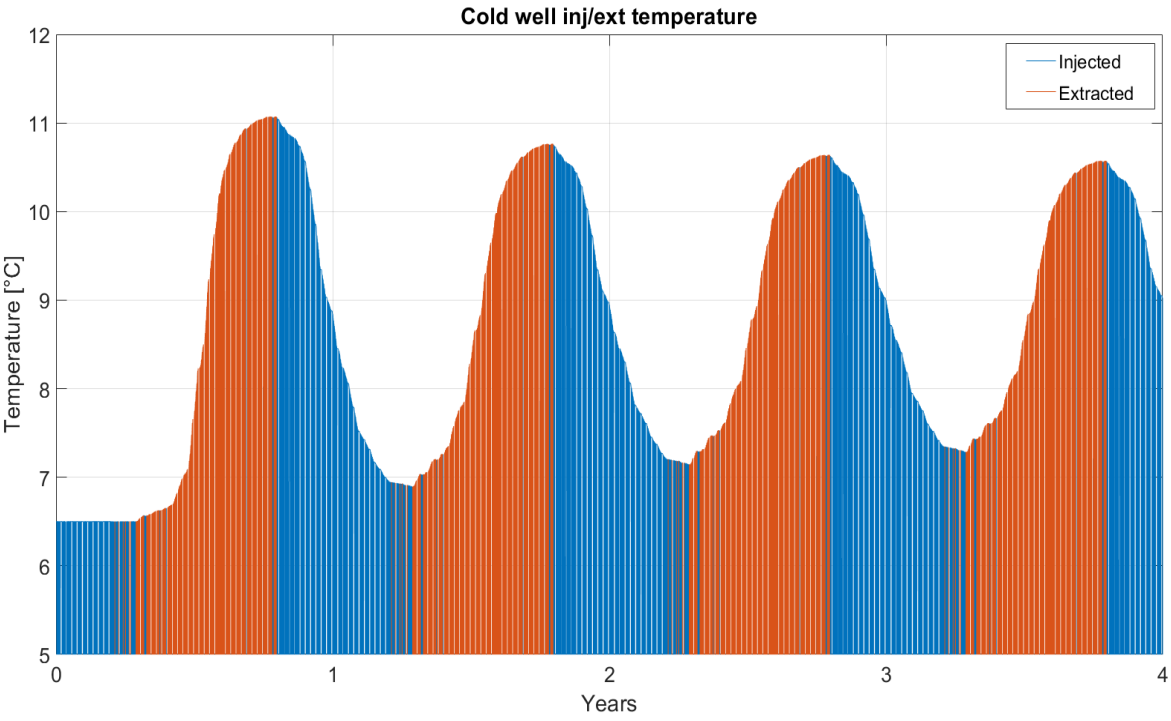

Figure 58: Balanced case, cold well inj/ext temperature

Concerning the thermal interference, the injected volume and thermal radii values are showed below in table 14.

Yearly Vol_{inj} warm well	**Yearly Vol_{inj} cold well**	**R_{th}, warm well**	**R_{th}, cold well**	**3 x Average R_{th}**
155810 m^3	153910 m^3	52 m	51.5 m	155.55 m

Table 14: Balanced case, thermal radii

In conclusion, the warm and cold aquifer temperatures at different distances from the injection site are reported in figure 59 and 60.

Wells must be placed at 155.55 m to avoid thermal interference.

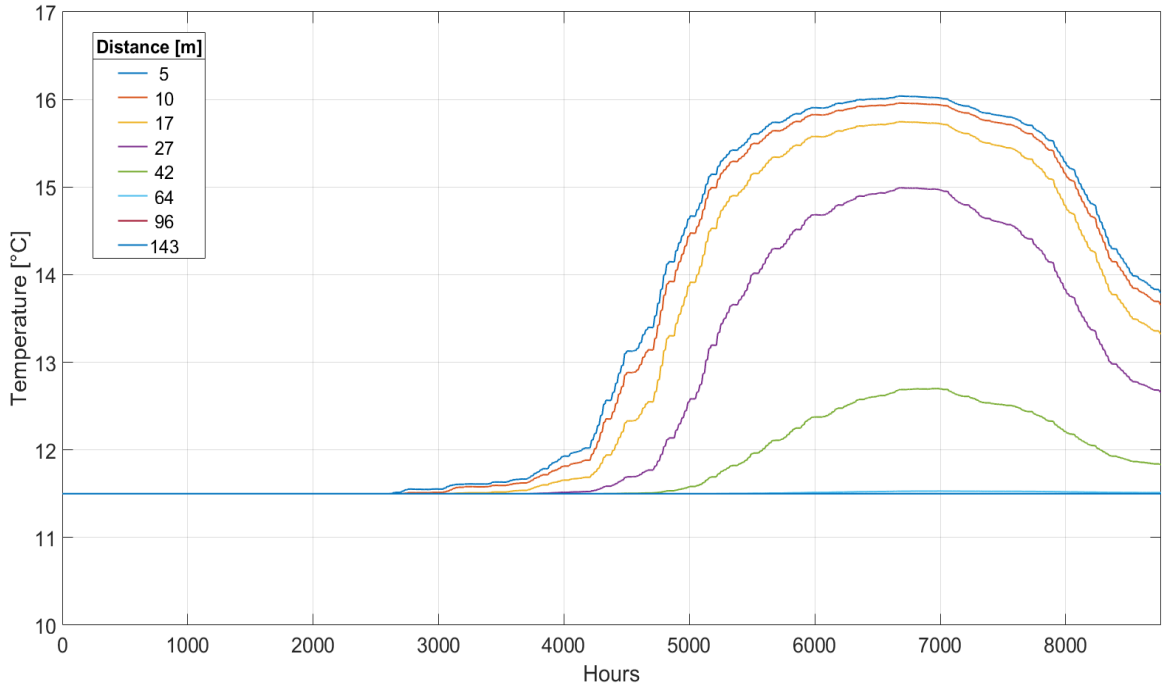

Figure 59: Balanced case, warm temp at different distance, 8760 h

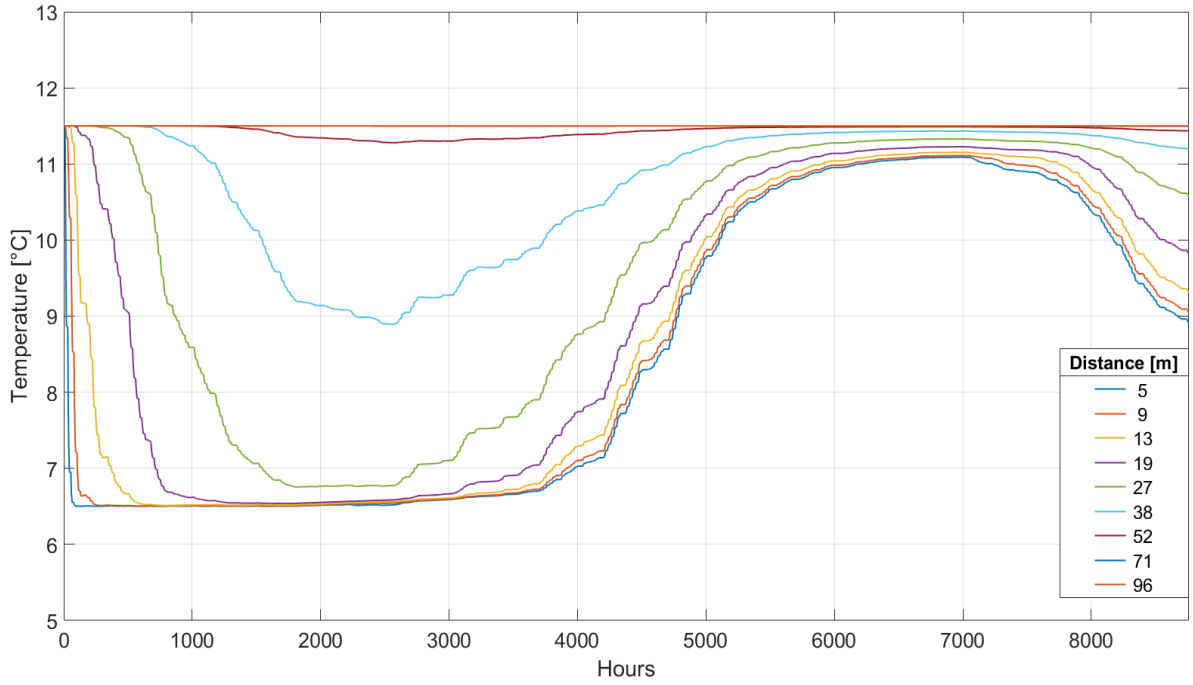

Figure 60: Balanced case, cold temp at different distance, 8760 h

4.4.3 Helsinki: heating dominant case

The third and final case analysed is a heating dominant example located in Helsinki. As the previous paragraphs, table 15 reports related information.

Undisturbed Ground Temperature/ Initial Temperature	7 °C
***EnergyPlus* multiplier**	
Internal Mass	70 %
People	60 %
Light	50 %
Electrical equipment	70 %
Yearly energy demand demands	
Heating	2114.4 MWh
Cooling	536.11 MWh

Table 15: Heating dominant case, data

Figure 61, 62 and 63 show thermal loads and air temperature, monthly energy histogram and flow rate respectively as in the previous cases.

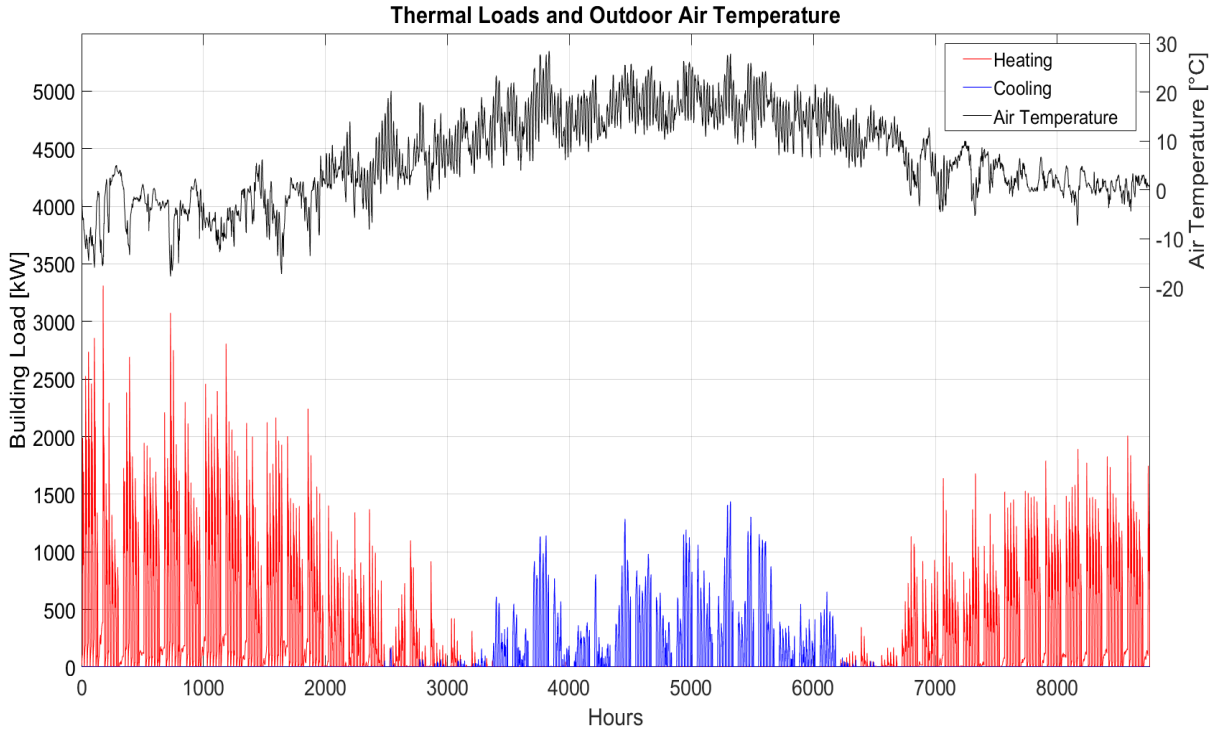

Figure 62: Heating dominant case, thermal loads and air temperature

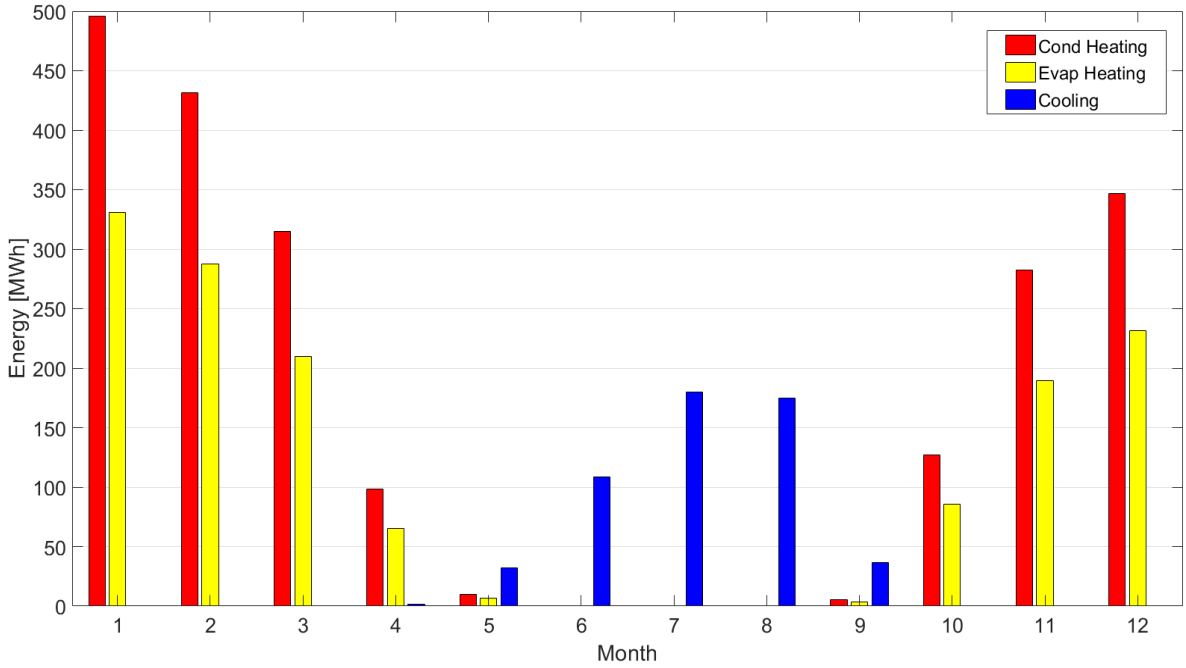

Figure 61: Heating dominant case, energy histogram

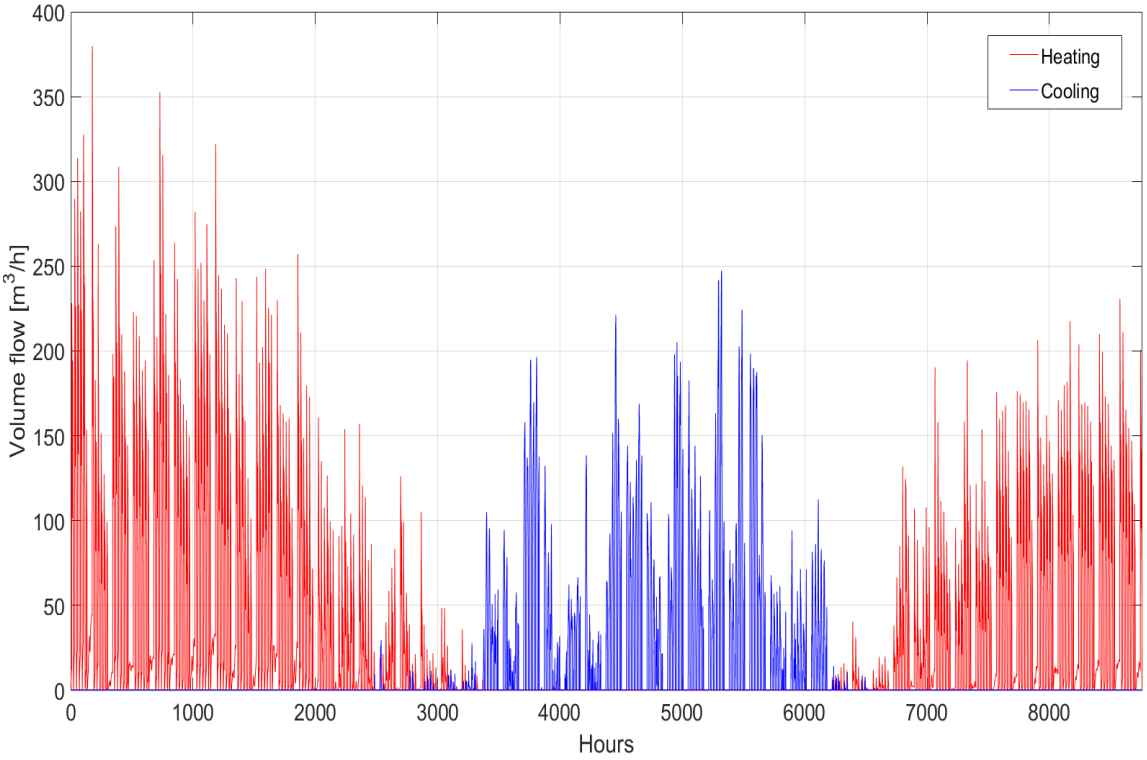

Figure 63: Heating dominant case, volumetric flow rate

As it is shown in figure 64, the heating dominant case presents a peak in temperature (8.3 / 3.3 °C, warm and cold wells) for the first year, while the trend slowly starts to decrease, highlighted for the first ten years. Due to the model's thermal load for cooling, the heat injected in the aquifer is too small to reach the temperature of the cold well close to the undisturbed ground.

Like the cooling dominant case, it seems that the trend tends to become linear after many years.

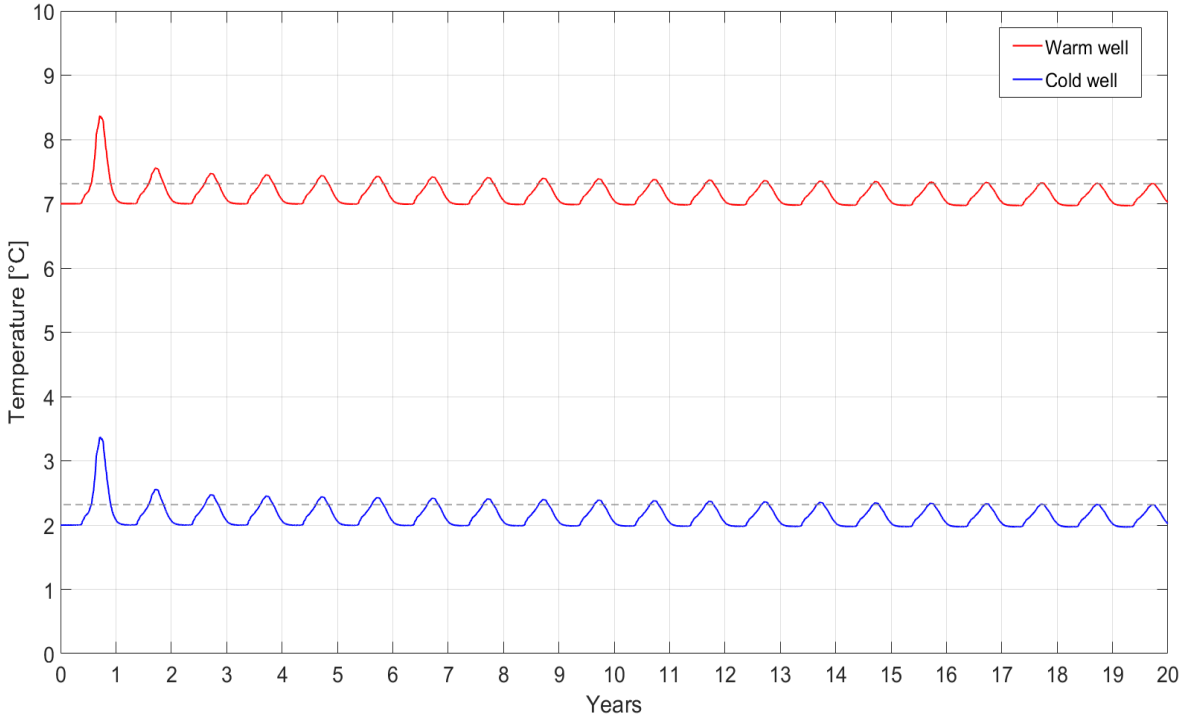

Figure 64: Heating dominant case, wells temperatures 20 years

For this case study, the coefficient of performance, shown in figure 65, takes on lower values as the evaporator side has much lower temperatures, while the annual hours of operation are 4675 h, more than half a year.

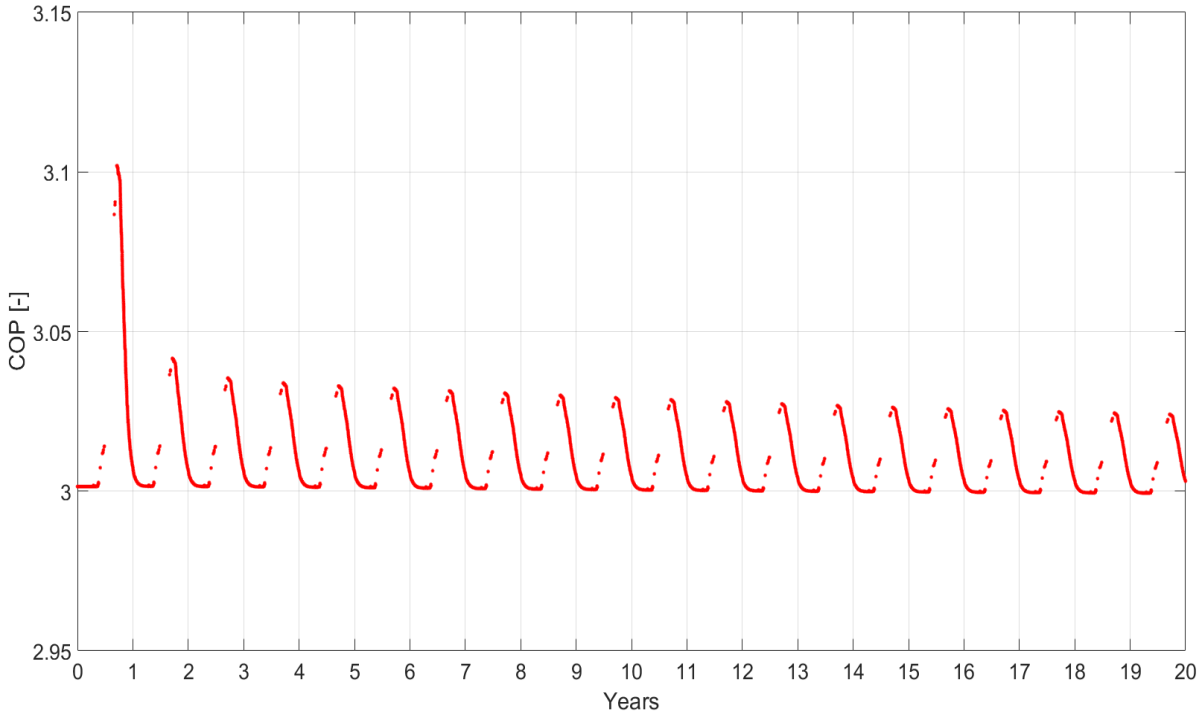

Figure 65: Heating dominant case, COP

Figure 66 and 67 reports injected and extracted water temperature for warm and cold well respectively.

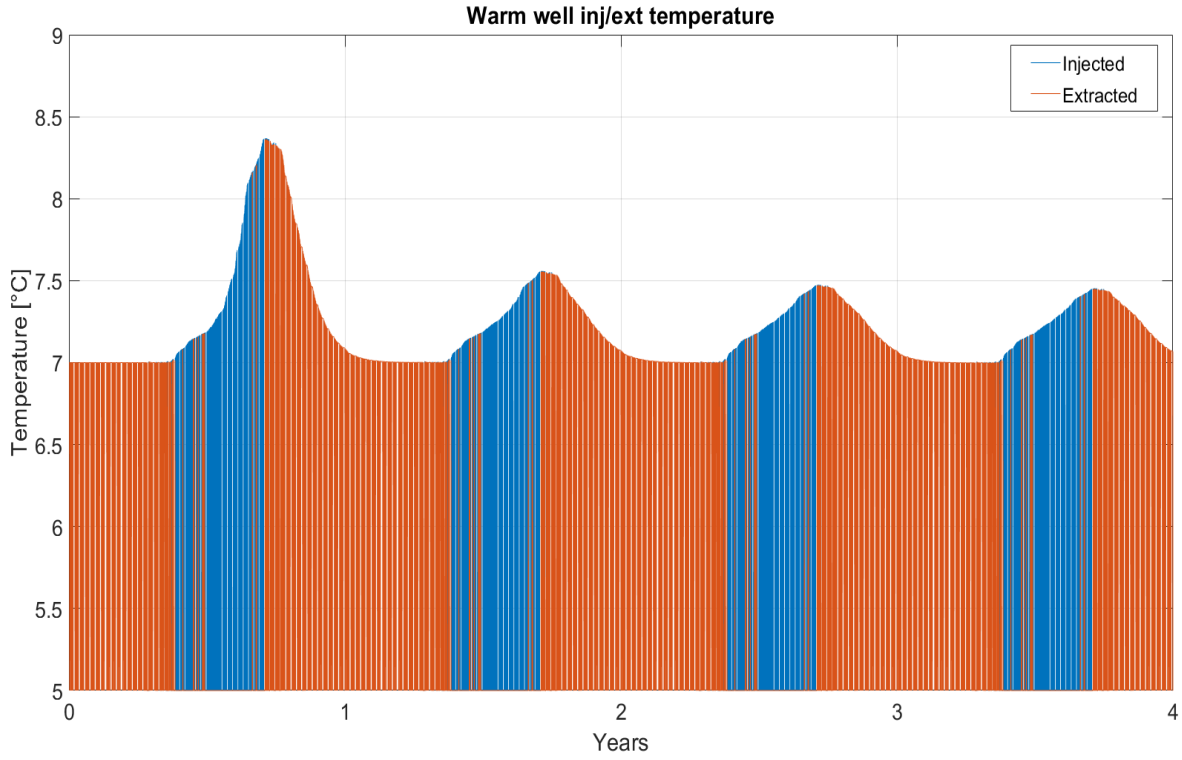

Figure 66: Heating dominant case, warm well inj/ext temperature

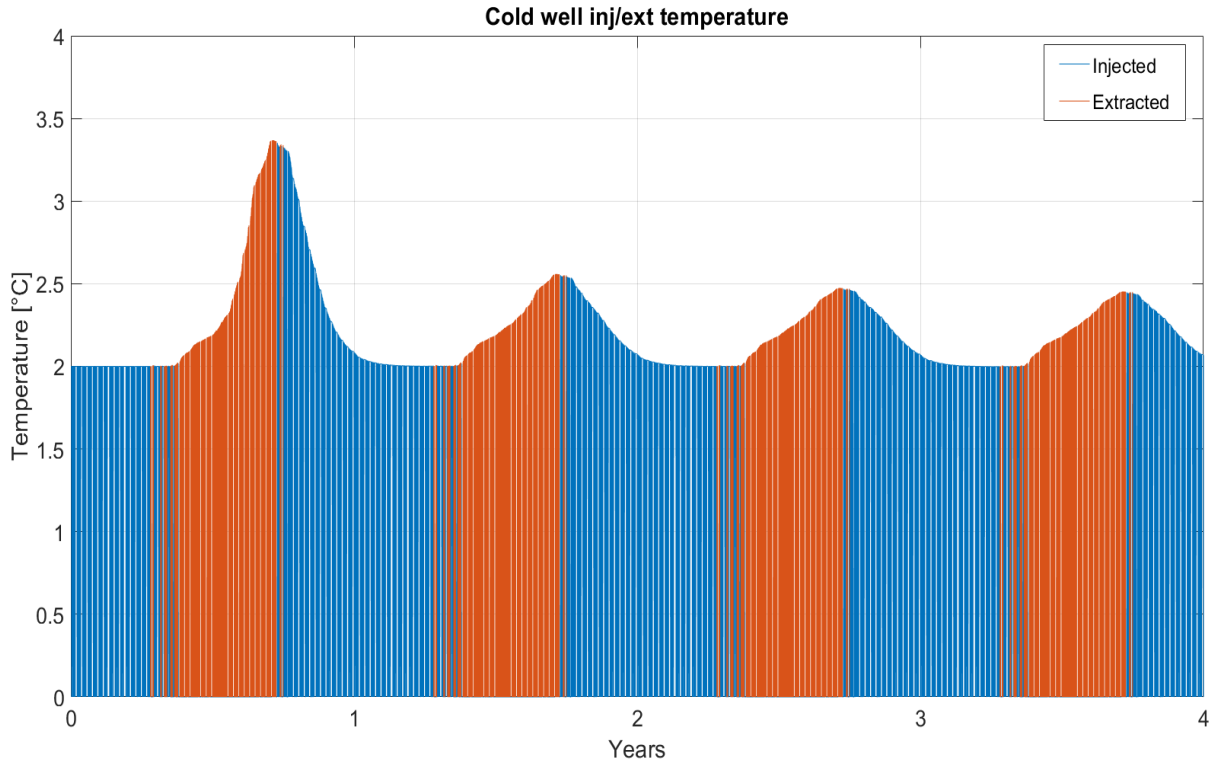

Figure 67: Heating dominant case, cold well inj/ext temperature

As with the other cases, the same considerations (reported in table 16) about the installation distance between the wells were made.

Yearly Vol_{inj} warm well	**Yearly Vol_{inj} cold well**	**R_{th}, warm well**	**R_{th}, cold well**	**3 x Average R_{th}**
91815 m^3	242710 m^3	39.88 m	64.85 m	157.2 m

Table 16: Heating dominant case, thermal radii

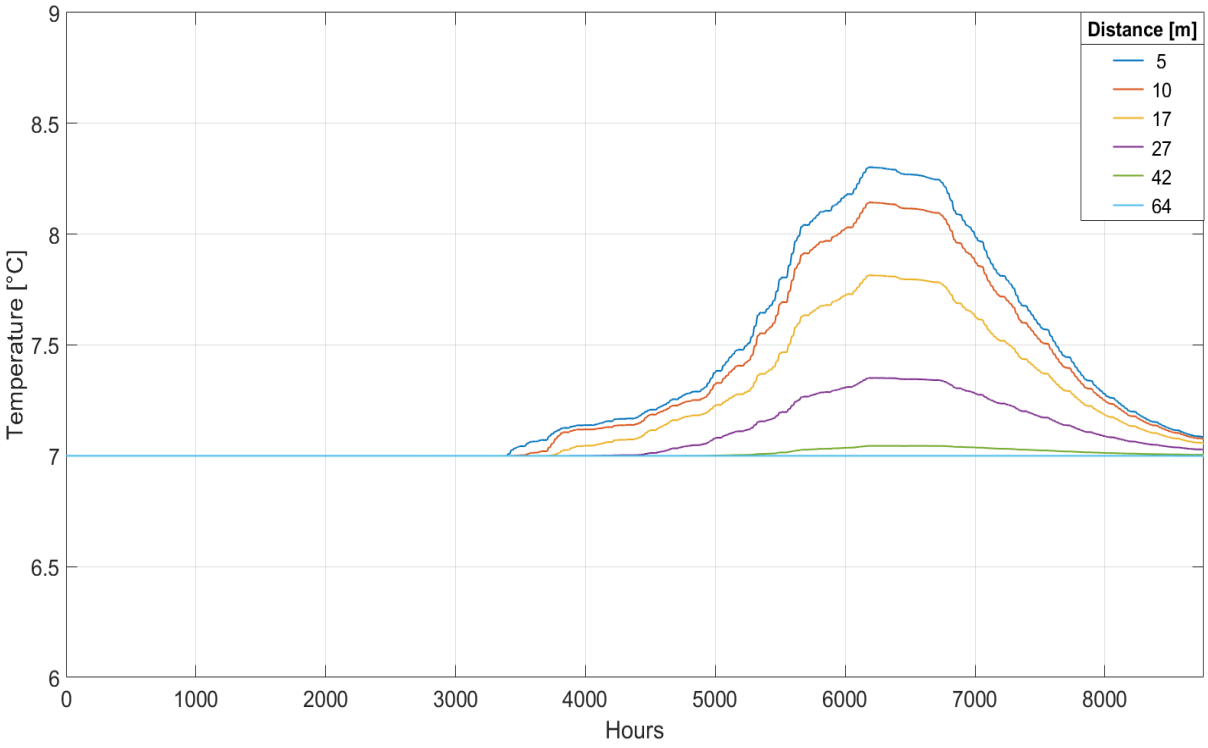

Figure 68: Heating dominant case, warm temp at different distance, 8760 h

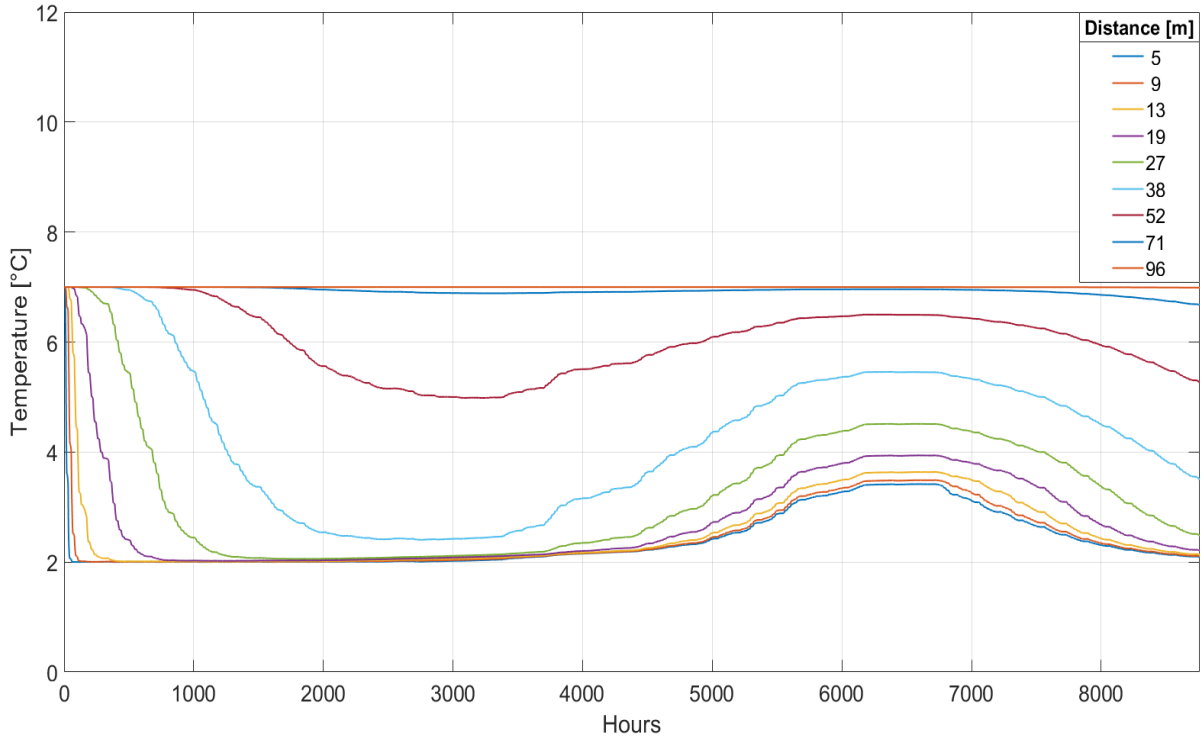

Figure 69: Heating dominant case, cold temp at different distance, 8760 h

4.4.4 Tests with different properties

Finally, several situations were analysed. Using data from the balanced case located in Frankfurt, some aquifer and system parameters were modified to examine how much temperatures changed over time.

First, different thicknesses of the aquifer (15 m, 25 m, 40 m and 50 m) have been used. The results are reported in figure 70.

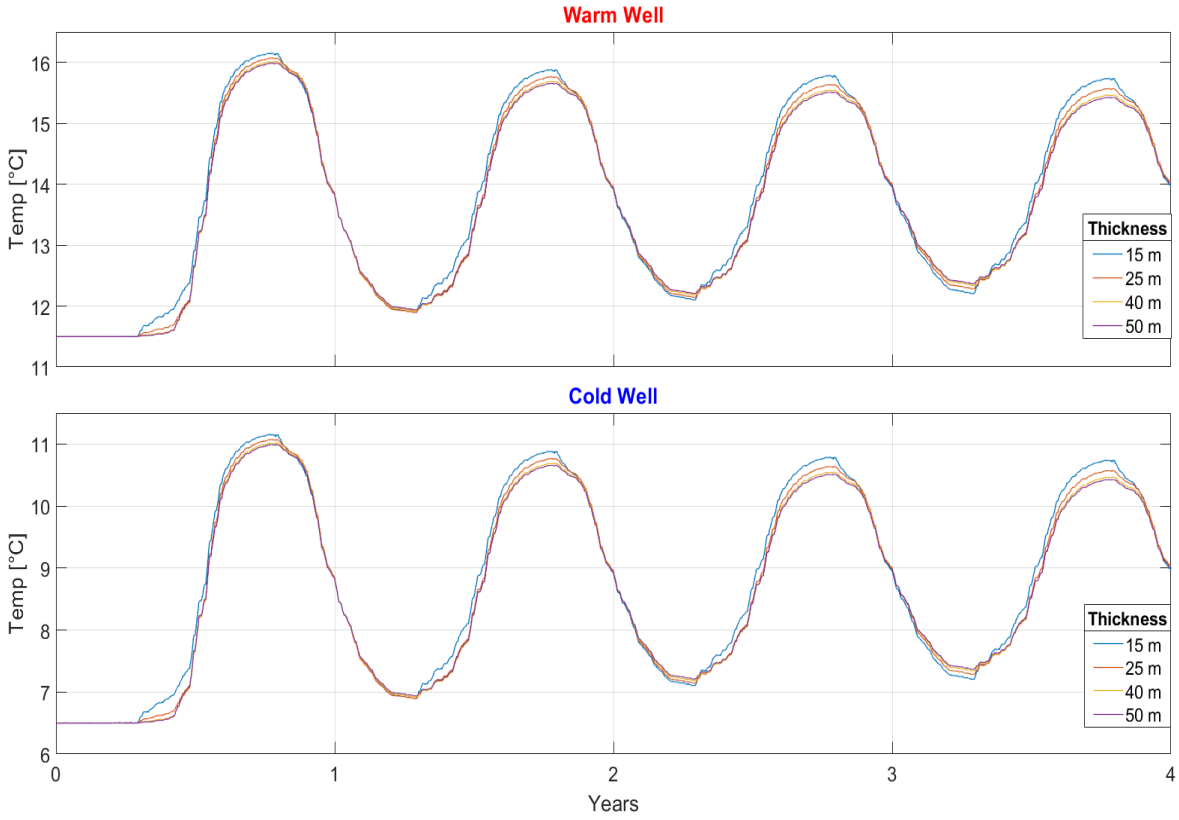

Figure 70: Balanced case, well temperatures with different aquifer thickness

In the case of different aquifer thicknesses, it is noted that:

- In the first time step (heating mode), there are no marked differences as the entire aquifer is at initial temperature coincident with the ground and the cold well assumes temperatures decreased by the constant ΔT; this will be noted in all the following cases also.
- As the thickness decreases, temperatures are slightly higher during the heating phase and lower for the cooling phase. This is explained by the smaller amount of water present and different values of capacitance (decreased due to lower annulus volumes) and thermal resistance (increased).

Similar behaviour is noted with different porosity of the aquifer (figure 71):

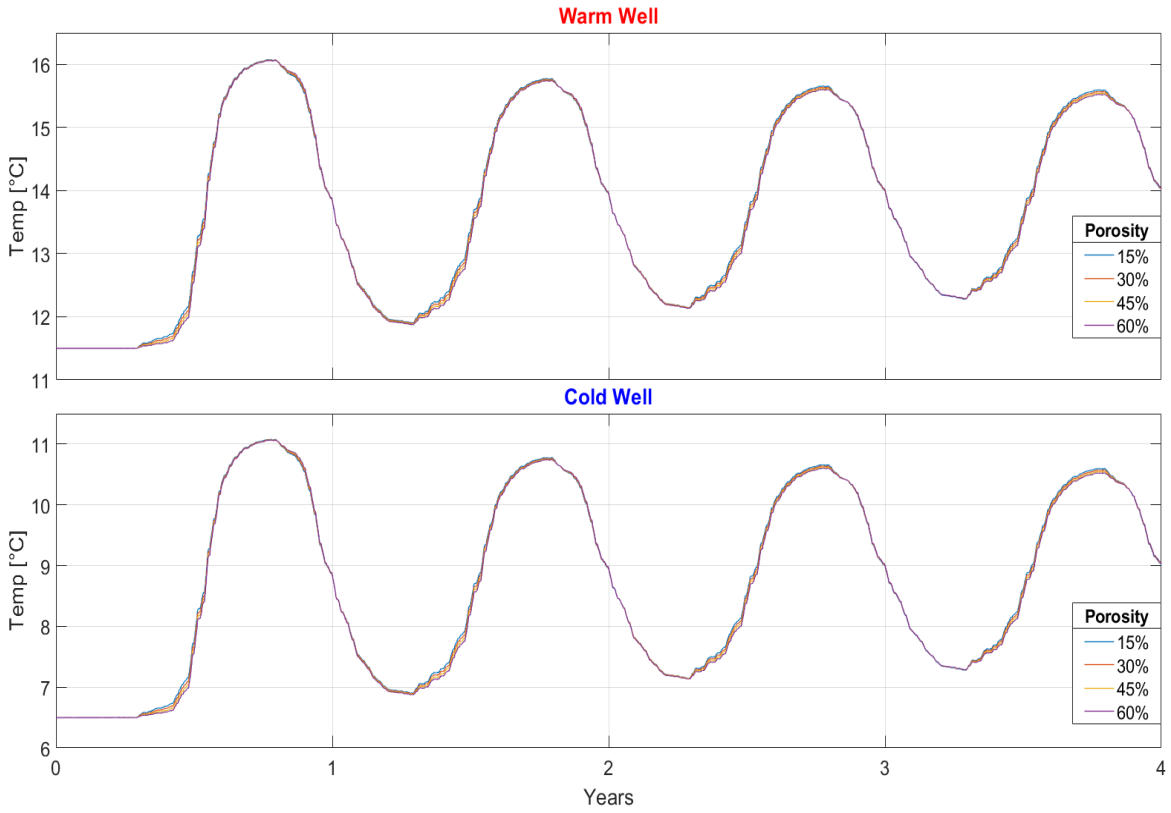

Figure 71: Balanced case, well temperatures with different aquifer porosity

When porosity increases, temperatures are slightly reduced. Increases in porosity decrease the aquifer thermal conductivity (increasing of the thermal resistance) and also increase the aquifer volumetric capacitance.

Regarding the leakage coefficient, it is important to remember how it was implemented in the model[15].

As illustrated in figure 72, as the leakages increase, so do the temperatures during the cooling phases. During summer seasons, water from the cold well is extracted, while from the last nodes of the aquifer, which are at similar temperatures to the undisturbed ground, more water flows than the nominal one

[15] See Chapter 2.7 *Water Leakages.*

(requested). This amount increases the temperature in the cold well, from which water is extracted and then injected in warm well, increasing its temperature.

During the heating period, the opposite effect happens as the leakages increase. The warm well temperature slightly decreases because more water from the last nodes comes closer to extraction site at about ground temperature, therefore decreasing the extracted temperature and also the water temperature injected into the cold well.

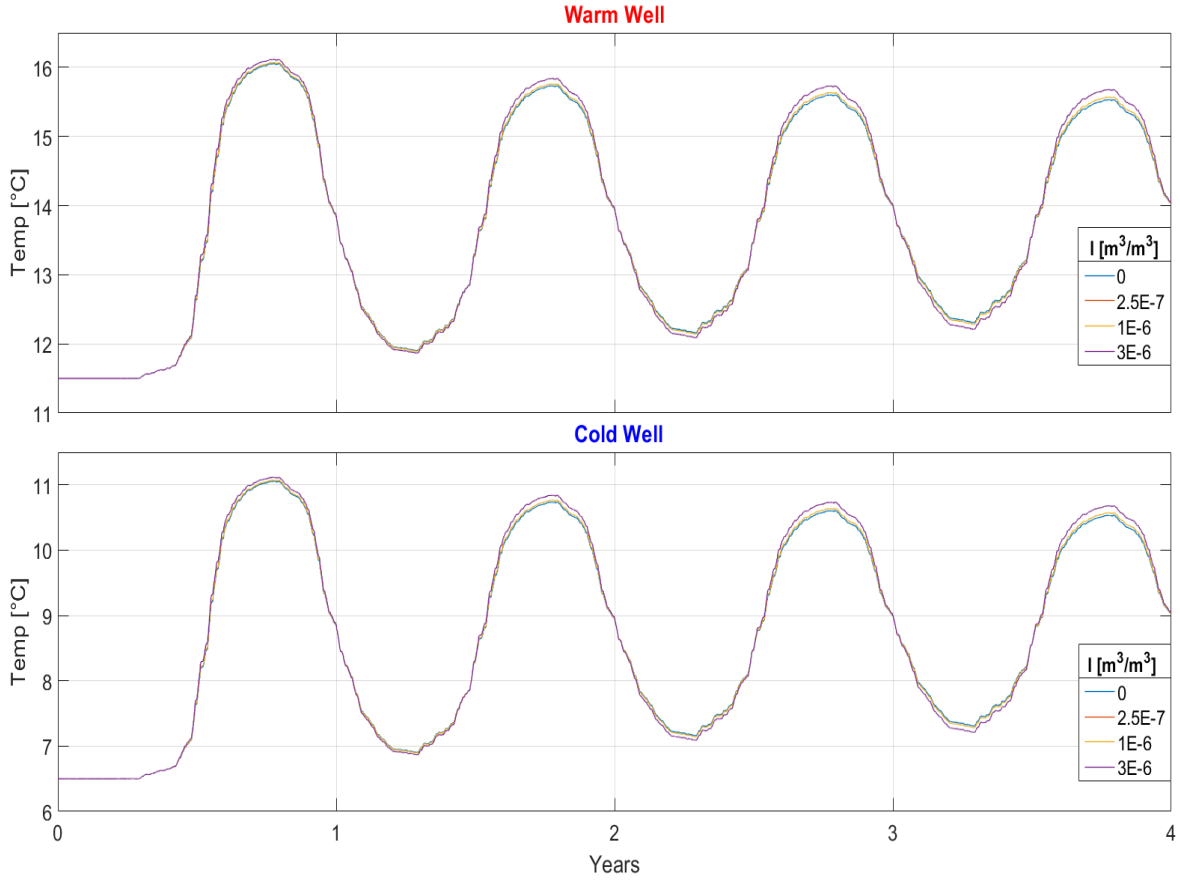

Figure 72: Balanced case, well temperatures with different leakages coef.

As it is shown in the previous figure 72, there is only a small difference between the case of neglecting the leakage equal to 2.5×10^{-7} m^3_w/m^3_{aq}, the value used for all the previous case studies performed.

The temperature differences between injected and extracted temperatures have been modified.

In figure 73, the blue lines represent the well temperatures with ΔT equal to 5°C for both heating and cooling; the trend is very linear due to this balanced value.

In case of higher cooling ΔT and lower heating ΔT, temperatures are increased due to higher injected temperature in the warm well and lower temperature in the cold one. It is vice versa for the opposite case.

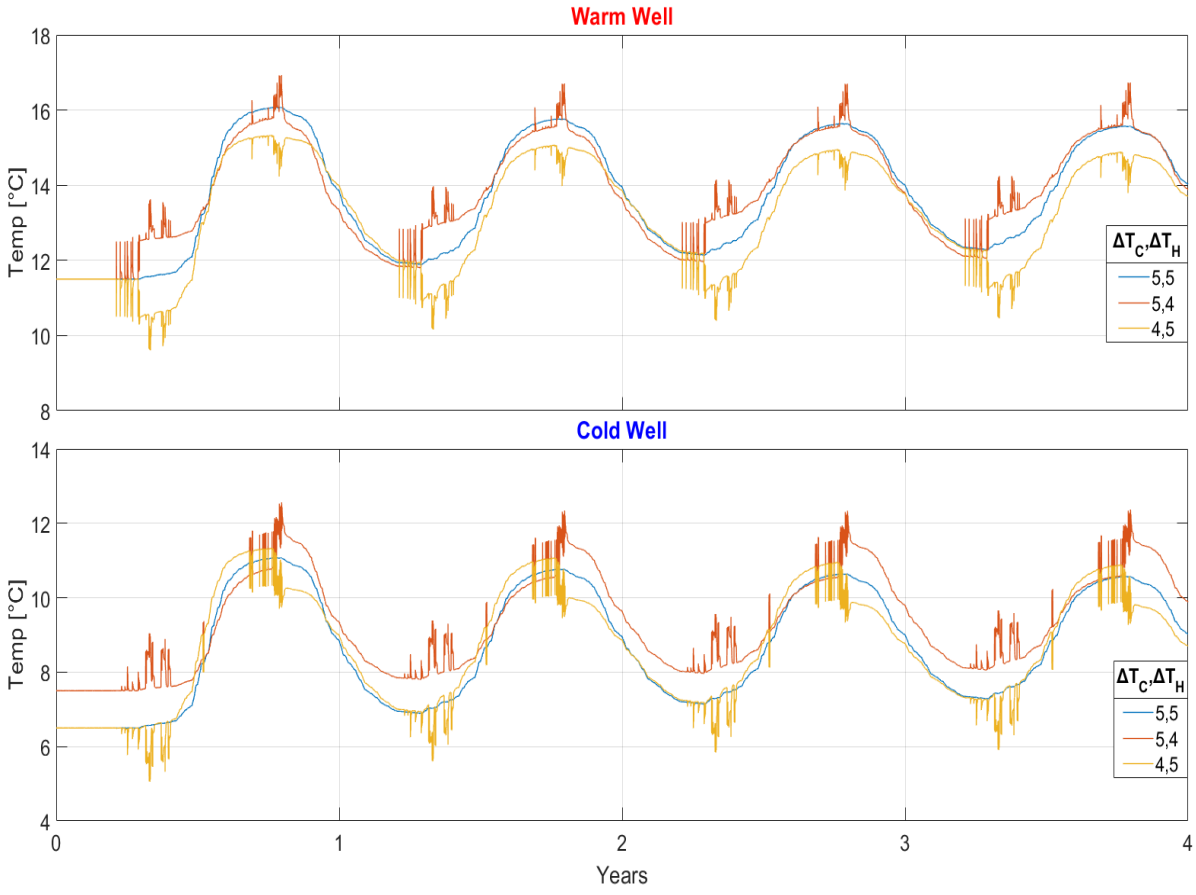

Figure 73: Balanced case, well temperatures with different ΔT

Conclusions:

The intent of this thesis has been to develop a simple and flexible aquifer thermal energy storage model for building/district energy simulation tools.

This has been possible thanks to the simple discretization used to model the aquifer system and all the assumptions made. The validations performed, especially the one with the real data of an ATES, have generated very satisfactory results, which also made it possible to analyse several hypothetical case studies in a quite accurate way using low computation effort in comparison to more complex models.

Obviously, the real design of an ATES requires fluid dynamics tools for thermohydraulic study in addition to geological and economic feasibility analyses.

The goal of this model is to provide a tool to perform "early planning" analysis of an ATES. The tool is able to be connected with data from an energy simulation that calculates the aquifer temperatures from which it is possible to get an idea of the system performance.

In the future, this model will be enhanced with a more detailed and complete design of the system, as for example adding more warm and cold ground-water wells, calculating the consumption of the submersible water pumps and the greenhouse gas emissions avoided with the ATES. Additional case studies with different conditions can be added also. Moreover, the *MATLAB* code used for the proposed model could be rewritten using different software, such as *Modelica*, which allows a more realistic simulation with an elaborated HVAC system.

In this way, the model remains simple and concise and it could be fully integrated in large-scale building and district energy tools.

Appendix: *MATLAB* code

```
% Varesano Davide, master degree in "Energy Engineering",
% Università degli Studi di Padova
% Department of Industrial Engineering
% Master thesis
% "Aquifer Thermal Energy Storage: development of a simplified model for
% building and district simulation tools"

% Main script for case studies

% General instructions:
% In loads matrix, please load an xlsx file with 3 columns respectively
% 1st Heating loads [J], 2nd Cooling loads [J], 3rd air temperature [°C]
% subscript H stands for heating, C for cooling

% Input values can be load with an excel file or inserted manually,
% in case of excel file, please take care to correctly enter the values
% in the right cells

% Please note: in case of error "Index in position 1 exceeds array bounds.
% Index must not exceed 'number of nodes, try to insert a number of nodes
% n at least 3 more than the active nodes (actnodes are calculated based
% on maximum domain radius and expansion coefficient)

clear all; close all; clc;
tic; % Starting time

loads=readmatrix('Loads_Air.csv'); % Loads

INPUT=readmatrix('input.xlsx'); % Input values,
k=size(loads,1); % [h] Time step

Q1_H=zeros(k,1); Q2_C=zeros(k,1); T_air=zeros(k,1);

for j=1:k
    Q1_H(j)=loads(j,1)/3600;  % [W]
    Q2_C(j)=loads(j,2)/3600;  % [W]
    T_air(j)=loads(j,3);      % [°C]
end

% Starting Data

r_max=INPUT(8,1);     % [m]
n=INPUT(8,2);         % [/] number of nodes (must be at least actnodes+3)
T_g=INPUT(8,3);       % [°C] Undisturbed Ground Temperature
cp_w=INPUT(1,1);      % [J/kgK] water specific heat
cp_s=INPUT(1,2);      % [J/kgK] sand specific heat
rho_s=INPUT(1,3);     % [kg/m3] sand density
rho_w=INPUT(1,4);     % [kg/m3] water density
h=INPUT(1,5);         % [m] aquifer thickness
deltaTAU=INPUT(8,4);  % [s] equal to energy simulation timestep
c_exp=INPUT(8,5);     % [/] expansion coefficient
ri1=INPUT(1,6);       % [m] grout/well radius
fi=INPUT(1,7);        % [/] porosity
```

```
lambda_w=INPUT(1,8);  % [W/m K]
lambda_s=INPUT(1,9);  % [W/m K]
lambda_aq= fi*lambda_w+(1-fi)*lambda_s; % [W/m K]

V=zeros(n,1);  % Volume array
R=zeros(n,1);  % Thermal resistances array
C=zeros(n,1);  % Thermal capacities array
s=zeros(n,1);  % annulus thickness [m]
re=zeros(n,1); % Ext radius
actnodes=0;    % active nodes
% (inside the r_max boundary, where are placed the lumped parameters)

l=INPUT(8,6); % leakage coef.

% Axial layers

lambda1=INPUT(15,3); lambda2=INPUT(16,3);
lambda3=INPUT(18,3); lambda4=INPUT(19,3);

h1=INPUT(15,4); h2=INPUT(16,4);
h3=INPUT(18,4); h4=INPUT(19,4);

R1=0.5*h1/lambda1*(1/(pi*r_max)^2); % Thermal Resistances
R2=0.5*h2/lambda2*(1/(pi*r_max)^2);
R3=0.5*h3/lambda3*(1/(pi*r_max)^2);
R4=0.5*h4/lambda4*(1/(pi*r_max)^2);

C_sp1=INPUT(15,5); C1=C_sp1*(pi*r_max^2*h1);
C_sp2=INPUT(16,5); C2=C_sp2*(pi*r_max^2*h2);
C_sp3=INPUT(18,5); C3=C_sp3*(pi*r_max^2*h3);
C_sp4=INPUT(19,5); C4=C_sp4*(pi*r_max^2*h4);

% Plant Data

T_WLC=INPUT(26,1);   % [°C] Water temp leaving the condenser in heating mode
DT_H=INPUT(26,2); DT_C=INPUT(26,3); % fixed deltaT
eta_c=INPUT(26,4);   % Carnot efficiency
DT_pp=INPUT(26,5);   % deltaT pinch point

COP_H=NaN(k,1);
Q2_H=zeros(k,1);  V_flowH=zeros(k,1); Q1_Hn=zeros(k,1); Q2_Cn=zeros(k,1);
Q1_C=zeros(k,1);  V_flowC=zeros(k,1); T_inj2=zeros(k,1); T_inj1=zeros(k,1);

% Calculation of active nodes
r2=ri1;
s0=c_exp*ri1;
for i=1:n
    s(i,1)=s0*c_exp;
    r_ext(i)=r2+s(i,1);
    s0=s(i,1);
    r2=r_ext(i);
end
r_ext=r_ext';

s1=c_exp*ri1;
for i=1:n+1 % loop for calculation of thermal resistances and capacities
  while re<=r_max
```

```
  actnodes=actnodes+1;

  % Axial thermal Resistances
  ri(actnodes)=ri1;
  re(actnodes)=ri1+s1;

  for o=1:actnodes-1
  R_ax(o)=h/lambda_aq/(2*pi*(re(o).^2-ri(o).^2));  % axial
  end

  s(actnodes,1)=c_exp*s1;
  r_M(actnodes)=((re(actnodes).^2+ri1^2)./2).^0.5;  % baricentric radius
  V(actnodes)=pi*h*(re(actnodes).^2-ri1.^2);
  C_s_aq=fi*rho_w*cp_w+(1-fi)*rho_s*cp_s; % aquifer volumetric heat capacity
  C(actnodes)=C_s_aq*V(actnodes);

  if actnodes==1
  R(1)=log(r_M(actnodes)/ri1)/(2*pi*lambda_aq*h); %1st thermal resistance
  else
  o=r_M(actnodes);
  d=r_M(actnodes-1);
  R(actnodes)=log(o/d)/(2*pi*lambda_aq*h);
  end
  s1=s(actnodes);
  ri1=re(actnodes);
  end
end
r_M=r_M';

r_M=r_M([1:actnodes-1],1);
r_M2=[INPUT(1,6);r_M];     % + well radius
V=V([1:actnodes],1);
R=R([1:actnodes],1);
C=C([1:actnodes-1],1);

Tp_1=T_g.*ones(n,1);  % [°C] initial temperature warm well
Tp_2=T_g.*ones(n,1);  % [°C] initial temperature cold well
Tg_1=Tp_1([1:(actnodes+3)],1); % Starting temperature
Tg_2=Tp_2([1:(actnodes+3)],1);

R0=R(1);

% Construction of the matrix system
A1=zeros(actnodes-1,2);
A12=zeros(actnodes-1,2);

for i=1:actnodes-1
    R_2(i)=1/(R_ax(i)+R2);
    R_3(i)=1/(R_ax(i)+R3);
    A1(i,2)=R_2(i);
    A12(i,1)=R_3(i);
end

B1=zeros(2,actnodes+3);
B1(1,1)=-1/R1-1/(R1+R2)-C1/deltaTAU;
B1(1,2)=1/(R1+R2);
B1(2,1)=1/(R1+R2);
```

```
d=0;
for i=1:actnodes-1
    f=R_ax(i);
        d=-1/(R2+f)+d;
end
B1(2,2)=-1/(R1+R2)+d-C2/deltaTAU;

for i=1:actnodes-1
    B1(2,2+i)=R_2(i);
end
B2=zeros(2,actnodes+3);
B2(2,actnodes+3)=-1/R4-1/(R3+R4)-C4/deltaTAU;
B2(2,actnodes+2)=1/(R3+R4);
B2(1,actnodes+3)=1/(R3+R4);
d=0;

for i=1:actnodes-1
    f=R_ax(i);
        d=-1/(R3+f)+d;
end
B2(1,actnodes+2)=-1/(R3+R4)+d-C3/deltaTAU;

for i=1:actnodes-1
    B2(1,2+i)=R_3(i);
end
B1w=zeros(2,actnodes+4);
B1w(1,1)=-1/R1-1/(R1+R2)-C1/deltaTAU;
B1w(1,2)=1/(R1+R2);
B1w(2,1)=1/(R1+R2);
d=0;

for i=1:actnodes-1
    f=R_ax(i);
        d=-1/(R2+f)+d;
end
B1w(2,2)=-1/(R1+R2)+d-C2/deltaTAU;

for i=1:actnodes-1
    B1w(2,3+i)=R_2(i);
end
B2w=zeros(2,actnodes+4);
B2w(2,actnodes+4)=-1/R4-1/(R3+R4)-C4/deltaTAU;
B2w(2,actnodes+3)=1/(R3+R4);
B2w(1,actnodes+4)=1/(R3+R4);

for i=1:actnodes-1
    B2w(1,3+i)=R_3(i);
end
d=0;

for i=1:actnodes-1
    f=R_ax(i);
        d=-1/(R3+f)+d;
end
B2w(1,actnodes+3)=-1/(R3+R4)+d-C3/deltaTAU;

for i=1:actnodes-1
```

```
    R_2w(i)=1/(R_ax(i)+R2);
    R_3w(i)=1/(R_ax(i)+R3);
    A1w(1,2)=0;
    A1w(i+1,2)=R_2w(i);
    A12w(1,2)=0;
    A12w(i+1,1)=R_3w(i);
    A12w(i,2)=0;
end

for i=1:k

% Heating period (Heat Pump)

 if Q1_H(i)>Q2_C(i)
    Q1_Hn(i)=Q1_H(i)-Q2_C(i);   % simultaneous load --> heat recover
    % Q1_Hn= load without opposite (minimum) load
    COP_H(i)=eta_c*(T_WLC+273.15+DT_pp)/(T_WLC+DT_pp-(Tg_1(3)-DT_H-DT_pp));
    Q2_H(i)=Q1_Hn(i)*(1-1/COP_H(i));
    V_flowH(i)=Q2_H(i)/(rho_w*cp_w*DT_H);

for w=1:actnodes
    V_flowHW(i,w)=V_flowH(i)*(1+V(w)*l); % Withdrawal
    V_flowHI(i,w)=V_flowH(i)*(1-V(w)*l); % Injection
end


% Withdraw from warm well

    for w = 2: actnodes
        a=R(w);
        b=R(w-1);
        aa=C(w-1);
        bb=R_ax(w-1);
  W(w,w)=-1/a-1/b-rho_w*cp_w*V_flowHW(i,w)-aa/deltaTAU-1/(bb+R2)-1/(bb+R3);
  W(w+1,w)=1/a;
  W(w,w+1)=1/a+rho_w*cp_w*V_flowHW(i,w);

  W(1,1)=-1/R0-rho_w*cp_w*V_flowHW(i,1);
  W(1,2)=1/R0+rho_w*cp_w*V_flowHW(i,1);
  W(2,1)=1/R0;

  end

  W=W([1:actnodes],[1:actnodes]);
    A3_F=[A1w,W];       % WITH NEW MATRIX
    A3_F=[A3_F,A12w];
    A3_F=[B1w;A3_F];    % + UPPER PART
    A3_F=[A3_F;B2w];    % + LOWER PART

for w=1:actnodes+4
           if w==1
            z=Tg_1(w);
           bw(w,1)=-T_air(i)/R1-C1/deltaTAU*z;   % Top node
        elseif w==2
            z=Tg_1(w);
           bw(w,1)=-C2/deltaTAU*z;               % Top aquifer
        elseif w==3
```

```
            bw(w,1)= 0;                              % Start
         elseif w==actnodes+2
             z=Tg_1(w-1);
             p=C(w-3);
            bw(w,1)= -T_g/R(actnodes)-p/deltaTAU*z-rho_w.../// 
                *cp_w*V_flowHW(i,actnodes)*T_g;             % End
         elseif w==actnodes+3
             z=Tg_1(w-1);
            bw(w,1)=-C3/deltaTAU*z;                  % Down aquif
         elseif w==actnodes+4
             z=Tg_1(w-1);
            bw(w,1)= -T_g/R4-C4/deltaTAU*z;          % Down node
         else
             z=Tg_1(w-1);
             p=C(w-3);
            bw(w,1)=-p/deltaTAU*z;                   % Central
         end
end

x=A3_F\bw;
Tg_1=[x(1:2);x(4:actnodes+4)];
D(i,2:actnodes+5)=x;

% Injection to cold well

for w = 1: actnodes-1
    A(w,w)= -1/R(w)-1/R(w+1)- C(w)/deltaTAU-rho_w*cp_w*V_flowHI(i,w).../// 
        -1/(R_ax(w)+R2)-1/(R_ax(w)+R3);
    A(w+1,w)=1/R(w+1)+rho_w*cp_w*V_flowHI(i,w+1);
    A(w,w+1) =1/R(w+1);
end

A=A([1:actnodes-1],[1:actnodes-1]);
A1_F=[A1,A];         % INJ NEW MATRIX
A1_F=[A1_F,A12];
A1_F=[B1;A1_F];      % + UPPER PART
A1_F=[A1_F;B2];      % + LOWER PART

T_inj2(i)=Tg_1(3)-DT_H; % Temperature of injected water

for w=1:actnodes+3
          if w==1
            b1(w,1)=-T_air(i)/R1-C1/deltaTAU*Tg_2(w);    % Top node
         elseif w==2
            b1(w,1)=-C2/deltaTAU*Tg_2(w);                % Top aquifer
         elseif w==3
            b1(w,1)= -T_inj2(i)/R0-C(1)/deltaTAU*Tg_2(w)-.../// 
                rho_w*cp_w*V_flowHI(i,1)*T_inj2(i); % Start
         elseif w==actnodes+1
            b1(w,1)= -T_g/R(actnodes)-C(actnodes-1)/deltaTAU*Tg_2(w); % End
         elseif w==actnodes+2
            b1(w,1)=-C3/deltaTAU*Tg_2(w);                % Down aquif
         elseif w==actnodes+3
            b1(w,1)= -T_g/R4-C4/deltaTAU*Tg_2(w);        % Down node
         else
            b1(w,1)=-C(w-2)/deltaTAU*Tg_2(w);            % Central
         end
```

```
   end
x=A1_F\b1;
Tg_2=x;
E(i,2:3)=x(1:2);
E(i,4)=T_inj2(i);
E(i,5:actnodes+5)=x(3:actnodes+3);

% Cooling period (Heat Exchanger)

  elseif Q2_C(i)>Q1_H(i)
         Q2_Cn(i)=Q2_C(i)-Q1_H(i); % heat recovery
         Q1_C(i)=Q2_Cn(i);
         V_flowC(i)=Q1_C(i)/(rho_w*cp_w*DT_C);

for w=1:actnodes
    V_flowCW(i,w)=V_flowC(i)*(1+V(w)*l); % Withdrawal
    V_flowCI(i,w)=V_flowC(i)*(1-V(w)*l); % Injection
end

% Withdraw from cold well

    for w = 2: actnodes
        a=R(w);
        b=R(w-1);
        aa=C(w-1);
        bb=R_ax(w-1);
  W(w,w)=-1/a-1/b-rho_w*cp_w*V_flowCW(i,w)-aa/deltaTAU-1/(bb+R2)-1/(bb+R3);
  W(w+1,w)=1/a;
  W(w,w+1)=1/a+rho_w*cp_w*V_flowCW(i,w);

  W(1,1)=-1/R0-rho_w*cp_w*V_flowCW(i,1);
  W(1,2)=1/R0+rho_w*cp_w*V_flowCW(i,1);
  W(2,1)=1/R0;
    end

  W=W([1:actnodes],[1:actnodes]);
    A3_F=[A1w,W];
    A3_F=[A3_F,A12w];
    A3_F=[B1w;A3_F];
    A3_F=[A3_F;B2w];

for w=1:actnodes+4
            if w==1
            z=Tg_2(w);
           bw(w,1)=-T_air(i)/R1-C1/deltaTAU*z;      % Top node
        elseif w==2
            z=Tg_2(w);
           bw(w,1)=-C2/deltaTAU*z;                  % Top aquif
        elseif w==3
           bw(w,1)= 0;                              % Start
        elseif w==actnodes+2
            z=Tg_2(w-1);
            p=C(w-3);
           bw(w,1)= -T_g/R(actnodes)-p/deltaTAU*z-.../// 
               rho_w*cp_w*V_flowCW(i,actnodes)*T_g;  % End
        elseif w==actnodes+3
            z=Tg_2(w-1);
```

```
            bw(w,1)=-C3/deltaTAU*z;                % Down aquif
        elseif w==actnodes+4
            z=Tg_2(w-1);
            bw(w,1)= -T_g/R4-C4/deltaTAU*z;       % Down node
        else
            z=Tg_2(w-1);
            p=C(w-3);
            bw(w,1)=-p/deltaTAU*z;                 % Central
        end
    end
x=A3_F\bw;
Tg_2=[x(1:2);x(4:actnodes+4)];
E(i,2:actnodes+5)=x;

% Injection to warm well

for w = 1: actnodes-1
    A(w,w)= -1/R(w)-1/R(w+1)- C(w)/deltaTAU-rho_w*cp_w*V_flowCI(i,w)...///
        -1/(R_ax(w)+R2)-1/(R_ax(w)+R3);
    A(w+1,w)=1/R(w+1)+rho_w*cp_w*V_flowCI(i,w+1);
    A(w,w+1) =1/R(w+1);
end


A=A([1:actnodes-1],[1:actnodes-1]);
A1_F=[A1,A];
A1_F=[A1_F,A12];
A1_F=[B1;A1_F];
A1_F=[A1_F;B2];


T_inj1(i)=Tg_2(3)+DT_C; % temperature of injected water

for w=1:actnodes+3
          if w==1
            b1(w,1)=-T_air(i)/R1-C1/deltaTAU*Tg_1(w);      % Top node
        elseif w==2
            b1(w,1)=-C2/deltaTAU*Tg_1(w);               % Top node
        elseif w==3
            b1(w,1)= -T_inj1(i)/R0-C(1)/deltaTAU*Tg_1(w)...///
                -rho_w*cp_w*V_flowCI(i,1)*T_inj1(i);      %  Start
        elseif w==actnodes+1
            b1(w,1)= -T_g/R(actnodes)-C(actnodes-1)/deltaTAU*Tg_1(w); % End
        elseif w==actnodes+2
            b1(w,1)=-C3/deltaTAU*Tg_1(w);               % Down aquif
        elseif w==actnodes+3
            b1(w,1)= -T_g/R4-C4/deltaTAU*Tg_1(w);      % Down node
        else
            b1(w,1)=-C(w-2)/deltaTAU*Tg_1(w);           % Central
        end
    end
x=A1_F\b1;
Tg_1=x;
D(i,2:3)=x(1:2);
D(i,4)=T_inj1(i);
D(i,5:actnodes+5)=x(3:actnodes+3);
```

```
% Storage

elseif Q1_H(i)==0 && Q2_C(i)==0
for w = 1: actnodes-1
    S(w,w)= -1/R(w)-1/R(w+1)- C(w)/deltaTAU-rho_w*cp_w*0-.../// 
        1/(R_ax(w)+R2)-1/(R_ax(w)+R3);
    S(w+1,w)=1/R(w+1)+rho_w*cp_w*0;
    S(w,w+1) =1/R(w+1);
end


S=S([1:actnodes-1],[1:actnodes-1]);
A2_F=[A1,S];        % STORAGE NEW MATRIX
A2_F=[A2_F,A12];
A2_F=[B1;A2_F];
A2_F=[A2_F;B2];

% Warm well
for w=1:actnodes+3
        if w==1
           b2(w,1)=-T_air(i)/R1-C1/deltaTAU*Tg_1(w);   % Top node
        elseif w==2
           b2(w,1)=-C2/deltaTAU*Tg_1(w);          % Top aquif
        elseif w==3
           b2(w,1)= -Tg_1(w)/R0-C(1)/deltaTAU*Tg_1(w)-.../// 
               rho_w*cp_w*0*Tg_1(w); % start
        elseif w==actnodes+1
           b2(w,1)= -T_g/R(actnodes)-C(actnodes-1)/deltaTAU*Tg_1(w); % End
        elseif w==actnodes+2
           b2(w,1)=-C3/deltaTAU*Tg_1(w);         % Down aquif
        elseif w==actnodes+3
           b2(w,1)= -T_g/R4-C4/deltaTAU*Tg_1(w);  % Down node
        else
           b2(w,1)=-C(w-2)/deltaTAU*Tg_1(w);  % Central
        end
    end

x=A2_F\b2;  % array temperature at time step P
Tg_1=x;
D(i,2:3)=x(1:2);
D(i,4)=Tg_1(3);
D(i,5:actnodes+5)=x(3:actnodes+3);


% Cold well
for w=1:actnodes+3
        if w==1
           b2(w,1)=-T_air(i)/R1-C1/deltaTAU*Tg_2(w);   % Top node
        elseif w==2
           b2(w,1)=-C2/deltaTAU*Tg_2(w);          % Top aquif
        elseif w==3
           b2(w,1)= -Tg_2(w)/R0-C(1)/deltaTAU*Tg_2(w)-.../// 
               rho_w*cp_w*0*Tg_2(w)% Start
        elseif w==actnodes+1
           b2(w,1)= -T_g/R(actnodes)-C(actnodes-1)/deltaTAU*Tg_2(w); % End
        elseif w==actnodes+2
           b2(w,1)=-C3/deltaTAU*Tg_2(w);      % Down aquif
```

```
        elseif w==actnodes+3
           b2(w,1)= -T_g/R4-C4/deltaTAU*Tg_2(w);  % Down node
        else
           b2(w,1)=-C(w-2)/deltaTAU*Tg_2(w);  % Central
        end
    end

x=A2_F\b2;
Tg_2=x;
E(i,2:3)=x(1:2);
E(i,4)=Tg_2(3);
E(i,5:actnodes+5)=x(3:actnodes+3);

end
D(i,1)=i;
E(i,1)=i;
end

% Yearly working COP hours
COPhours=length(find(COP_H>0))/20;

% Total leakage (last node)
totH=100-V_flowH(8)*100/V_flowHI(8,actnodes);
totC=100-V_flowC(4480)*100/V_flowCI(4480,actnodes);

% Total Yearly Injected Volume
totV_H=sum(V_flowC(1:8760)*deltaTAU); % in warm well
totV_C=sum(V_flowH(1:8760)*deltaTAU); % in cold well

% Thermal interference radius
R_th1=sqrt(sum(V_flowC(1:8760)*deltaTAU)*rho_w*cp_w/(pi*h*C_s_aq)); % warm
R_th2=sqrt(sum(V_flowH(1:8760)*deltaTAU)*rho_w*cp_w/(pi*h*C_s_aq)); % cold
R_thAVE=(R_th1+R_th2)/2; % average thermal radius

% Figures

% Temperature Graph
plot(1:k,D([1:k],4),'-r',LineWidth=1.5)
hold on
plot(1:k,E([1:k],4),'-b',LineWidth=1.5)
axis([0 k 6 20])
grid on
xlabel('Years', FontSize=20)
ylabel('Temperature [°C]',FontSize=20)
legend('Warm well','Cold well',FontSize=15)
xticks([0:k/20:k])
set(gca, 'XTickLabel', num2cell(0:20))
g = gcf;
g.WindowState = 'maximized';
saveas(gcf,'WellTemperature.fig')

% Other graph
figure
plot(1:8760,Q1_Hn([1:8760])/(1000),'-r')
hold on
plot(1:8760,Q2_Cn([1:8760])/(1000),'-b')
ylabel('Building Load [kW]', FontSize=15)
```

```
hold on
yyaxis right
plot(1:8760,T_air([1:8760]),'-k')
grid on
title('Thermal Loads and Outdoor Air Temperature', FontSize=20)
xlabel('Hours', FontSize=20)
ylabel('Air Temperature [°C]', FontSize=15)
legend('Heating','Cooling','Air Temperature',FontSize=15)
g = gcf;
g.WindowState = 'maximized';
saveas(gcf,'Loads.fig')

figure
plot(1:8760,V_flowH([1:8760])*3600,'-r')
hold on
plot(1:8760,V_flowC([1:8760])*3600,'-b')
grid on
title('Water Flow', FontSize=20)
xlabel('Hours', FontSize=15)
ylabel('Volume flow [m^3/h]', FontSize=20)
legend('Heating','Cooling', FontSize=14)
g = gcf;
g.WindowState = 'maximized';
saveas(gcf,'Volumeflow.fig')

% Temperatures at different distance from well
figure % Warm well
plot(D([1:8760],1),D([1:8760],11:4:41),LineWidth=1);
legend([num2str(round(r_M2(8:4:38)))])
axis([0 8760 6 20])
grid on
xlabel('Hours', FontSize=20)
ylabel('Temperature [°C]', FontSize=20)
title('Warm Temperature at different distance', FontSize=15)
g = gcf;
g.WindowState = 'maximized';
saveas(gcf,'WarmWelldistance.fig')

figure % Cold well
plot(E([1:8760],1),E([1:8760],11:3:31),LineWidth=1);
legend([num2str(round(r_M2(8:3:28)))])
axis([0 8760 6 20])
grid on
xlabel('Hours', FontSize=20)
ylabel('Temperature [°C]', FontSize=20)
title('Cold Temperature at different distance', FontSize=20)
g = gcf;
g.WindowState = 'maximized';
saveas(gcf,'ColdWelldistance.fig')

% Injected/Extracted temp. Warm well
figure
plot(1:k,T_inj1,1:k,T_inj2+DT_H)
axis([0 k/5 5 20])
grid on
xlabel('Years', FontSize=20)
ylabel('Temperature [°C]', FontSize=20)
```

```
legend('Injected','Extracted', FontSize=14)
xticks([0:k/20:k])
set(gca, 'XTickLabel', num2cell(0:4))
title('Warm well inj/ext temperature', FontSize=20)
g = gcf;
g.WindowState = 'maximized';
saveas(gcf,'WarmWellinjext.fig')

% Injected/Extracted temp. Cold well
figure
plot(1:k,T_inj2,1:k,T_inj1-DT_C)
axis([0 k/5 5 15])
grid on
xlabel('Years', FontSize=20)
ylabel('Temperature [°C]', FontSize=20)
legend('Injected','Extracted', FontSize=14)
xticks([0:k/20:k/4])
set(gca, 'XTickLabel', num2cell(0:4))
title('Cold well inj/ext temperature',FontSize=20)
g = gcf;
g.WindowState = 'maximized';
saveas(gcf,'ColdWellinjext.fig')

% COP
figure
plot(1:k,COP_H,'-r.', LineWidth=2, MarkerSize=10)
axis([0 k 0 5])
grid on
xlabel('Years', FontSize=20)
ylabel('COP heating [-]', FontSize=20)
xticks([0:k/20:k])
set(gca, 'XTickLabel', num2cell(0:20))
g = gcf;
g.WindowState = 'maximized';
saveas(gcf,'COP.fig')

% Histograms
figure
ist1=[sum(Q1_Hn(1:743)) sum(Q2_H(1:743)) sum(Q2_Cn(1:743));.../// 
 sum(Q1_Hn(744:1415)) sum(Q2_H(744:1415)) sum(Q2_Cn(744:1415));.../// 
 sum(Q1_Hn(1416:2159)) sum(Q2_H(1416:2159)) sum(Q2_Cn(1416:2159));.../// 
 sum(Q1_Hn(2160:2879)) sum(Q2_H(2160:2879)) sum(Q2_Cn(2160:2879));.../// 
 sum(Q1_Hn(2880:3623)) sum(Q2_H(2880:3623)) sum(Q2_Cn(2880:3623));.../// 
 sum(Q1_Hn(3624:4343)) sum(Q2_H(3624:4343)) sum(Q2_Cn(3624:4343));.../// 
 sum(Q1_Hn(4344:5087)) sum(Q2_H(4344:5087)) sum(Q2_Cn(4344:5087));.../// 
 sum(Q1_Hn(5088:5831)) sum(Q2_H(5088:5831)) sum(Q2_Cn(5088:5831));.../// 
 sum(Q1_Hn(5832:6551)) sum(Q2_H(5832:6551)) sum(Q2_Cn(5832:6551));.../// 
 sum(Q1_Hn(6552:7295)) sum(Q2_H(6552:7295)) sum(Q2_Cn(6552:7295));.../// 
 sum(Q1_Hn(7296:8015)) sum(Q2_H(7296:8015)) sum(Q2_Cn(7296:8015));.../// 
 sum(Q1_Hn(8016:8760)) sum(Q2_H(8016:8760)) sum(Q2_Cn(8016:8760));.../// 
   ]/1000000;% MWh
gr=bar(ist1);
gr(1).FaceColor=[1 0 0]; gr(2).FaceColor=[1 1 0];
gr(3).FaceColor=[0 0 1];
ylabel('Energy [MWh]')
xlabel('Month')
legend('Cond Heating','Evap Heating','Cooling')
```

```
g = gcf;
g.WindowState = 'maximized';
saveas(gcf,'istog.fig')

% .csv file with result
for j=1:actnodes
txt = [r_M2(j)];
headerS{j} =sprintf('%d',txt);
headerS2{j} =sprintf('[degree C]');
end
title3={'meters'};
title4={'hours'};
T3=[title3, headerS;title4, headerS2];
writecell(T3,'RESULTSwarm.csv');
writematrix(D,'RESULTSwarm.csv','WriteMode','append');
writecell(T3,'RESULTScold.csv');
writematrix(E,'RESULTScold.csv','WriteMode','append');

toc % Elapsed time
```

Index of figures:

Index of tables:

Bibliography:

[1]. IEA, 2021 Global Status Report for Building and Construction

[2]. ASHRAE, 2019 ASHRAE Handbook-HVAC application, Chapter 35

[3]. Nordell B., Snijders A., Stiles L. "The use of aquifers as thermal energy storage (TES) systems"

[4]. Paul Fleuchausa, Bas Godschalkb, Ingrid Stobera, Philipp Bluma. "Worldwide application of aquifer thermal energy storage" application of aquifer thermal energy storage"

[5]. Andersson O., Sellberg B. "Swedish ATES Applications: Experiences after Ten Years"

[6]. U.S. Geological Survey. "Modeling Ground-Water Flow with MODFLOW and Related Programs"

[7]. Basar Bozkaya, Rongling Li, Timilehin Labeodan, Rick Kramer, Wim Zeiler. "Development and evaluation of a building integrated aquifer thermal storage model"

[8]. Elisa Scalco, Angelo Zarrella, Alessandro Maccarini, Alireza Afshari. "An aquifer thermal energy storage model for efficient simulations of district systems"

[9]. Carotenuto A., Fucci F., La Fianza G., Reale F. "Physical model and demonstration of an aquifer thermal energy store" 1991,11(2-3):169:180;

[10]. Julian E. Mindel, Peter Alt-Epping, Antoine Armandine Les Landes, Stijn Beernink, Daniel T. Birdsell, Martin Bloemendal, Virginie Hamm, Simon Lopez, Charles Maragna, Carsten M. Nielsen, Sebastia Olivella, Marc Perreaux, Maarten W. Saaltink, Martin O. Saar, Daniela Van den Heuvel, Rub´en Vidal, Thomas Driesner. "Benchmark study of simulators for thermo-hydraulic modelling of low enthalpy geothermal processes"

[11]. HEATSTORE, "Interim report on UTES-type/site-specific simulators based on academic/research codes"

[12]. Stijn Beernink, Martin Bloemendal, Rob Kleinlugtenbelt, Niels Hartog. "Maximizing the use of aquifer thermal energy storage systems in urban areas: effects on individual system primary energy use and overall GHG emissions"

Other references consulted:

- Basar Bozkaya, Rongling Li, Wim Zeiler. "A dynamic building and aquifer co-simulation method for thermal imbalance investigation"
- Wijbrand Sommer, Johan Valstar, Ingo Leusbrock, Tim Grotenhuis, Huub Rijnaarts. "Optimization and spatial pattern of large-scale aquifer thermal energy storage"
- Benno Drijver, Martijn van Aarssen, Bas de Zwart. "High-temperature aquifer thermal energy storage (HT-ATES): sustainable and multi-usable"
- Oleg Todorova, Kari Alannea, Markku Virtanena, Risto Kosonen. "A method and analysis of aquifer thermal energy storage (ATES) system for district heating and cooling: A case study in Finland"
- Martin Bloemendal, Niels Hartog. "Analysis of the impact of storage conditions on the thermal recovery efficiency of low-temperature ATES systems"
- Martin Bloemendal, Marc Jaxa-Rozenc, Theo Olsthoorn. "Methods for planning of ATES systems"